

Updating Current Strategies for Estimating a Source Term for a Tailings Storage Facility

Report to the
Water Research Commission

by

KN van Zweel
Centre for Water Sciences and Management
North-West University

WRC Report No. 2850/1/22
ISBN 978-0-6392-0460-4

August 2022



Obtainable from

Water Research Commission
Private Bag X03
Gezina
PRETORIA 0031

orders@wrc.org.za or download from www.wrc.org.za

DISCLAIMER

This report has been reviewed by the Water Research Commission (WRC) and approved for publication. Approval does not signify that the contents necessarily reflect the views and policies of the WRC, nor does mention of trade names or commercial products constitute endorsement or recommendation for use.

EXECUTIVE SUMMARY

Since the promulgation of the Waste Classification Act in 2013 and the subsequent cost implications of installing liners to disposal sites, research on techniques to obtain accurate source terms for disposal sites has become more relevant than ever. A study conducted for the Water Research Commission outlines a strategy for developing a geochemical model for the purposes of predicting potential acidic leachate qualities emanating from a disposal site. The strategy incorporates various well-documented static and kinetic laboratory procedures. There is, however, a knowledge gap when the results obtained from these procedures must be incorporated in a geochemical model and the model must be calibrated to field conditions.

It is accepted that the rate of pyrite oxidation in backfilled pits and waste storage facilities is governed by the rate of oxygen ingress. Several mathematical models to describe the kinetics of a heterogeneous reaction have been developed over the years. These models all describe in-situ leaching behaviour by focusing on the leaching behaviour of the individual particles in the tailings. All three these modelling approaches assume the particle is spherical and that the reaction front moves radially towards the centre of the particle. However it is important to note that by understanding the oxygen transport behaviour in tailings material and accurately tracking the extent of pyrite oxidation and quantifying the redox controls with depth, a more accurate geochemical model can be constructed.

The aims of this project with the focus on tailings storage facilities were therefore to:

1. Develop field techniques to measure oxygen concentration and redox profiles. The data obtained from these procedures will aid in determining the source term of a tailings storage facility.
2. Determine the influence of governing factors such as migration rate of phreatic head, oxygen ingress and particle size distribution on the accuracy of geochemical models following current geochemical investigation strategies.
3. Comment on shortcoming of current geochemical investigation strategies and help improve and update these strategies

In order to achieve these aims eight boreholes were drilled in a gold tailings dam. The borehole depth was determined by visually observing a colour change in the tailings and by assessing pH and oxidation reduction potential (ORP) readings that were done during the drilling of the boreholes. The boreholes were equipped with sets of small chambers covered with a membrane and tube bundles leading up to the surface in order to measure the oxygen concentration of each installed chamber. Profiles were recorder for oxygen concentration, redox, electrical conductivity, pH and moisture content. Samples were taken for geochemical classification and particle size distribution. It is important to note that it would have been ideal if a much larger array of boreholes were drilled to obtain a better understanding of the special variation of the measured parameters. It is also recommended for future work to plan for long term monitoring of these boreholes to get a sense of the temporal variation.

A conceptual model was developed based on the assumption that the total sulphur represents the initial pyrite content in the tailings material, and the conversion of pyrite can be calculated from the sulphur speciation data. The conversion represents the extent to which pyrite has been oxidized with depth. The pyrite conversion shows an almost an inverse profile of the moisture profile with depth. This trend was observed in all the boreholes. The conversion of pyrite with depths profiles shows that, in horizons that have a high volumetric moisture percentage, oxidation rates of pyrite are significantly lower compared to sample points in the depth profile that were drier. The results suggest that points in the depth profiles of the boreholes that show a higher degree of saturation will have a lower oxidation rate. It is assumed that the degree of saturation of the material will be a rate determining step in the oxidation of pyrite.

The modelling software Geostudio SEEP/W was used to model the unsaturated flow in the tailings material over time. The Gas Consumption and Exothermic Reaction add-in in SEEP/W was used to account for the oxygen sink due to pyrite oxidation. The results obtained from this model was only used to calculate the possible variance in the soil moisture over time as a function of seasonality. The output of the SEEP/W model was further used as input for the geochemical model.

PYROX was used to model the oxygen transport in the tailings material. The model numerically solves Fick's law of mass transport that contains an oxygen sink that represents the oxygen consumed by pyrite oxidation. The results of this study indicate that the unsaturated flow regime of a tailings storage facility may govern the rate of oxidation of pyrite though controlling the rate of oxygen ingress into the tailings. Several uncertainties such as the depth and downward migration rate of the phreatic head made calibrating the PYROX model challenging. Variation in soil moisture at the respective nodes of the PYROX model were calculated with SEEP/W by assuming that the phreatic head was static for the timespan of the model. This is a limitation of the modelling approach and it is accepted that it may not be representative of the physical process. Furthermore, horizons of very fine particles (can be seen as nodes with a high moisture content in the moisture profiles) were observed. It was also noted that these horizons acted like barriers and shielded material underneath it from oxidation. The geochemical model assumes that the material in the unoxidized zone is homogeneous and did not compensate for this shielding effect or the possible existence of preferential flow paths like the fissures.

It was concluded that the data requirements to better understand the global behaviour of the geochemical evolution of the tailings are primarily hydrological in nature. This implies better understanding of parameters such as particle size distribution, influence of preferential flow paths, downward migration the phreatic head and the spatial and temporal variation of soil moisture as a function of the aforementioned parameters.

In order to address the uncertainties identified, a larger array of boreholes with greater depths (intercept the saturated zone in the tailings storage facility) will be required to get a sense of the spatial variability the parameters governing the unsaturated material moisture content. By better comprehending the unsaturated flow regime of tailings storage facilities, more accurate field scale geochemical models can be constructed to model potential risks that may be associated with these sites.

ACKNOWLEDGEMENTS

The project team would firstly like to thank the WRC for providing funding for the project.

Dr Yazeed Van Wyk, taking over as research manager and patience with the project team's challenges

The inputs from the reference group are gratefully acknowledged.

Thank you Johan Fourie with assisting with the field work and analyses.

Finally thank you to all the students who assisted with the research.

CONTENTS

EXECUTIVE SUMMARY	iii
ACKNOWLEDGEMENTS	iv
CONTENTS	v
LIST OF FIGURES	vii
LIST OF TABLES	ix
ACRONYMS AND ABBREVIATIONS	x
GLOSSARY	xi
CHAPTER 1: BACKGROUND	1
1.1 INTRODUCTION	1
1.2 PROJECT AIMS	2
CHAPTER 2: LITERATURE SURVEY	3
2.1 INTRODUCTION	3
2.2 OXYGEN TRANSPORT	3
2.2.1 Fick's second law	3
2.2.2 Pyrite oxidation	3
2.2.3 Shrinking Core Model	4
2.2.4 Modelling tailings storage facilities	5
CHAPTER 3: METHODOLOGY	7
3.1 FIELD WORK	7
3.1.1 Oxygen concentration profiles	7
3.1.2 Moisture content profiles	9
3.1.3 Oxidation reduction potential	9
3.2 LABORATORY WORK	10
3.2.1 Static tests	10
3.2.2 Kinetic tests	10
3.2.3 Additional analysis	10
CHAPTER 4: NUMERICAL MODELS	12
4.1 CONCEPTUAL MODEL	12
4.1.1 Pyrite conversion	12
4.1.2 Influence of volumetric moisture percentage	12
4.1.3 Unsaturated flow model	15
4.1.3.1 Geostudio	15
4.1.3.2 Model setup	15
4.1.3.3 Model calibration	15
4.1.4 Oxygen transport modelling	16
4.1.4.1 PYROX	16

4.2	MODEL SETUP	16
CHAPTER 5: RESULTS AND DISCUSSION		18
5.1	FIELD MEASUREMENTS	18
5.1.1	Particle size distribution	20
5.1.2	Laboratory analysis	21
5.1.2.1	Sulphide content	21
5.1.2.2	Acid Base Accounting	24
5.1.2.3	X-ray diffraction results	24
5.1.3	Model results	27
5.1.3.1	Moister profiles	27
5.1.3.2	Oxygen profiles (PYROX)	29
CHAPTER 6: CONCLUSION		32
6.1	FIELD WORK	32
6.2	LABORATORY ANALYSIS	32
6.3	MODEL RESULTS	32
Bibliography		34
APPENDIX A: ICP MS Results		37
APPENDIX B: Particle Size Distribution		44
APPENDIX C: XRD Results		48
APPENDIX D: Sulphur Speciation Results		54

LIST OF FIGURES

Figure 1: Schematic drawing of the three leach models discussed by Davis and Ritchie (1986).....	4
Figure 2: Show a schematic drawing of a tailings heap. The transport of oxygen into the heap and to the reacting particles is mathematically described by Fick's second law with an oxygen sink term (refer to equation 1 & 2, section 2.2.1). The reaction kinetics of the reacting particles is mathematically described by the shrinking core model (Molson et al., 2005).	6
Figure 3: Schematic drawing of oxygen chamber installation in a monitoring borehole	7
Figure 4: Location map of the monitoring/data boreholes	8
Figure 5: Chemical and physical parameter profiles of Borehole RF1	12
Figure 6: Chemical and physical parameter profiles of Borehole RF2	13
Figure 7: Chemical and physical parameter profiles of Borehole RF3	14
Figure 8: Chemical and physical parameter profiles of Borehole RF6	14
Figure 9: Results obtained from SEEP/W showing gas concentration variation as a function of time. The model accounted for wet and dry periods.	15
Figure 10: DEM of the tailings heap indicating where the boreholes was drilled and where the cross section was selected for the numerical model.	16
Figure 11: Schematic of the PYROX model	17
Figure 12: Data obtained from RF1	18
Figure 13: Data obtained from RF2	19
Figure 14: Data obtained from RF3	19
Figure 15: Data obtained from RF4	20
Figure 16: Sulphur speciation results for BH RF 1	22
Figure 17: Sulphur speciation results for BH RF 2	22
Figure 18: Sulphur speciation results for BH RF 3	23
Figure 19: Sulphur speciation results for BH RF 4	23
Figure 20: Modelled volumetric moister percentage curve compared to the measured volumetric moister curve for BH RF1	27
Figure 21: Modelled volumetric moister percentage curve compared to the measured volumetric moister curve for BH RF2	28
Figure 22: Modelled volumetric moister percentage curve compared to the measured volumetric moister curve for BH RF3	28
Figure 23: Modelled volumetric moister percentage curve compared to the measured volumetric moister curve for BH RF4	29
Figure 24: Modelled oxygen concentration curve (PYROX) compared to the measured oxygen concentration curve for BH RF1	30
Figure 25: Modelled oxygen concentration curve (PYROX) compared to the measured oxygen concentration curve for BH RF2	30

Figure 26: Modelled oxygen concentration curve (PYROX) compared to the measured oxygen concentration curve for BH RF3	31
Figure 27: Modelled oxygen concentration curve (PYROX) compared to the measured oxygen concentration curve for BH RF4	31
Figure 28: Particle size distribution curve for borehole RF 1	44
Figure 29: Particle size distribution curve for borehole RF 2	45
Figure 30: Particle size distribution curve for borehole RF 3	46
Figure 31: Particle size distribution curve for borehole RF 4	47
Figure 32: XRD analysis results for RF 2.1	48
Figure 33: XRD analysis results for RF 2.2	48
Figure 34: XRD analysis results for RF 2.3	48
Figure 35: XRD analysis results for RF 2.4	49
Figure 36: XRD analysis results for RF 2.5	49
Figure 37: XRD analysis results for RF 2.6	49
Figure 38: XRD analysis results for RF 2.7	50
Figure 39: XRD analysis results for RF 2.8	50
Figure 40: XRD analysis results for RF 2.9	50
Figure 41: XRD analysis results for RF 2.10	51
Figure 42: XRD analysis results for RF 2.11	51
Figure 43: XRD analysis results for RF 2.12	51
Figure 44: XRD analysis results for RF 2.13	52
Figure 45: XRD analysis results for RF 3 unoxidized composite sample	52
Figure 46: XRD analysis results for RF 1 unoxidized composite sample	52
Figure 47: XRD analysis results for RF 1 oxidized composite sample	53
Figure 48: XRD analysis results for RF 3 oxidized composite sample	53
Figure 49: XRD analysis results for RF 1 transition zone sample	53

LIST OF TABLES

Table 1: Monitoring borehole information	9
Table 2: Summation of laboratory test work	11
Table 3: Input parameters for the model	17
Table 4: D50 values with depth for BH RF 1	20
Table 5: D50 values with depth for BH RF 2	21
Table 6: D50 values with depth for BH RF 3	21
Table 7: D50 values with depth for BH RF 4	21
Table 8: Acid Base Accounting for Borehole RF 4	24
Table 9: XRD results.....	25
Table 10: XRF results	26
Table 11: 1:20 Leach test laboratory results	37
Table 12: Humidity leach cell week 1 results.....	39
Table 13: Humidity leach cell week 2 results.....	40
Table 14: Humidity leach cell week 3 results.....	41
Table 15: Humidity leach cell week 4 results.....	42
Table 16: Humidity leach cell week 5 results.....	43
Table 17: RF 1 sulphur speciation data	54
Table 18: RF 2 sulphur speciation data	54
Table 19: RF 3 sulphur speciation data	55
Table 20: RF 4 sulphur speciation data	55

ACRONYMS AND ABBREVIATIONS

a	Radius of particle obtained from the D50 values for each sampled depth
ABA	Acid base accounting
ABAT	Acid base accounting technique
ABATE	Acid base accounting technique and evaluation
AMD	Acid mine drainage
AP	Acid potential
D ₁	Bulk diffusion coefficient
D ₂	Diffusion coefficient for the forming ash layer shielding the shrinking particle
D50	Particle size
H	Henry's constant
ICP-MS	Inductively coupled plasma mass spectrometry
L	Depth of borehole
mM	Millimole
mV	millivolt
NAG	Net Acid Generation
NP	Neutralization Potential
NNP	Net Neutralization Potential
(NPR) (NP:AP)	Neutralizing Potential Ratio
ORP	Oxidation reduction potential
[O ₂] _a	Concentration of oxygen in the pore space
r	Radius of the core of the particle that has not yet reacted
R	Particle radius
r _B	Density of the particle
SCM	Shrinking Core Model
UNOX	Unoxidised
WRC	Water Research Commission
XRD	X-ray diffraction
XRF	X-ray fluorescence
θ	Gas filled porosity of the material
θ	Volumetric moisture content
ρ	Bulk density of the tailings material
Φ	Porosity

GLOSSARY

Acid mine drainage: The outflow of acidic water from for example a mining site. In most cases, this acid comes primarily from oxidation of iron sulphide.

Diffusion coefficient: The quantity of a substance that in diffusing from one region to another passes through each unit of cross section per unit of time when the volume-concentration gradient is unity

Geochemistry: This is the study of the origin, evolution and distribution of chemical elements on earth which are contained in the rock-forming minerals and the products derived from it, as well as water and atmosphere.

Geochemical model: Geochemical modelling is the practice of using chemical thermodynamics, chemical kinetics, or both, to analyse the chemical reactions that affect geologic systems, commonly with the aid of a computer.

Leaching: This is a process of extracting a substance from a material such as tailings normally by means of a liquid. This process is also referred to as extraction

Moisture content: This is the quantity of water contained in a material such as soil or tailings

Neutron Depth Probe: This is a probe that measures the moisture content in soil, tailings etc.

Oxidation reduction potential: The oxidation reduction potential (ORP) is a water quality parameter and it provides an indication of the amount of oxygen in the water

Oxidation: This occurs when an atom, molecule, or ion loses one or more electrons in a chemical reaction. When oxidation occurs, the oxidation state of the chemical species increases.

Oxygen diffusion: The oxygen diffusion rate (ODR) is a measure of the mobility of oxygen in a medium such as sulphidic tailings which can lead to oxidation reactions.

Oxidized zone: A zone that forms as a result of chemical decomposition of unstable minerals under the action of surface waters and groundwater, as well as the oxygen and carbon dioxide present in the air and dissolved in these waters.

Particle size distribution: The particle-size distribution (PSD) of a granular material, is a list of values or a mathematical function that defines the relative amount, typically by mass, of particles present according to size.

Pyrite: The mineral pyrite, or iron pyrite, also known as fool's gold, is an iron sulphide with the chemical formula FeS_2 . Pyrite is considered the most common form of sulphide minerals.

Pyrite oxidation: The weathering of pyrite includes the oxidation of pyrite by oxygen. Sulphur is oxidized to sulphate and ferrous iron is released.

Redox: This is a type of chemical reaction in which the oxidation states of atoms are changed.

Unsaturated zone: The unsaturated zone is the portion of the subsurface above the groundwater table. The soil and rock in this zone contains air as well as water in its pores

This page was intentionally left blank

CHAPTER 1: BACKGROUND

1.1 INTRODUCTION

Since the promulgation of the Waste Classification Act in 2013 and the subsequent cost implications of installing liners to waste disposal sites, research on techniques to obtain accurate source terms for disposal sites has become more relevant than ever.

A study conducted for the Water Research Commission (WRC) by Usher et al. (2002) outlines a strategy for developing a geochemical model for the purposes of predicting potential acidic leachate qualities emanating from a disposal site. The strategy incorporates various well-documented static and kinetic laboratory procedures. There is, however, a knowledge gap when the results obtained from these procedures must be incorporated in a geochemical model and the model must be calibrated to field conditions.

It is accepted that the rate of pyrite oxidation in backfilled pits and waste storage facilities is governed by the rate of oxygen ingress (Davis & Ritchie, 1986 (a, b &c); Mayer et al., 2002). Several mathematical models to describe the kinetics of a heterogeneous reaction have been developed over the years. These models were developed for describing leaching behaviour of copper tailings. Davis and Ritchie (1986b) refer to three primary types that all describe in-situ leaching behaviour by focusing on the leaching behaviour of the individual particles in the tailings. All three these modelling approaches assume the particle is spherical and that the reaction front moves radially towards the centre of the particle (Davis & Ritchie, 1986b).

The best-known and widely used of these models is the Shrinking Core Model (SCM). This mathematical model describes the kinetics for a solid-gas and solid-liquid system (Levenspiel, 1999). In the well-known work done by Davis and Ritchie (1986b) and later also by Molson et al. (2005), the shrinking core model is used to describe the reaction kinetics of pyrite oxidation in tailings material. In this approach it is assumed that the rate of oxygen diffusion of the reaction sites is the rate limiting step. This is also discussed as an important factor in the oxidation of pyrite soils by Appelo and Postma (2005). It is noted that oxygen transport is only important in the unsaturated zone. In the saturated zone, the approximate amount of oxygen available for pyrite oxidation is 0.33 mM O₂, suggesting that the unsaturated zone is the most reactive and the greatest source of sulphate oxidation.

The bulk diffusion coefficient D_1 , governing the transport of oxygen through the pore space of the tailings material is a function of void space, degree of saturation of the tailings material and temperature (Reardon & Moddle, 1985). Thus, is important to understand the variability of moisture content with depth in these systems and the migration of the phreatic head and the subsequent change in depth of the unsaturated zone with time.

In order to understand the equilibrium chemistry in the tailings material redox profiles are also required. In acid mine drainage (AMD) it is fair to assume that the dominant redox couple would be Fe²⁺ / Fe³⁺. The concentrations of both ions will be a function of the extent of pyrite oxidation. Yibas et al. (2010) conducted a study for the WRC focusing on kinetic development of oxidation zones. In the study by Yibas et al. (2010) oxygen profiles were obtained for the various tailings storage facilities that formed part of the study. The profiles were used to identify three distinct zones. The oxidized zone, the transition zone and the unoxidized zone. The data obtained gives a good indication of the number of tailings that has not yet reacted. It does, however, not address the transient behaviour that is expected from the tailings storage facilities.

The last step of the acid-base accounting technique and evaluation (ABATE) strategy (Usher et al., 2002) consists of kinetic modelling. The data input up to this point includes acid base accounting (ABA), mineralogy, particle size distribution, and static and kinetic tests. The strategy relies on kinetic tests to obtain acid

generation rates. The rates obtained from these tests, however, do not accurately represent the acid generation rates expected in the tailings material as the kinetic leach test do not account for physical parameters influencing the rate of acid generation.

By understanding the oxygen transport behaviour in tailings material and accurately tracking the extent of pyrite oxidation and quantifying the redox controls with depth, a more accurate geochemical model can be constructed.

1.2 PROJECT AIMS

1. Develop field techniques to measure oxygen concentration-and redox profiles in tailings storage facilities. The data obtained from these procedures will aid in determining the source term of a tailings storage facility.
2. Determine the influence of governing factors such as migration rate of phreatic head, oxygen ingress and particle size distribution have on the accuracy of geochemical models following current geochemical investigation strategies.
3. Comment on shortcoming of current geochemical investigation strategies and help improve and update these strategies with specific reference to the ABAT strategy (Usher et al., 2002).

CHAPTER 2: LITERATURE SURVEY

2.1 INTRODUCTION

The consensus regarding the modelling of AMD in waste storage facilities is that oxygen transport in the waste material is the rate determining step in the oxidation of pyrite. The first studies that looked at this behaviour were conducted by Davis and Ritchie (1986a, b and c) and later also by Molson et al. (2005). In both these mentioned studies, the shrinking core model was used to mathematically describe the reaction kinetics of pyrite oxidation.

This approach is also discussed as an important factor in the oxidation of pyrite soils by Appelo and Postma (2005). It is further noted that the oxygen transport is only important in the unsaturated zone. In the saturated zone, the approximate amount of oxygen available for pyrite oxidation is 0.33 mM O₂, indicating that the unsaturated zone is the most reactive and the greatest source of sulphate oxidation.

2.2 OXYGEN TRANSPORT

Davis and Ritchie (1986a) assume that the rate of unreacted core shrinkage is much slower than the oxygen diffusion rate within the particle (Levenspiel, 1999). It is assumed that the reaction at the surface of the particle is instantaneous and that ash layer diffusion is the rate determining step.

2.2.1 Fick's second law

It is assumed that the oxygen transport in from the atmosphere to the reaction sites in the tailings material occur by diffusion only. Davis and Ritchie (1986a) used Fick's second law with a consumption term to describe the diffusion process mathematically:

$$(\partial U_A)/\partial t = D_1 \times (\partial^2 U_A)/(\partial z^2) - q(z,t) \quad [1]$$

The model describes a two-stage diffusion process to the reaction sites. The first stage consists of oxygen diffusion through the air-filled pores. D₁ is the diffusion coefficient for this stage. The term on the left, (∂U_A)/∂t, represent the change in pore oxygen concentration. The consumption term in equation 1 (q(z,t)) represents the change in volume due to the oxidation of pyrite, and can be expressed as follows (Molson et al., 2005):

$$q(z,t) = D_2 \times ((3(1-\theta))/R^2) \times (r/(R-r)) \times [O_2]_a / H \quad [2]$$

In equation 2, H is Henry's constant [kg/m³] and [O₂]_a represent the concentration of oxygen in the pore space. D₂ represents the diffusion coefficient for the forming ash layer shielding the shrinking particle. The parameter θ represent the gas filled porosity of the material. R represent the particle radius and r represent the radius of the core of the particle that has not yet reacted. The concentration of oxygen dissolving into the water film surrounding the particle is calculated using Henry's law, where H represents Henry's constant for a given temperature.

2.2.2 Pyrite oxidation

Younger (2000) suggests that a general reaction equation for the oxidation of pyrite can be written as follows:



In the reaction, iron disulfide is oxidized, causing the formation of acid and the release of sulfate in the water. The ferrous iron (Fe^{2+}) can further be oxidized to Ferric iron (Fe^{3+}). The ferric iron can then either be hydrolysed to form ferric hydroxide ($Fe(OH)_3$), also known as yellow boy, or the ferric iron can act as a catalyst in oxidation of iron disulfide (Skousen et al., 2002). There are several reactions contributing to a buffer effect to low pH due to oxidation of pyrite. The most obvious of which is the dissolution of Calcite ($CaCO_3$) (Bain et al., 2001) and other carbonate rock forming minerals (Dolomite and Aragonite) (Appelo and Postma, 2005). The presence of buffering minerals affects the mobility of dissolved metals, for example the precipitation of gypsum may occur due to the increase of Ca^{2+} at the calcite dissolution front, thereby providing an upper limit on dissolved calcium and SO_4 concentrations (Bain et al., 2001).

2.2.3 Shrinking Core Model

A number of mathematical models to describe the kinetics of a heterogeneous reaction have developed over the years. These models were developed for describing leaching behaviour of copper tailings material. Davis and Richie (1986b) refer to three primary types that all describe in-situ leaching behaviour by focusing on the leaching behaviour of the individual particles in the tailings material. According to Davis and Richie (1986c), the three models differ in the assumptions made about the reaction rate compared to the reactant transport rate to the reaction sites.

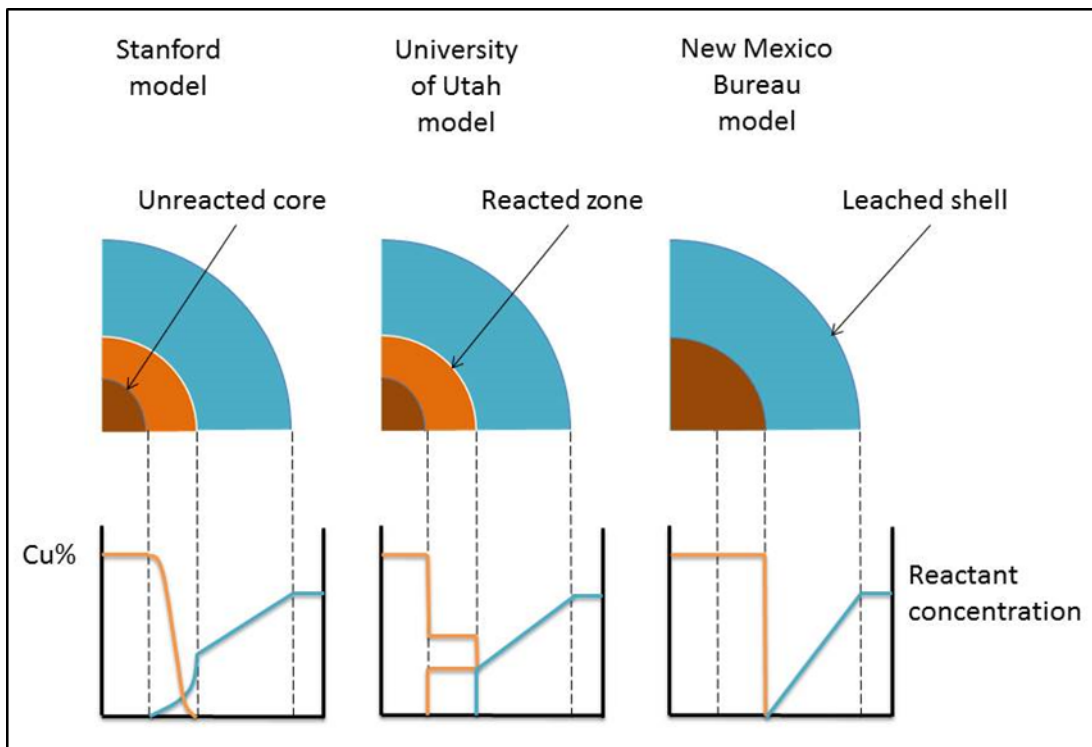


Figure 1: Schematic drawing of the three leach models discussed by Davis and Ritchie (1986)

All three these modelling approaches assume the particle is spherical and that the reaction front moves radially towards the centre of the particle (Davis & Richie, 1986a, b & c).

The most well-known and widely used of these models is the SCM. This mathematical model describes the kinetics for a solid-gas and solid-liquid system (Levenspiel, 1999). The model finds its application in geochemistry by describing the oxidation of pyrite in tailings leaching scenarios. For a heterogeneous reaction in which a fluid reacts with a solid the following reaction applies:



The rate of reaction can be controlled by three mechanisms, the first of which is diffusion through the gas film. This is not discussed further in this work as it is assumed that the reaction of the particles occurs at the water-solid interface. The second rate-determining step is the diffusion of reactant through the ash layer and can mathematically be described as follows:

$$-\frac{dN_A}{dt} = r_{\text{mineral}} = 4\pi r^2 D_2 \frac{dC_A}{dr} \quad [5]$$

where r is the radius of the unreacted core [m] and D_2 is the diffusion coefficient of the reactant through the ash layer [m^2/s]. The ash layer or alteration rim refers to the reacted crust that forms around the unreacted core (Figure 1). The third rate determining step in chemical rate controls and can be mathematically expressed as follows:

$$-\frac{1}{4\pi r^2} \frac{dN_B}{dt} = r_{\text{Mineral}} = \frac{-b}{4\pi r^2} \frac{dN_A}{dt} = bk'' C_{Ag} \quad [6]$$

where k'' is the first order rate constant for the surface reaction and C_{ag} is the gas phase concentration of the reactant diffusing through the ash layer [moles/l]. Levenspiel (1999) shows that the abovementioned rate controlling steps can be combined to account for the influence of all three rate-controlling steps:

$$-\frac{dr}{dt} = r_{\text{Mineral}} = \frac{bC_A/\rho_B}{\frac{(R-r)r}{RD_2} + \frac{1}{k''}} \quad [7]$$

where R is the radius of the initial unreacted particle and the density of the particle is denoted by ρ_B [kg/m^3]. Ardejani et al. (2008) used this approach to describe the kinetic oxidation of pyrite.

2.2.4 Modelling tailings storage facilities

Previously substantial work has been done on the importance of chemical, physical and microbiological factors influencing the weathering of rate of pyrite (Linklater et al., 2005; Molson et al., 2005). Leaching of metals contained in the constituents of either ores for the purpose of mining the leached product or spoils and tailings dams relies on the oxidation of insoluble sulphide bearing minerals to soluble sulphates (Davis & Ritchie, 1986 a). Water transports the soluble oxidation products through the gangue where further oxidation, dissolution and precipitation can take place (Brown et al., 1999). Therefore, the concentrations of chemical components in the effluent of spoils and tailings material are space and time-dependent processes, which in turn depend on the pyrite oxidation rate, water infiltration rate and chemical oxidation rates (Pantelis et al., 2002).

Several mathematical models that describe the leaching process in tailings storage facilities, have been developed over the last couple of years (Davies & Ritchie, 1986 a, b & c; Molson et al., 2005; Linklater et al., 2004; Pantelis et al., 2002). In the work done by Davies and Ritchie (1986a, b & c) it was assumed that oxygen is transported into the tailings by means of diffusion. In the work done by Lefebvre et al. (2001) it is shown that convective flow of oxygen caused by heat production of pyrite oxidation can also determine the rate of oxygen supply. In the work done by Pantelis et al. (2002) the tailings storage facilities is modelled as a three-phase system consisting of gas-and water phases flowing through a rigid solid porous phase. In the model it was

assumed for simplicity that the sulphide containing minerals consist entirely of pyrite. There was also not compensated for the temperature dependence of diffusion coefficients, viscosities and thermal conductivities. This was done under the assumption that physical conditions in the spoils tailings material reach pseudo-steady which can last in most cases for decades or longer.

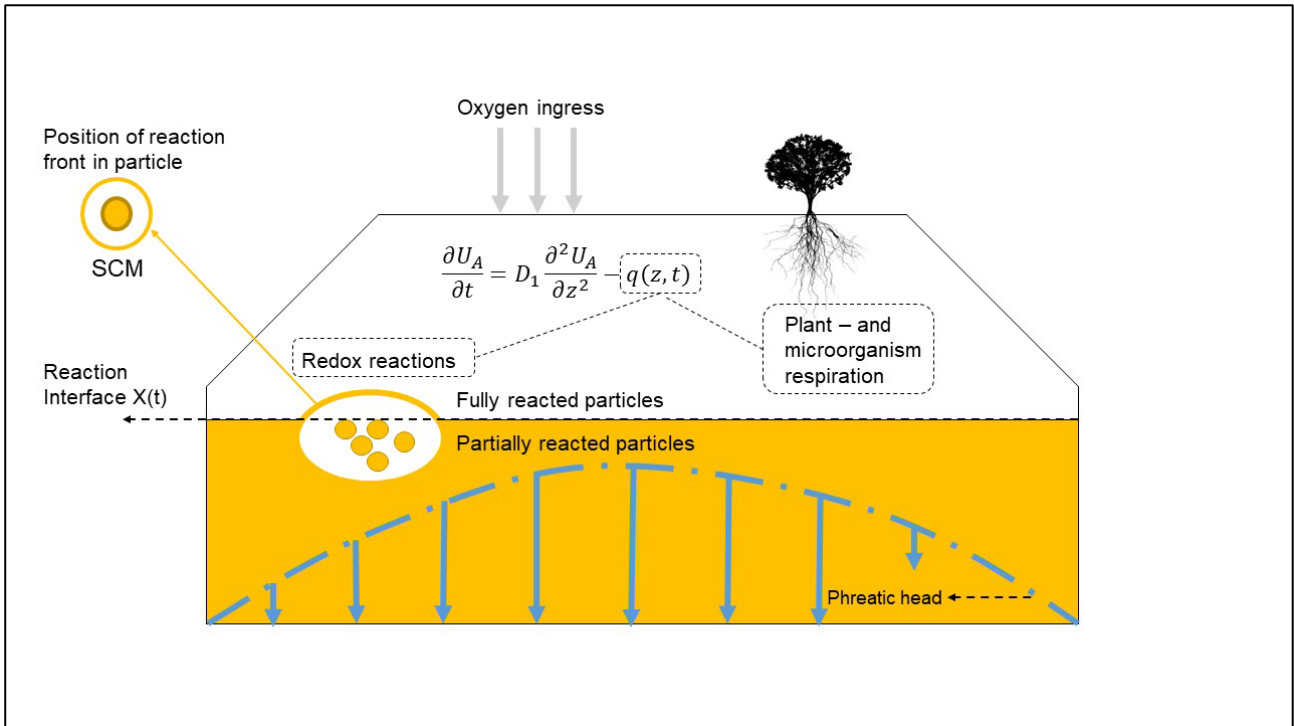


Figure 2: Show a schematic drawing of a tailings heap. The transport of oxygen into the heap and to the reacting particles is mathematically described by Fick's second law with an oxygen sink term (refer to equation 1 & 2, section 2.2.1). The reaction kinetics of the reacting particles is mathematically described by the shrinking core model (Molson et al., 2005).

In the conceptual model presented in Figure 2 it is shown that the rate at which a waste tailings heap is reacting is a function of the oxygen ingress. The oxygen transport rate is in turn a function of both the gradient between the atmospheric oxygen concentration and the pore oxygen concentration, the thickness and moisture content of the unsaturated material.

CHAPTER 3: METHODOLOGY

3.1 FIELD WORK

3.1.1 Oxygen concentration profiles

Four boreholes were drilled in the tailings storage facility. The borehole depth was determined by visually observing a colour change in the tailings and by assessing pH and oxidation reduction potential (ORP) readings that was done during the drilling of the boreholes. The boreholes were equipped with sets of small chambers covered with a membrane and tube bundles leading up to the surface in order to measure the oxygen concentration of each installed chamber.

Figure 3 below shows a schematic drawing of the installed chambers in the borehole. Between each chamber a bentonite clay seal was installed to ensure that the reading obtained at a specific depth represent the oxygen concentration in the tailings, and that there is no leakage of gases between various depth intervals.

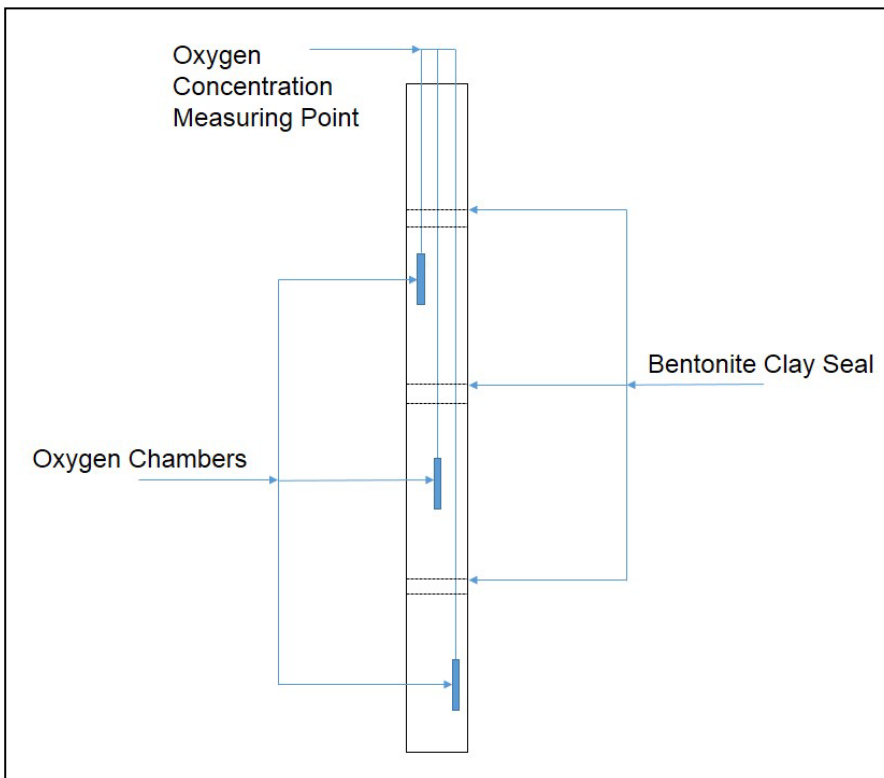


Figure 3: Schematic drawing of oxygen chamber installation in a monitoring borehole

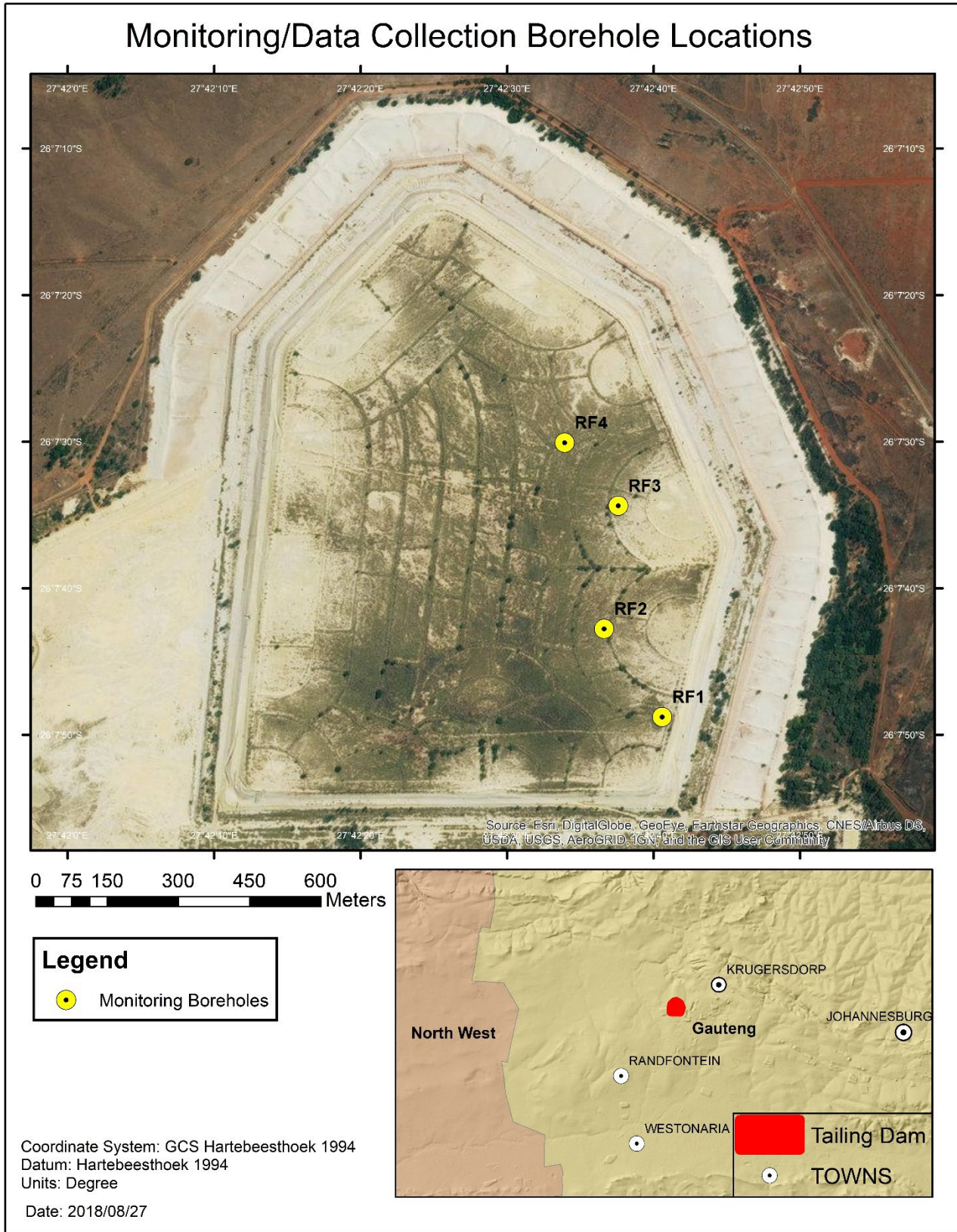


Figure 4: Location map of the monitoring/data boreholes

Table 1 shows the depths of the four respective boreholes drilled with a hand auger. Borehole RF 1 was drilled to a depth of 6 metres. It can be seen from Figure 4 that this borehole is located close to the side of the site. The 3 remaining boreholes drilled were drilled to depths ranging from 3 to 4 metres.

Table 1: Monitoring borehole information

Borehole ID		Depth		Coordinates	
				x	y
RF1	RF1-1	6	4.4	27.711275	-26.130217
RF2	RF2-1	3	2.4	27.710175	-26.128549
RF3	RF3-1	4	3.2	27.710443	-26.126214
RF4	RF3-1	3	2	27.709427	-26.12502

After installation of the tube bundles and chambers, the boreholes were left for around two hours to obtain equilibrium. The oxygen concentrations with depth were then measured with a PortaSens II Portable Gas Leak Detector. The probe is a hand-held device that measures oxygen displacement.

3.1.2 Moisture content profiles

Two sets of boreholes were drilled at each location, one set was used for the installation of the oxygen chambers and the other set for moisture content measurements. The second set of boreholes at each location were lined with a PVC casing. The boreholes were then used to obtain moisture content data with a Neutron Depth Probe.

The Neutron Depth Probe comprises two main components: a) a probe, which is lowered into an access tube located over the drilled hole which is inserted vertically into the tailings, and which contains a source of fast neutrons in the form of radioactive material such as Americium-241, Beryllium and Caesium-137, and a detector of slow neutrons; b) a ratemeter (battery powered and portable) to monitor the flux of slow neutrons scattered by soil (Hillel, 1980).

The theory behind this instrument as described by numerous researchers (Long & French, 1967; Visvalingam & Tandy, 1972; Gardner, 1986) is based on the principle that hydrogen, which has the same size and mass as a neutron, has a marked property of scattering and slowing neutrons (thermalizing effect). When a fast neutron is placed within the soil, it immediately becomes surrounded by a cloud of thermal neutrons. Using a detector thermal neutron density can easily be measured, insensitive to fast neutrons, which is placed in the vicinity of a fast source. Then the thermal neutron density can be converted to volumetric water content using the calibration curve which is linear over the range of interest.

Samples were also taken at depth intervals of 20 cm for each borehole for determining the gravimetric moisture content. These samples were weighed, dried in an oven for 24 hours at a 110°C and then re-weighed in order to obtain the gravimetric water content. This was done to obtain the volumetric water content at each node measurement for the neutron depth probe.

3.1.3 Oxidation reduction potential

Tailings samples were taken every 30 cm during the drilling of the boreholes for ORP measurements. The oxidation-reduction potential (ORP) of each sample was measured using a platinum electrode ORP meter (Eutech instrument). The ORP meter was calibrated to Standard Hydrogen Electrode potential using a 240-mV reference solution.

The measurements were taken as soon as the sample had been extracted via a hand auger. In order to minimize the exposure to atmosphere and the potential subsequent oxidation of the extracted material, a saturated paste was made by mixing 20 grams of sample material with 50 millilitres of deionized water. The sample paste was left for 10 minutes in order to equilibrate after which the ORP readings were obtained with the hand-held probe.

In addition to the ORP readings, pH and electrical conductivity were also measured for each sample in order to obtain depth profiles for the respective parameters.

3.2 LABORATORY WORK

3.2.1 Static tests

ABA is generally used as a first order classification procedure in acid rock drainage (ARD) prediction methodologies. ABA results provide information about the potential of a sample to generate ARD (Price, 1997); it is a valuable and widely used test that determines both the acid-generating and acid neutralizing potential of a sample (Skousen et al., 2002). Net Acid Generating (NAG) tests are also performed to aid in a better interpretation of the ABA results (Miller et al., 1997). The test procedure is not time consuming, is low cost and the analytical procedure is relatively simple (Usher et al., 2002)

There are however limitations to this test procedure. The most important of which is the fact that ABA does not address the transient behaviour of acid drainage, and this is also the case for all the static type tests. Usher et al. (2002) notes that the ABA test procedure assumes instant availability of reactants, simple reaction stoichiometry and account for size effects of solid reactants.

ABA and the other static tests listed in Table 2 where conducted in order to show how much of the data obtained from these tests helps to understand the field scale transient behaviour of tailings material.

3.2.2 Kinetic tests

In order to address the shortfalls of static testing Usher et al. (2002) recommends a kinetic leach test methodology adapted from the D5744-96 Standard Test Method (ASTM, 2001). The minimum suggested duration of this leach test is twenty weeks and is in some cases not enough time for sulphate production to stabilize. Humidity cell tests (HCT) supplement static tests in this regard and can assist in obtaining reaction rates and an indication of the potential mineral leaching behaviour of rock samples (Price, 1997). Currently one of the biggest challenges faced by environmental practitioners is to integrate site specific data obtained from HCT's into predictive geochemical models (Sunkavalli, 2014).

In this study the humidity leach cells where only run for a duration of 5 weeks. This was done in order to determine only to assess the leachability of secondary minerals in the material. It was assumed from the start from the study that that the oxidation rates obtained from the HLC's would not be scalable to field conditions as the HLC's do not account for the rate limiting effects of oxygen diffusion.

3.2.3 Additional analysis

Additionally, to the static- and kinetic tests that where performed, sulphur speciation was performed in order to assess the extent of conversion of pyrite. X-ray diffraction (XRD) and X-ray fluorescence (XRF) was also performed on the tailings material.

Table 2 Summation of laboratory test work

Laboratory test	Comment	Sample Information
Acid base accounting	Total S at 2200°C. AP (acid potential) determined from sulphide-S content (SAP) and total-S content (TAP)	BH RF 4 (samples were taken every 30 cm for the total depth of the borehole)
Sulphur speciation	Sulphide-S vs Sulphate-S vs del-S	BH RF 1, RF 2, RF 3 and RF 4 (30 cm sample increments for the whole depth of the borehole)
NAG Test	Net Acid Generation	BH RF 2 (samples were taken every 30 cm for the total depth of the borehole)
X-ray fluorescence (XRF) and X-ray diffraction (XRD)	XRF (major and trace) and XRD were performed in order to obtain a vertical profile of major and trace elements and mineral phases present	BH RF 2 (samples were taken every 30 cm for the total depth of the borehole)
Humidity leach test (5 weeks)	Columns were set up of composite samples of the oxidized zone, transition zone and unoxidized zone. ICP-MS was used to analyse the weekly leachate.	Five columns were set up; 1) RF 1 Ox (a composite sample of the oxidized zone of BH RF 1) 2) RF 1 TRANS (a composite sample of the transition zone of BH RF 1) 3) RF 1 UNOX (a composite sample of the unoxidized zone of BH RF 1) 4) RF 3 OX (a composite sample of the oxidized zone of BH RF 3) 5) RF 3 UNOX (a composite sample of the unoxidized zone of BH RF 3)
Static leach tests	1:20 leach	BH RF 2 (samples were taken every 30 cm for the total depth of the borehole)

CHAPTER 4: NUMERICAL MODELS

4.1 CONCEPTUAL MODEL

4.1.1 Pyrite conversion

If it is assumed that the total sulphur represents the initial pyrite content in the tailings material, and the conversion of pyrite can be calculated from the sulphur speciation data presented in Section 5.1.2.1. The conversion represents the extent to which pyrite has been oxidized with depth.

$$\text{conversion} = \frac{\text{Total Sulphur} - \text{Sulphide Sulphur}}{\text{Total Sulphur}}$$

4.1.2 Influence of volumetric moisture percentage

It can be seen in from the figures below that the pyrite conversion shows an almost an inverse profile of the moisture profile with depth. This trend was observed in all four the boreholes. The conversion of pyrite with depths profiles shows that in horizons that have a high volumetric moisture percentage oxidation rates of pyrite are significantly lower compared to sample points in the depth profile that were drier.

The profiles would suggest that points in the depth profiles of the four boreholes that show a higher degree of saturation will have a lower oxidation rate and it may be fair to assume that the degree of saturation of the material will be a rate determining step in the oxidation of pyrite in the tailings material.

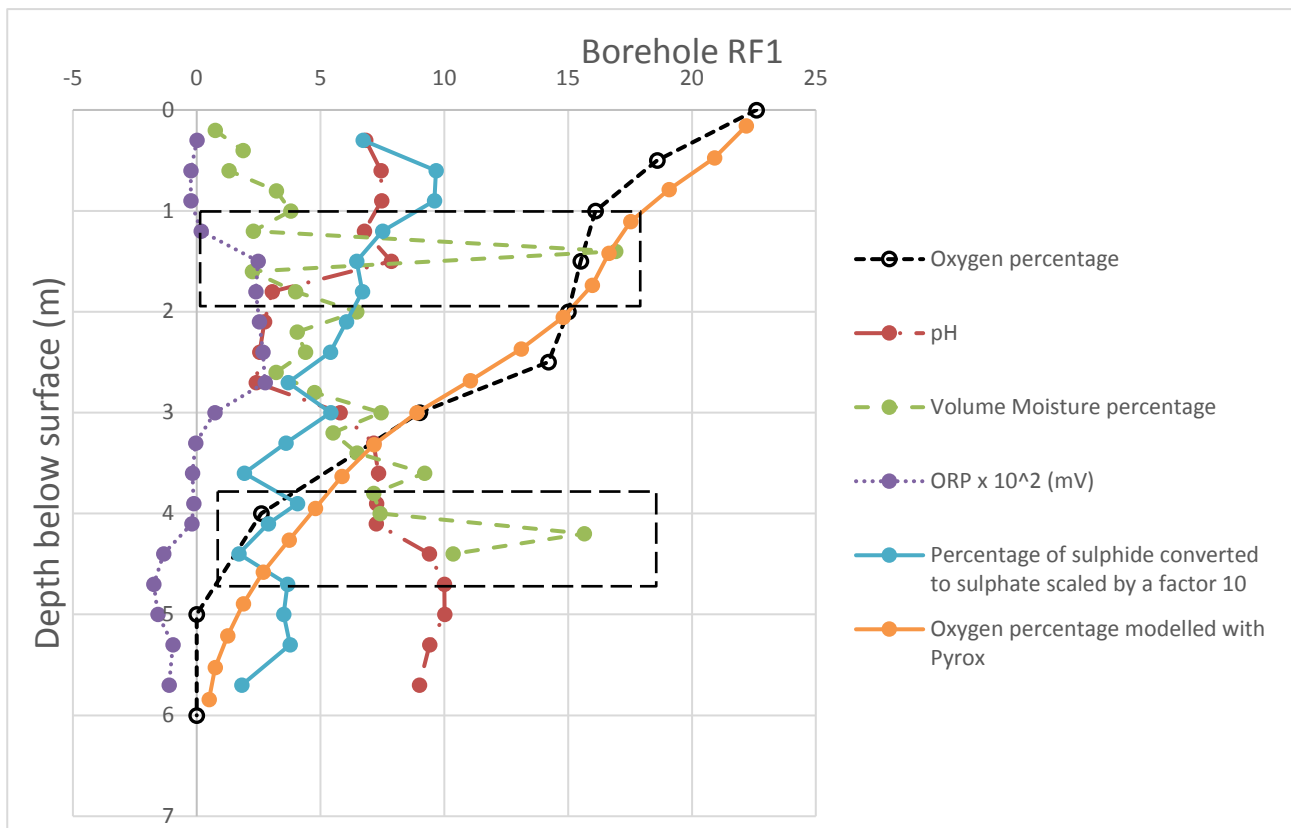


Figure 5: Chemical and physical parameter profiles of Borehole RF1

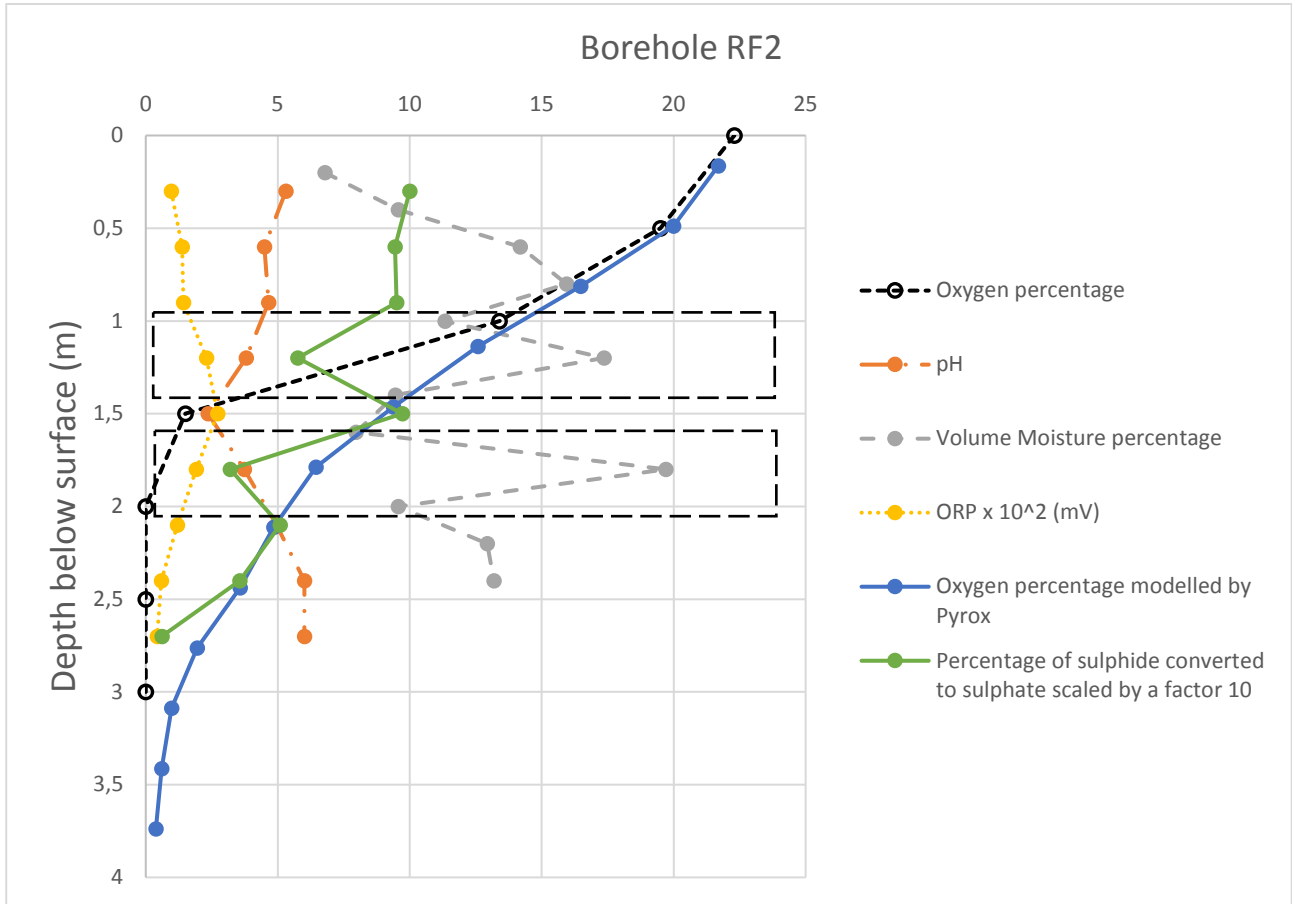


Figure 6: Chemical and physical parameter profiles of Borehole RF2

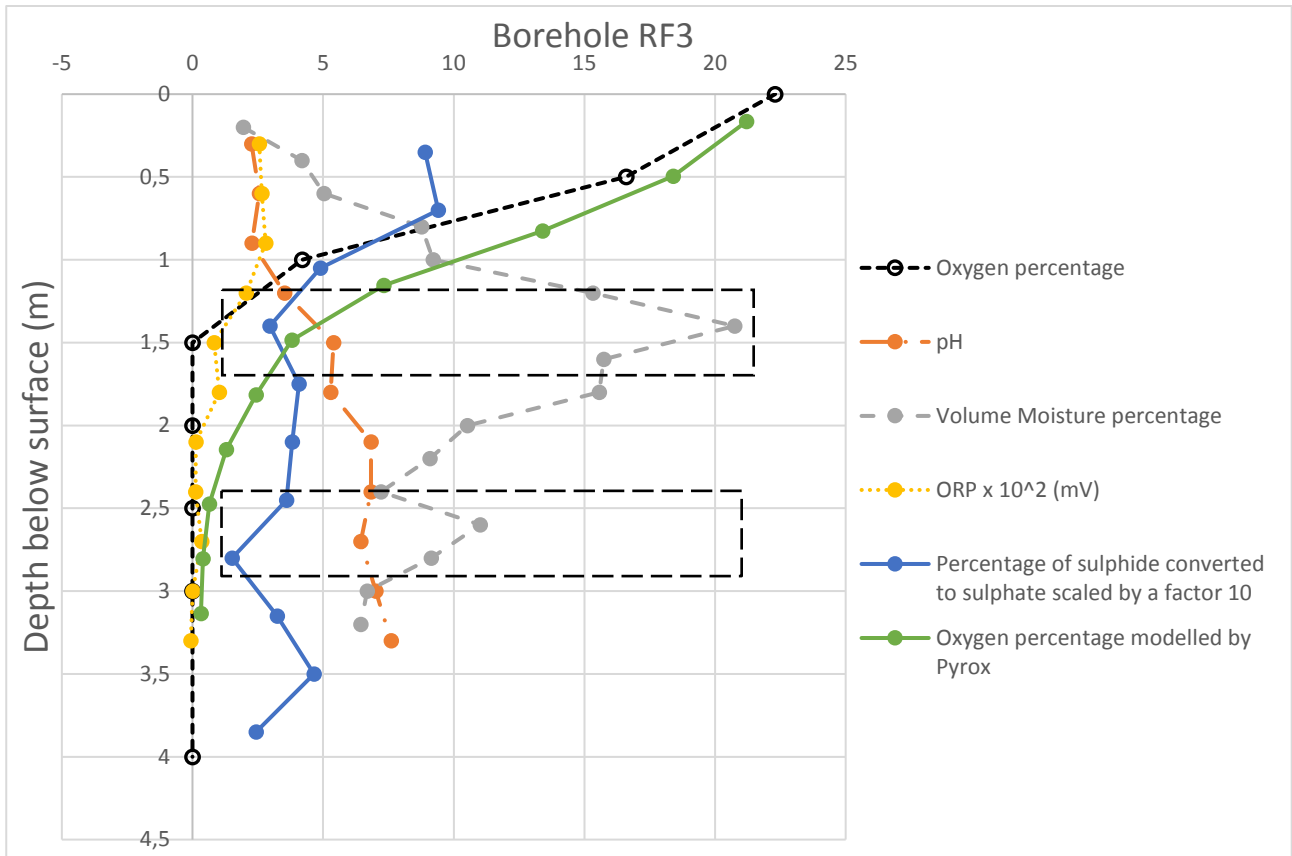


Figure 7: Chemical and physical parameter profiles of Borehole RF3

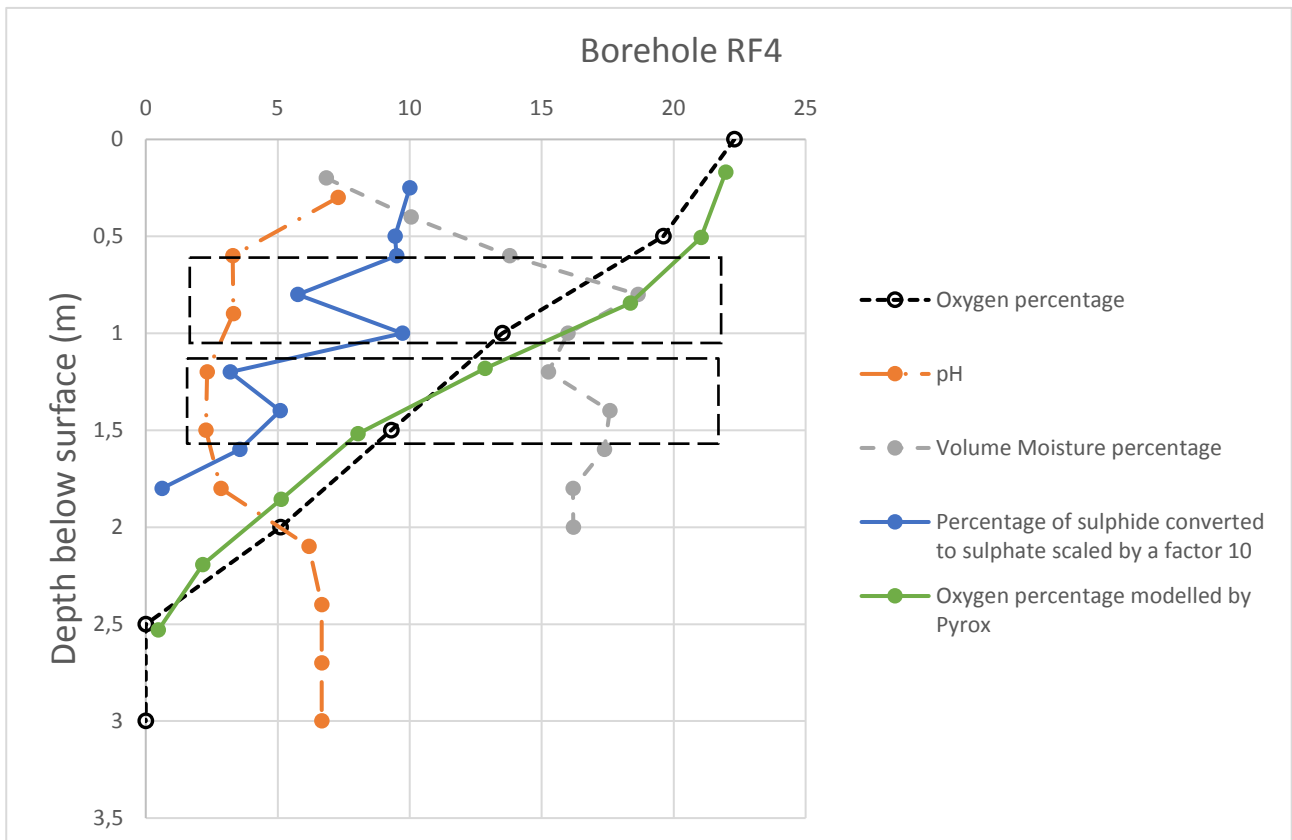


Figure 8: Chemical and physical parameter profiles of Borehole RF6

4.1.3 Unsaturated flow model

4.1.3.1 Geostudio

The modelling software Geostudio SEEP/W was used to model the unsaturated flow in the tailings material with time. The Gas Consumption and Exothermic Reaction add-in in SEEP/W was used to also account for the oxygen sink due to pyrite oxidation.

The depth of the phreatic head in the tailings storage facility was unknown. Therefore, it was assumed the migration of the phreatic head is very slow and to be static for the time period of the model. The results obtained from this model only served to calculate the possible variance in the soil moisture over time as a function of seasonality. The output of the SEEP/W model was used as input for the geochemical model.

4.1.3.2 Model setup

A 1D unsaturated flow model was constructed in Geostudio's SEEP/W package (Geoslope International Ltd., 2019). The following boundary conditions were assigned to the model:

- 1) No-flow boundary condition in the bottom boundary of the model;
- 2) Land-Climate interaction boundary (LCI)

4.1.3.3 Model calibration

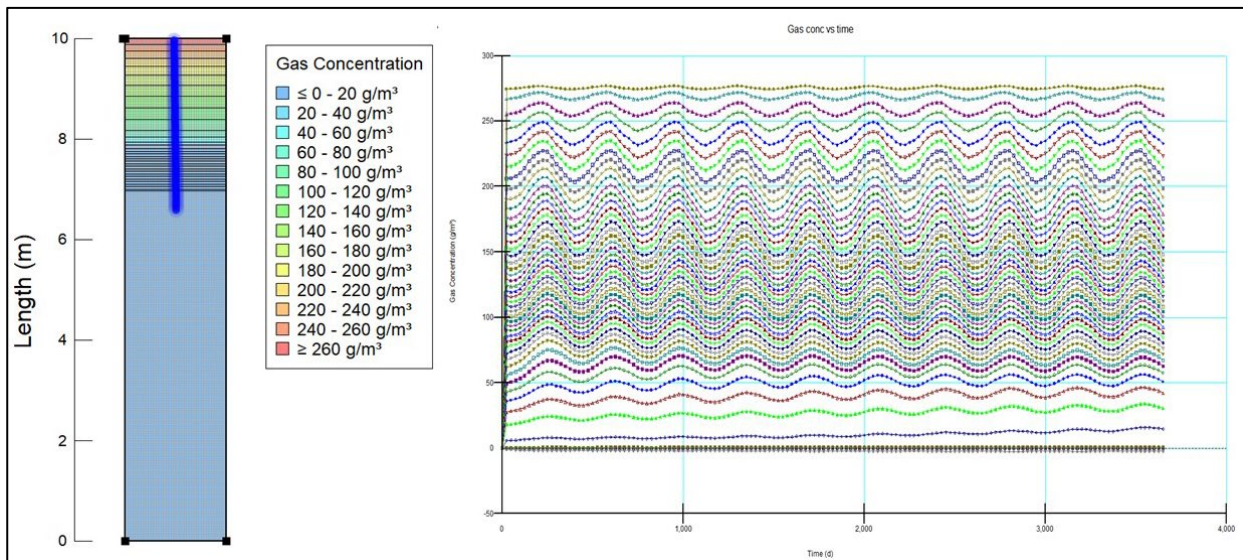


Figure 9: Results obtained from SEEP/W showing gas concentration variation as a function of time. The model accounted for wet and dry periods.

4.1.4 Oxygen transport modelling

4.1.4.1 PYROX

PYROX was used to model the oxygen transport in the tailings material. The model was developed by the Institute for Groundwater Research, University of Waterloo (Wunderley & Blowes, 1997). The model numerically solves Fick's law of mass transport that contains an oxygen sink that represents the oxygen consumed by pyrite oxidation.

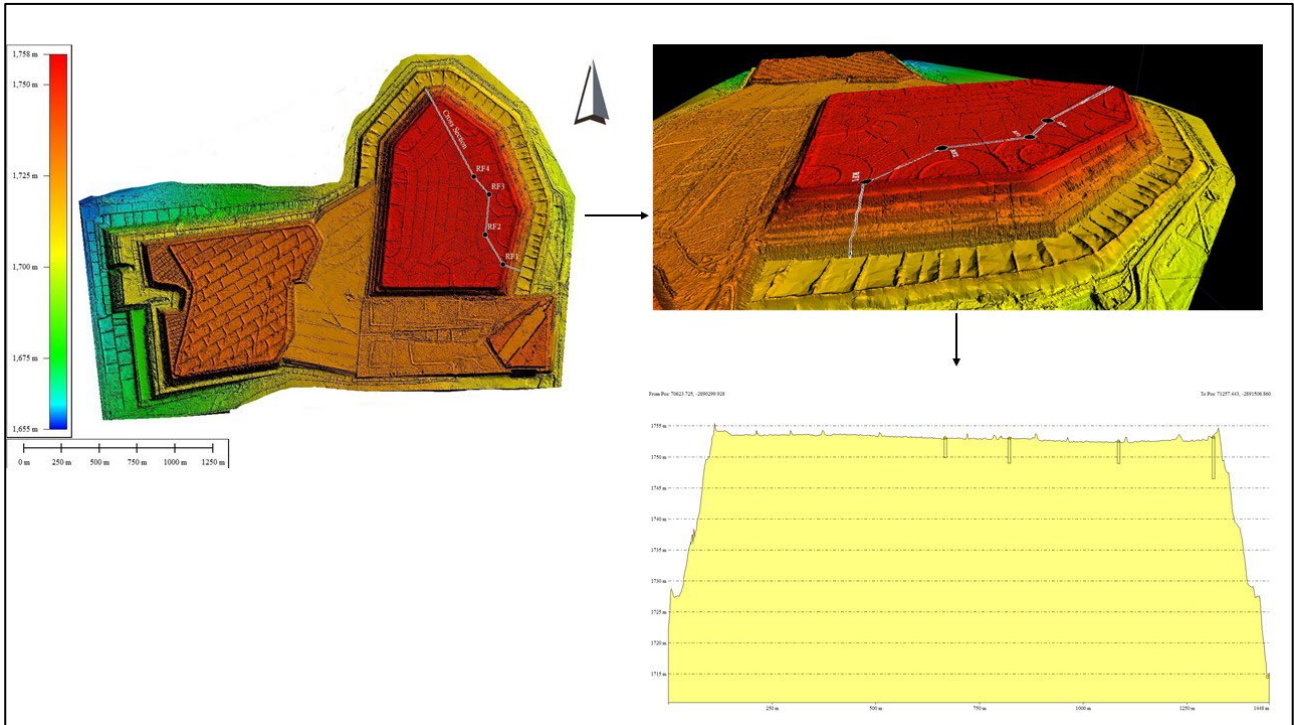


Figure 10: DEM of the tailings heap indicating where the boreholes was drilled and where the cross section was selected for the numerical model.

4.2 MODEL SETUP

The PYROX model requires for each node the data listed in Table 3. Each sample point with depth in the boreholes was modelled as a node in the programme. The software assumes that the material is an infinite slab and only considers diffusion for the means of transport of oxygen into the tailings heap as depicted in the schematic drawing in Figure 11. The diagram shows conceptually how the PYROX software calculate sulphate loads. The software calculates the sulphate load in kilogram per year for a defined depth L and a surface area of 1 m^2 . Furthermore, the programme assumes a steady state moisture profile for the whole simulation time.

The following details pertain to the parameters briefly explained in Table 3:

- 1) L – the depth of the profile that is being modelled. This value is equal to the depth of the borehole that is being modelled. The depth is divided into n number of nodes corresponding to the depth intervals sampled during the fieldwork campaign;
- 2) ρ – the bulk density of the tailings material was obtained from the study by Yibas et al. (2010). This study included the study site as part of a larger geochemical survey of tailings material of several tailings heaps in the Witwatersrand;

- 3) D_1 – this parameter represents the bulk diffusion coefficient. This parameter is estimated by fitting the model to the oxygen concentration measurements made during the fieldwork campaign;
- 4) D_2 – Is calculated by the PYROX code and is a function of the volumetric moisture content of the material;
- 5) a – is the particle size defined at each node and this values where obtained by determining the particle size distribution of the material at each depth increment for each respective borehole;
- 6) θ – The volumetric moisture content was obtained from the unsaturated flow model;
- 7) Φ – The porosity was obtained from the study by Yibas et al. (2010);
- 8) **pyrite(wt%)** – The pyrite content was obtained from performing a sulphur speciation laboratory analysis (section 5.1.2.1).

Table 3 Input parameters for the model

Parameter	Unit	Description
L	m	Depth of borehole
ρ	kg/m ³	Bulk density of the tailings material
D_1	m ² /s	Diffusion Coefficient of oxygen in pore space of dump calculated by PYROX
D_2	m ² /s	Diffusion Coefficient of oxygen in water – fitting parameter
a	D50	Radius of particle obtained from the D50 values for each sampled depth
θ		Volumetric moisture content
Φ		Porosity
pyrite(wt%)		This value is usually obtained from the ABA analysis, in the study the percentage unreacted pyrite was obtained from performing a laboratory sulphur speciation analysis.

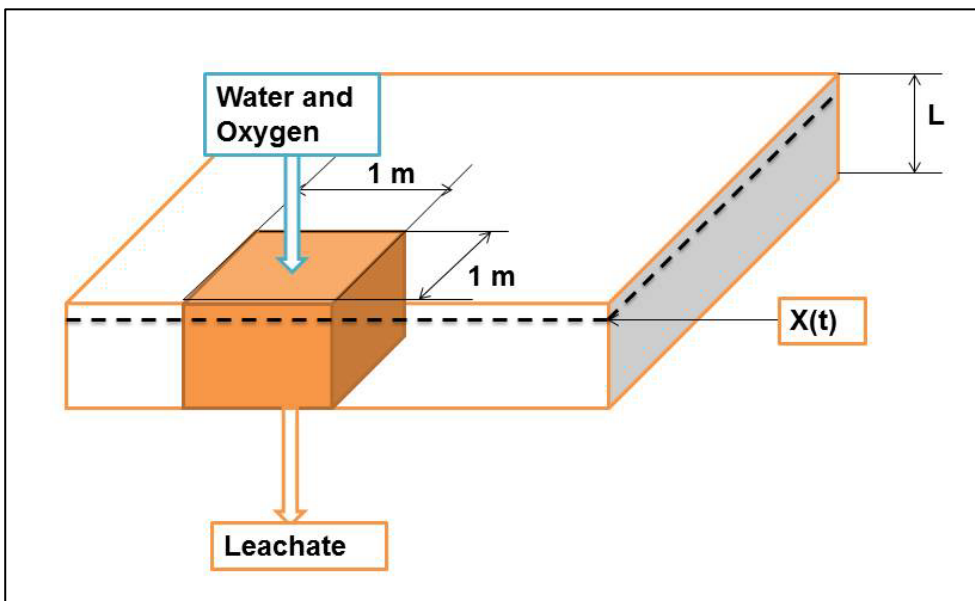


Figure 11: Schematic of the PYROX model

CHAPTER 5: RESULTS AND DISCUSSION

5.1 FIELD MEASUREMENTS

It can be seen from the figures below that the pH and ORP profiles are almost mirror images of each other. Furthermore, the inflexion point of these two profiles closely coincides where a colour change in the tailings material was observed (yellow to grey). It can also be seen from the oxygen profiles that this point is at a position between the transition zone and the unoxidised zone.

Borehole RF1 is located close to the side of the tailings dump and therefore explains the depth difference of the unoxidized zone compared to the other three boreholes that showed a reaction front depth of around 1.5 metres. Oxygen can diffuse into the dump from the sides of dump explaining the difference.

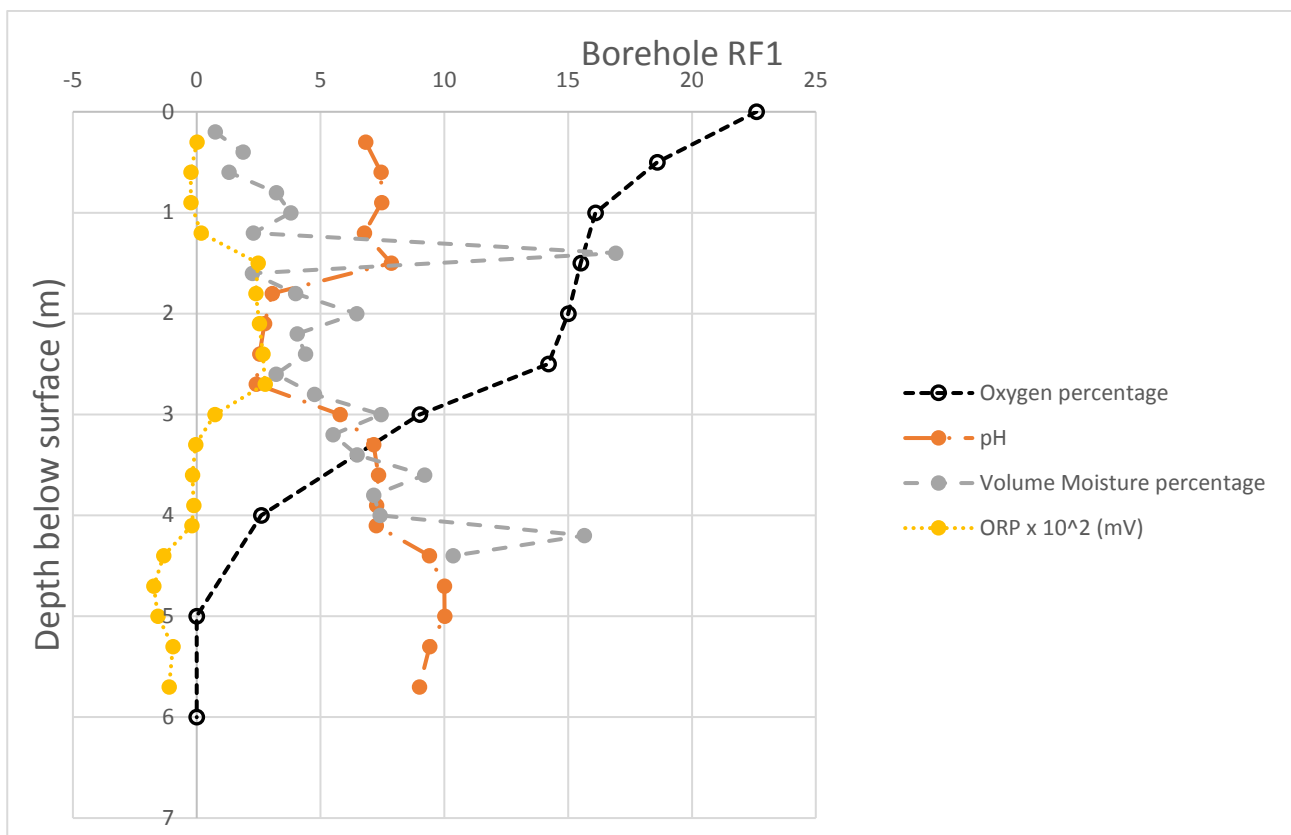


Figure 12: Data obtained from RF1

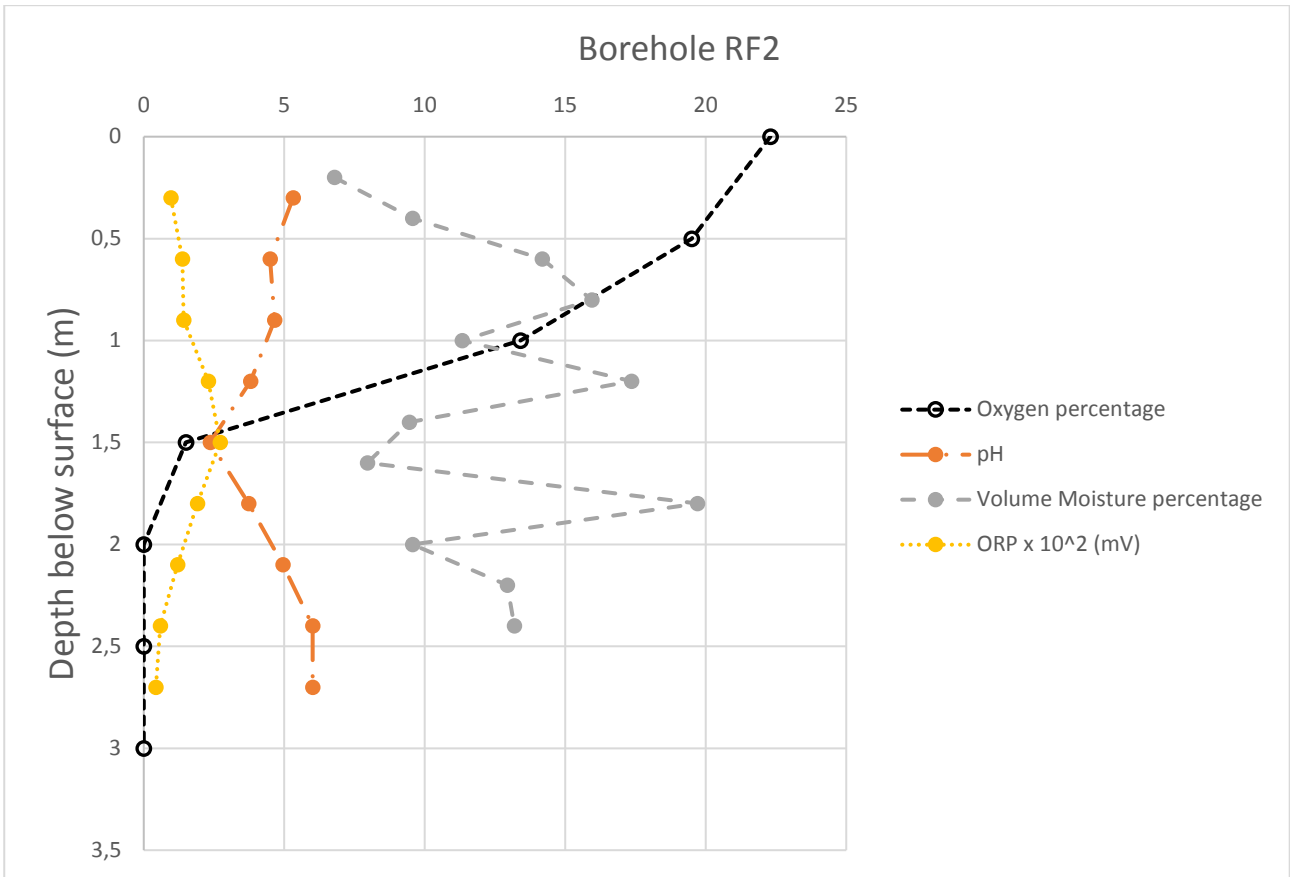


Figure 13: Data obtained from RF2

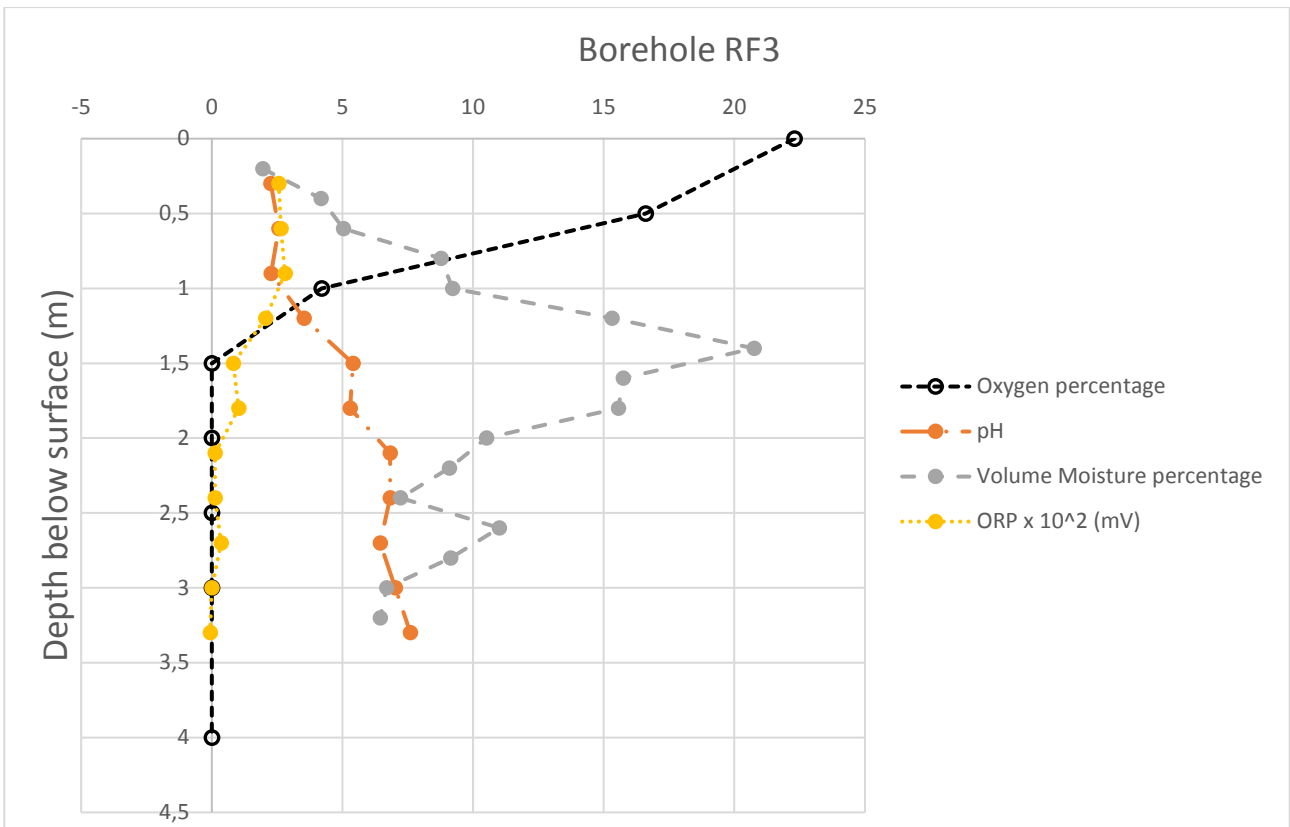


Figure 14: Data obtained from RF3

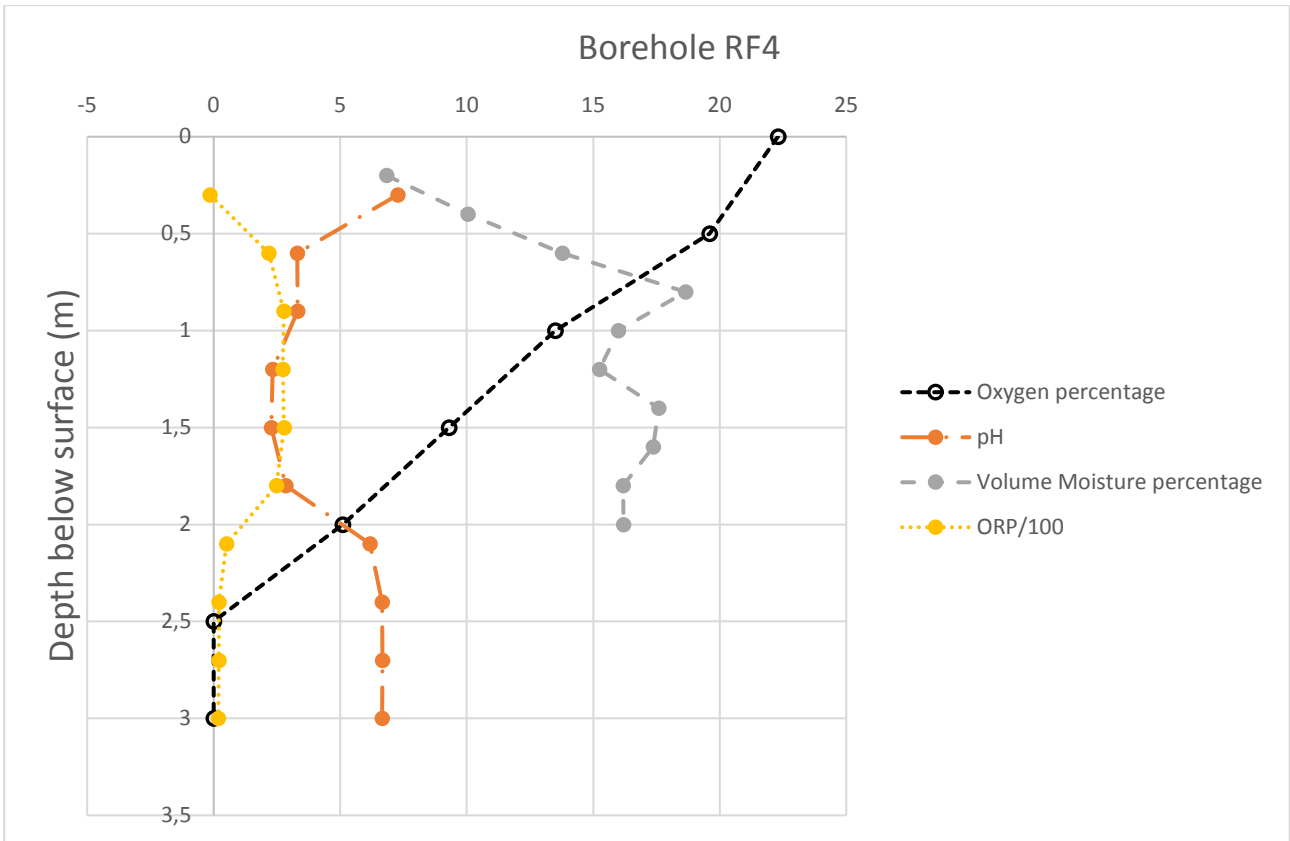


Figure 15: Data obtained from RF4

5.1.1 Particle size distribution

The data presented below is only that measured using the hydrometer method. The data shows a typical narrow range of fine sand and silt fractions that would have been the aim of milling and metallurgical processing. The fine fractions as presented below will include the main chemically reactive fractions of the tailings material whilst the coarse fractions will dominate/regulate the oxidative flux of the tailings.

Table 4: D50 values with depth for BH RF 1

Sample no.	Depth (cm)	D50 (mm)
RF 1.1	30	0.027695667
RF 1.2	60	-
RF 1.3	90	0.009810667
RF 1.4	120	0.010158923
RF 1.5	150	
RF 1.6	180	0.038616
RF 1.7	210	-
RF 1.8	240	-
RF 1.9	270	0.0179075
RF 1.10	300	0.012592375
RF 1.11	330	0.03100675
RF 1.12	360	0.0144449
RF 1.13	390	0.0123203
RF 1.14	410	0.015582
RF 1.15	440	0.03408275
RF 1.16	470	0.015582
RF 1.17	500	0.0119015
RF 1.18	530	0.056643625
RF 1.19	570	0.058759125

Table 5: D50 values with depth for BH RF 2

Sample no.	Depth (cm)	D50 (mm)
RF 2.1	30	-
RF 2.2	60	0.055791
RF 2.3	90	0.021974
RF 2.4	120	0.0092918
RF 2.5	150	-
RF 2.6	180	-
RF 2.7	210	-
RF 2.8	240	0.0126246
RF 2.9	270	-

Table 6: D50 values with depth for BH RF 3

Sample no.	Depth (cm)	D50 (mm)
RF 3.1	30	
RF 3.2	60	0.0316039
RF 3.3	90	0.0248991
RF 3.4	120	0.0248991
RF 3.5	150	0.0532312
RF 3.6	180	0.0429944
RF 3.7	210	0.047886
RF 3.8	240	
RF 3.9	270	0.0614522
RF 3.10	300	0.0428809
RF 3.11	330	0.036158

Table 7: D50 values with depth for BH RF 4

Sample no.	Depth (cm)	D50 (mm)
RF 4.1	30	0.0078508
RF 4.2	60	0.012829
RF 4.3	90	0.012829
RF 4.4	120	0.0127415
RF 4.5	150	0.0125257
RF 4.6	180	0.0132964
RF 4.7	210	0.012818
RF 4.8	240	0.0218985
RF 4.9	270	0.0588146
RF 4.10	300	0.0476106

5.1.2 Laboratory analysis

5.1.2.1 Sulphide content

The figures below show the total weight percentage of total sulphur, weight percentage of sulphide and the weight percentage of sulphate. For this data, the percentage conversion of pyrite (extent of pyrite oxidation with depth was calculated). This was shown in section 4.1. The variation in conversion correlated well with change in particle size and also moisture content, with wetter horizons in the tailings showing less conversion opposed to dryer horizons showing a greater conversion of pyrite.

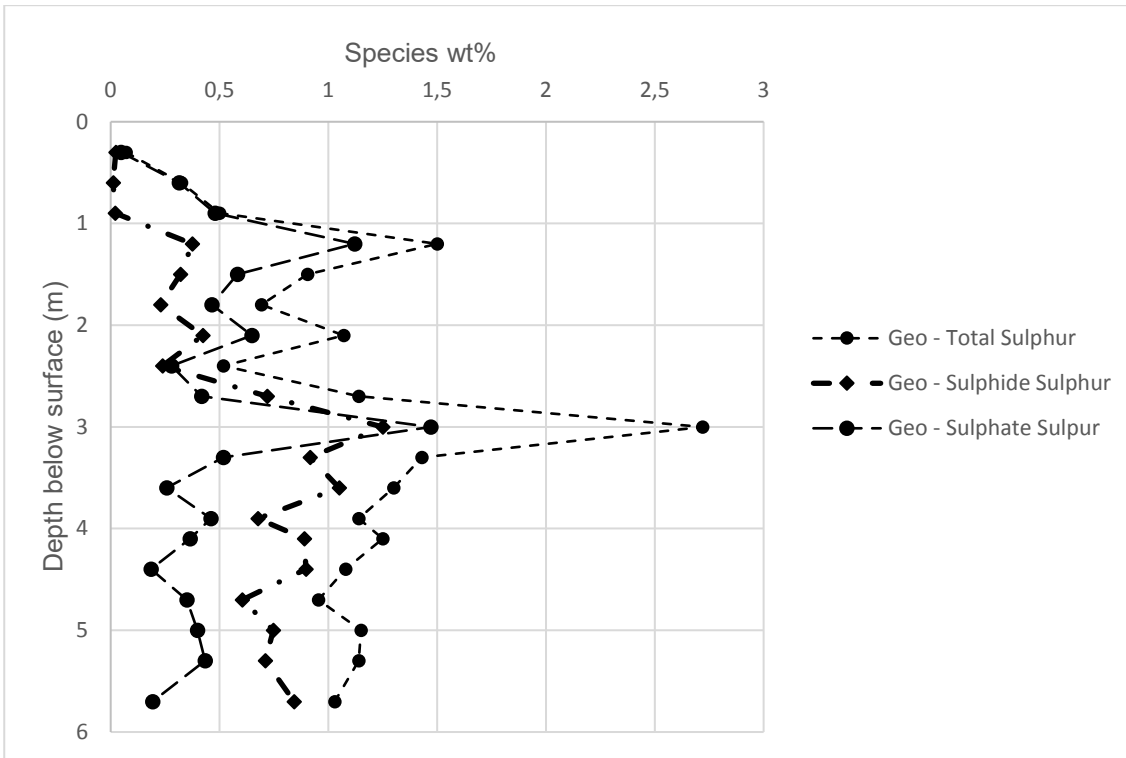


Figure 16: Sulphur speciation results for BH RF 1

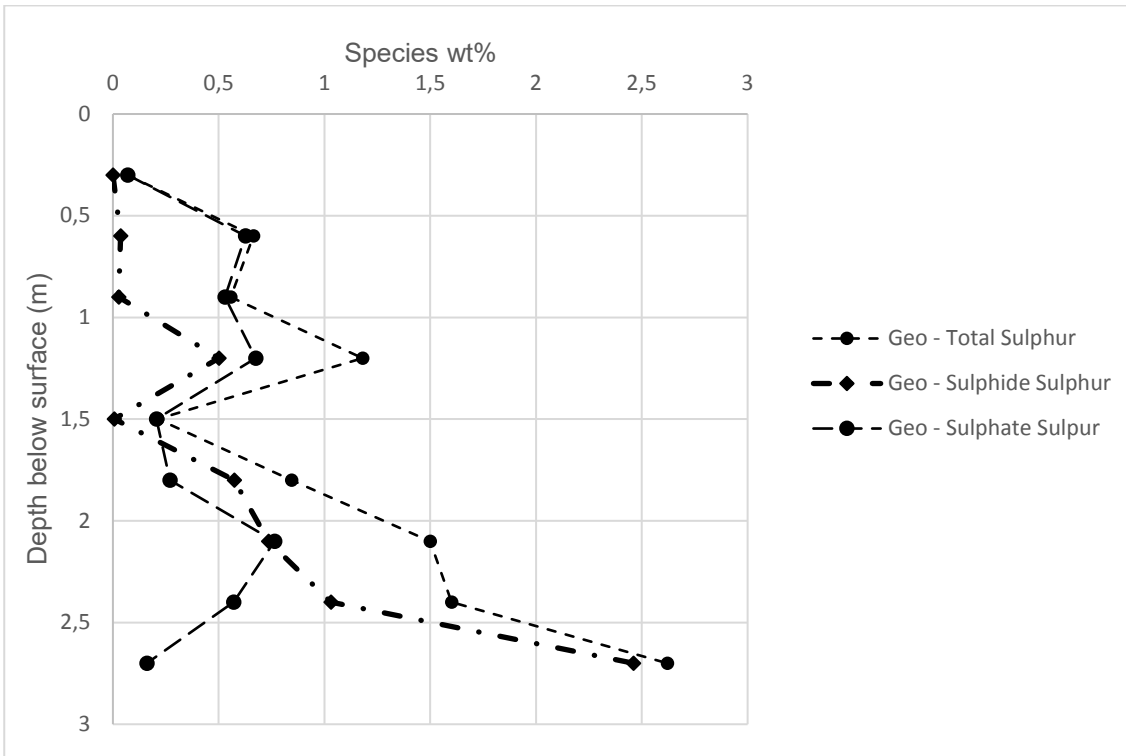


Figure 17: Sulphur speciation results for BH RF 2

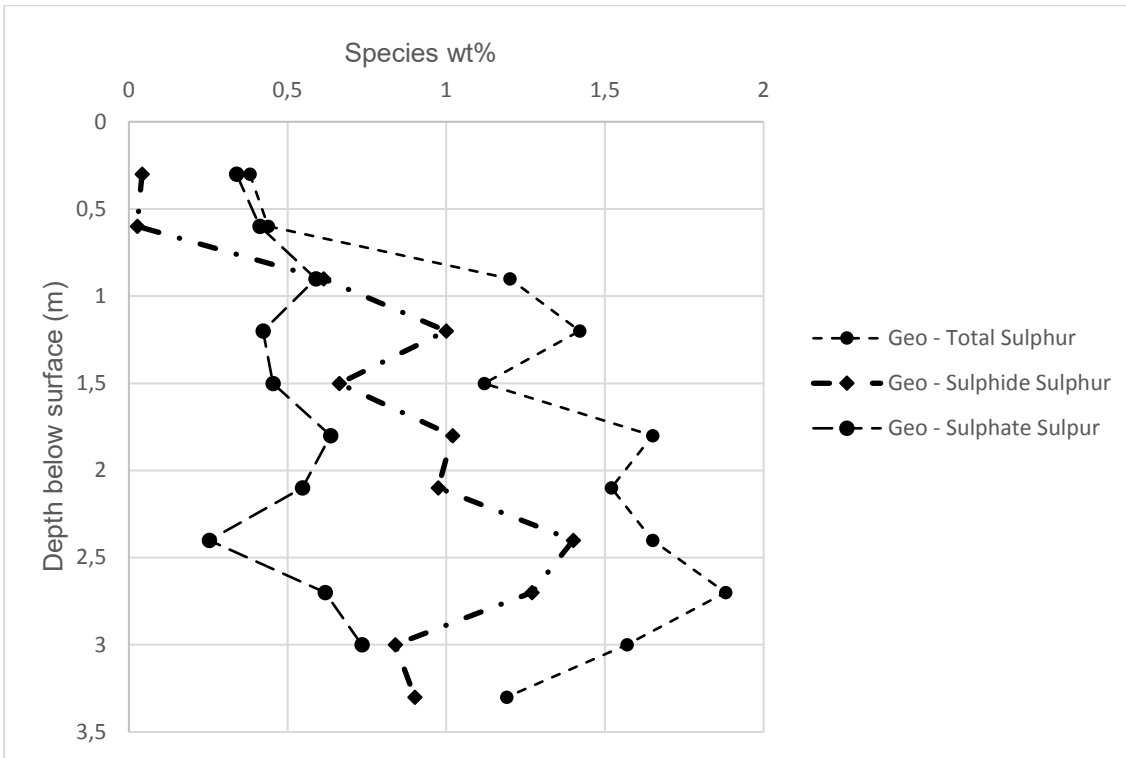


Figure 18: Sulphur speciation results for BH RF 3

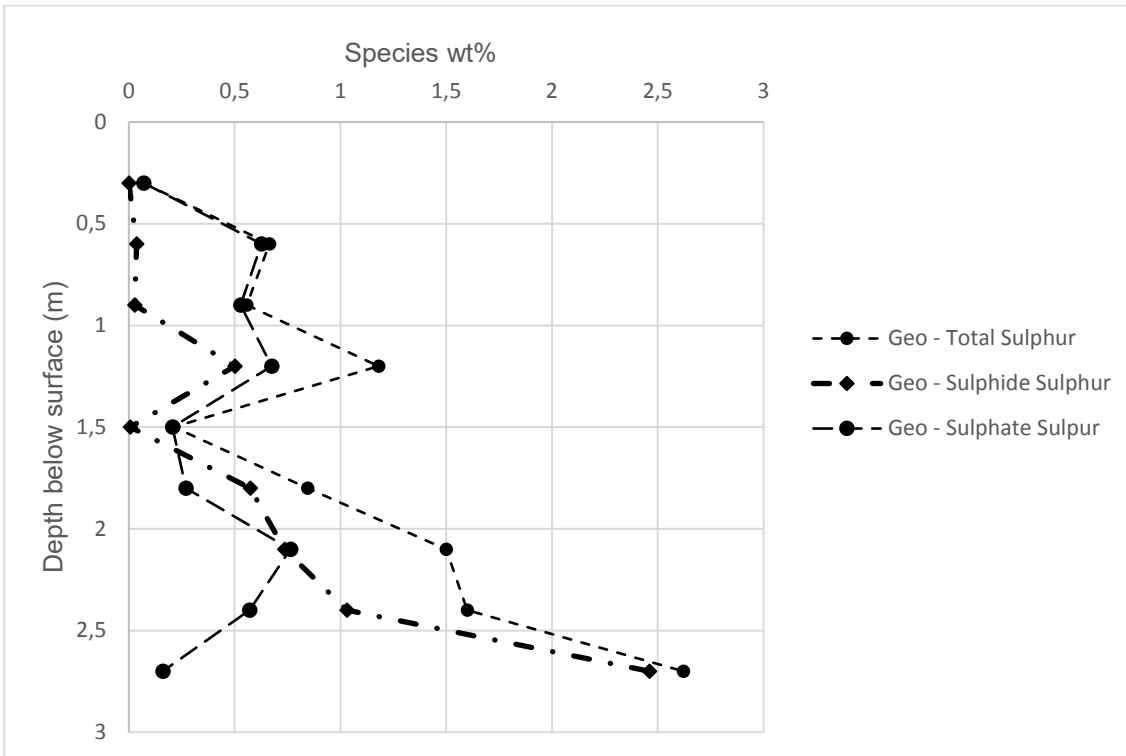


Figure 19: Sulphur speciation results for BH RF 4

5.1.2.2 Acid Base Accounting

Table 8: Acid Base Accounting for Borehole RF 4

Sample Number	Paste pH	Total Sulphur (%) (LECO)	Acid Potential (AP) (kg/t)	Neutralization Potential (NP)	Net Neutralization Potential (NNP)	Neutralizing Potential Ratio (NPR) (NP: AP)	NAG pH	Rock Type
RF 4.1	7.44	0.3	9.22	31.3	22.08	3.40	4.46	II
RF 4.2	7.76	0.17	5.45	23	17.55	4.22	5.01	III
RF 4.3	7.06	0.64	20.06	27.55	7.49	1.37	3.02	II
RF 4.4	4.22	0.64	20.05	32.4	12.35	1.62	2.37	II
RF 4.5	3.29	1.03	32.11	39.45	7.34	1.23	2.06	II
RF 4.6	2.65	1.08	33.63	60	26.38	1.78	2.29	II
RF 4.7	2.55	1.28	40.09	56.7	16.61	1.41	2.4	II
RF 4.8	7.53	0.9	28.21	22.5	-5.71	0.80	2.36	I
RF 4.9	7.59	0.82	25.76	28.15	2.39	1.09	2.5	II
RF 4.10	7.65	1.01	31.57	25.45	-6.12	0.81	2.42	I
RF 4.11	7.02	1.37	42.67	30.8	-11.87	0.72	2.28	I

5.1.2.3 X-ray diffraction results

Rietveld refinement was used to identify individual mineral phases from tailings samples as a bulk mineralogical investigation. The main phase, quartz, as presented in Table 10, occurs in all samples and ranges between 73.2 and 90.7%. Pyrite was only identified in samples RF2.13 and RF3 UNOX; however, mineral phases resulting from pyrite oxidation have been detected in all samples, but this does not mean that pyrite is not present in the samples, but that detection wasn't possible as the peak intensity of quartz and Fe containing minerals like biotite tends to overshadow pyrite. Both jarosite and gypsum as pyrite oxidation products were detected in all samples except ones where pyrite was directly identified suggesting that these samples have been oxidised to a well-developed stage. Mineral phases of pyrophyllite, illite and kaolinite represent mineral phases of mica transformation to clay minerals either as hydrothermal relic minerals in the original ore body or as secondary minerals that developed through the breakdown phyllosilicates under low pH conditions. The presence of calcite needs to be related to sample pH original ore mineralogy and site-specific interventions as a relative decrease is observed with depth, that may suggest amelioration or process alteration if for example uranium was extracted which would have needed high pH metallurgical processes.

Table 9: XRD results

Sample Name	Mineral wt%										
	Quartz	Pyrite	Pyrophyllite	Jarosite	Ilminite	Illite	Calcite	Kaolinite	Biotite	Gypsum	Phengite
RF 2.1	83.5%	-	4.8%	-	0.6%	3.8%	6.3%		1.5%	0.2%	-
RF 2.2	83.0%	-	4.3%	-	-	4.2%	5.9%	1.4%	1.1%	0.1%	-
RF 2.3	87.7%	-	2.5%	-	-	2.5%	5.9%	0.8%	0.6%	0.1%	-
RF 2.4	82.9%	-	0.3%	0.9%	-	3.6%	7.7%	0.9%	1.1%	-	-
RF 2.5	88.0%	-	2.5%	1.0%	-	2.7%	4.9%	0.5%	0.5%	-	-
RF 2.6	73.2%	-	15.9%	0.6%	-	0.4%	8.4%	0.4%	1.0%	-	-
RF 2.7	83.0%	-	11.5%	0.6%	-	1.2%	2.8%	0.7%	0.2%	-	-
RF 2.8	90.7%	-	4.7%	0.4%	-	1.9%	1.9%	-	0.4%	-	-
RF 2.9	83.8%	-	11.0%	0.3%	-	1.2%	2.8%	0.4%	0.5%	-	-
RF 2.10	86.4%	-	8.9%	0.4%	-	1.1%	2.6%	0.3%	0.1%	-	-
RF 2.11	83.8%	-	10.5%	0.2%	-	1.4%	3.5%	0.3%	0.3%	-	-
RF 2.12	84.8%	-	9.8%	0.5%	-	1.5%	2.3%	0.6%	0.6%	-	-
RF 2.13	78.4%	0.7%	18.4%	1.1%	-	-	0.2%	1.0%	-	-	0.2%
RF 3 UNOX	82.4%	1.8%	13.1%	0.7%	-	0.6%	0.7%	0.7%	-	-	-
RF 1 UNOX	82.0%	-	12.4%	0.7%	-	0.3%	3.9%	0.2%	0.4%	-	-
RF 1 OX	83.8%	-	10.1%	0.6%	-	0.6%	4.2%	0.3%	0.4%	-	-
TF 2 OX	86.8%	-	8.8%	0.4%	-	0.7%	2.8%	0.3%	0.2%	-	-
RF 1 TRANS	87.5%	-	8.5%	0.4%	-	1.1%	2.3%	-	0.2%	-	-

Table 10: XRF results

Sample name		RF 3 UNOX	RF1 UNOX	RF 1 OX	RF 3 OX	RF 1 TRANS	RF 2.1	RF 2.2	RF 2.3	RF 2.4	RF 2.5	RF 2.6	RF 2.7	RF 2.8	RF 2.9	RF 2.10	RF 2.11	RF 2.12	RF 2.13
Sum of Concentration	(%)	96.15	95.141	97.159	96.21	94.482	99.307	99.621	94.616	98.711	95.042	97.218	95.997	94.465	99.65	99.461	94.705	98.688	95.974
PbO	(%)	0.007	0.005	0.007	0.006	0.01	0.006	0.005	0.007	0.01	0.008	0.007	0.006	0.009	0.006	0.007	0.003	0.012	0.007
HfO2	(%)	nd	nd	Nd	nd	nd	nd	nd	nd	nd	nd	nd	nd	nd	nd	nd	nd	nd	nd
ZnO	(%)	0.004	0.006	0.007	0.003	0.002	nd	nd	nd	nd	0.006	0.007	0.003	0.002	nd	nd	nd	nd	0.004
CuO	(%)	0.004	0	Nd	nd	nd	nd	nd	nd	nd	0.001	nd	nd	nd	nd	nd	nd	nd	0.004
NiO	(%)	0.009	0.01	0.007	0.003	0.003	0.007	0.003	0.002	nd	0.009	0.008	0.004	0.002	0.007	0.003	0.002	nd	0.008
Fe2O3	(%)	4.609	3.336	2.483	2.294	2.79	2.962	2.787	2.595	3.13	3.319	2.481	2.299	2.783	2.954	2.795	2.579	3.119	4.617
Mn3O4	(%)	0.029	0.038	0.025	0.017	0.018	0.038	0.02	0.023	0.019	0.035	0.028	0.013	0.018	0.039	0.023	0.021	0.019	0.03
Cr2O3	(%)	0.03	0.032	0.032	0.024	0.026	0.027	0.024	0.022	0.03	0.031	0.031	0.025	0.025	0.026	0.025	0.023	0.032	0.03
V2O5	(%)	0.015	0.013	0.013	0.014	0.012	0.018	0.015	0.01	0.016	0.014	0.014	0.014	0.013	0.016	0.015	0.012	0.016	0.016
BaO	(%)	0.002	0.005	0.015	0.006	0.004	0.001	0.006	0.014	0.011	0.006	0.017	0.008	0.015	0.005	0.007	nd	0.011	0.007
TiO2	(%)	0.344	0.298	0.288	0.264	0.277	0.318	0.271	0.247	0.276	0.309	0.29	0.256	0.273	0.307	0.267	0.253	0.276	0.346
CaO	(%)	0.41	0.594	0.639	0.396	0.613	0.063	0.654	1.271	1.548	0.577	0.635	0.403	0.616	0.052	0.642	1.291	1.53	0.413
K2O	(%)	0.198	0.248	0.302	0.245	0.236	0.261	0.215	0.246	0.407	0.244	0.311	0.249	0.237	0.259	0.23	0.232	0.401	0.185
SO3	(%)	1.747	1.235	0.734	0.884	1.042	nd	0.491	1.188	1.706	1.235	0.733	0.886	1.065	nd	0.496	1.194	1.699	1.74
ZrO2	(%)	0.035	0.02	0.019	0.019	0.015	0.019	0.016	0.036	0.021	0.018	0.023	0.02	0.014	0.027	0.024	0.031	0.025	0.035
P2O5	(%)	0.016	0.023	0.025	0.02	0.023	0.03	0.026	0.021	0.026	0.018	0.022	0.018	0.023	0.016	0.023	0.024	0.029	0.017
SrO	(%)	nd	nd	Nd	nd	nd	nd	nd	nd	nd	nd	nd	nd	nd	nd	nd	nd	nd	nd
SiO2	(%)	84.429	83.163	85.914	87.051	84.732	89.533	89.367	83.561	83.778	83.135	85.945	86.838	84.686	89.872	89.189	83.637	83.769	84.285
Al2O3	(%)	4.248	6.11	6.646	4.952	4.654	6.024	5.721	5.373	7.698	6.072	6.659	4.946	4.667	6.062	5.715	5.403	7.73	4.221
MgO	(%)	0.001	0.001	0.001	0.001	0.001	0	0	0	0	0.001	0.001	0.001	0.001	0	0	0	0	0.001
Na2O	(%)	0.013	0.004	0.002	0.011	0.024	nd	nd	nd	0.035	0.004	0.006	0.008	0.016	0.002	nd	nd	0.02	0.008

5.1.3 Model results

5.1.3.1 Moisture profiles

The results obtained from the two numerical steps (SEEP/W and Pyrox) are presented below. The output obtained from SEEP/W was used to calculate a range for the moisture content values with depth in the tailings material. In the figures below show the range- and median moisture content compared to the values measured in the field. The modelled moisture content was lower than the field values for all 4 boreholes. This shift was caused by the upper limitation of the degree of saturation that can be defined in the PYROX model. The PYROX code experience numerical problems when the pore saturation is more than 94%, so the medium can never be fully saturated.

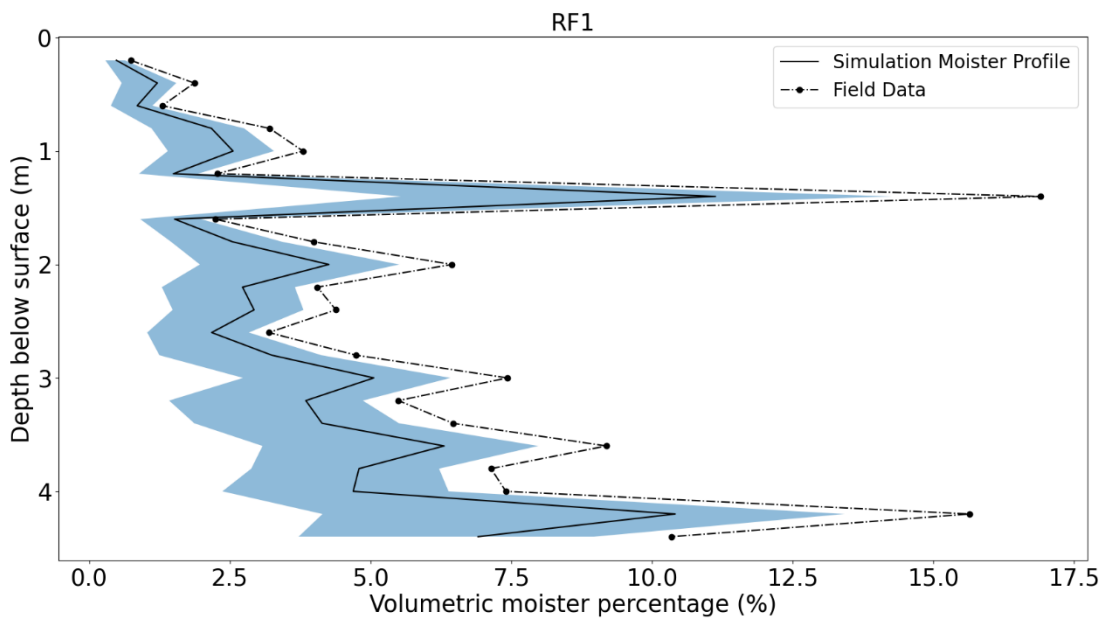


Figure 20: Modelled volumetric moisture percentage curve compared to the measured volumetric moisture curve for BH RF1

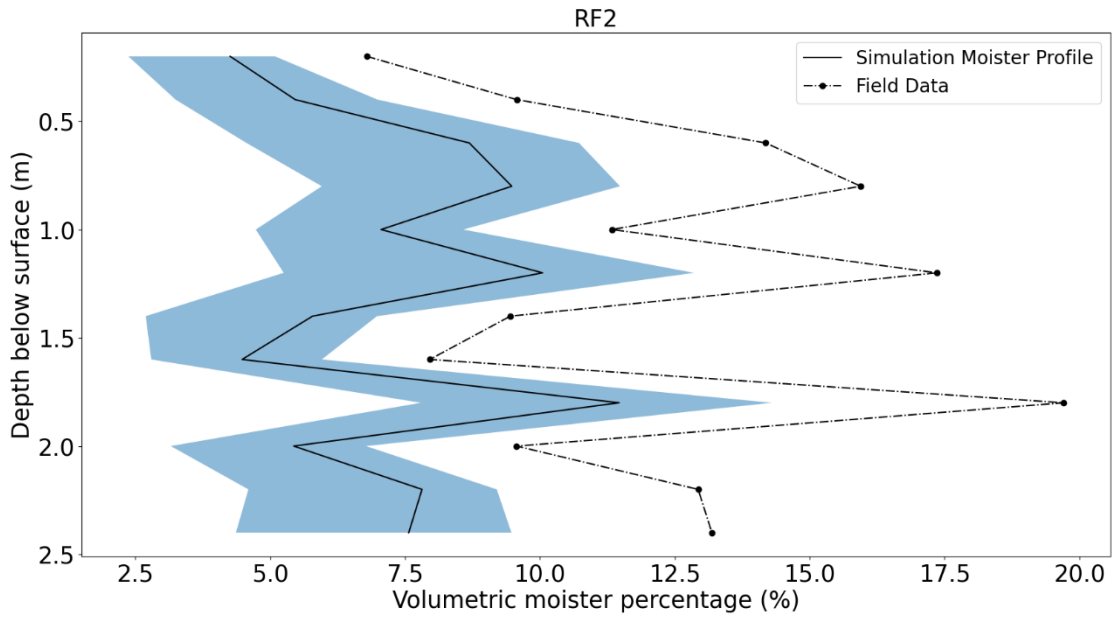


Figure 21: Modelled volumetric moister percentage curve compared to the measured volumetric moister curve for BH RF2

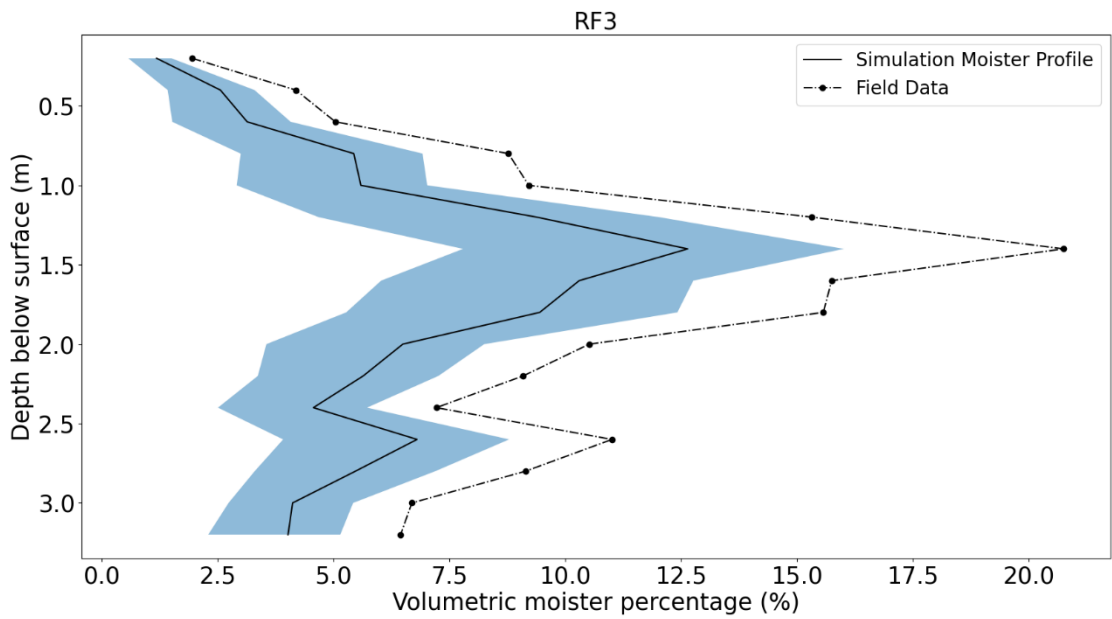


Figure 22: Modelled volumetric moister percentage curve compared to the measured volumetric moister curve for BH RF3

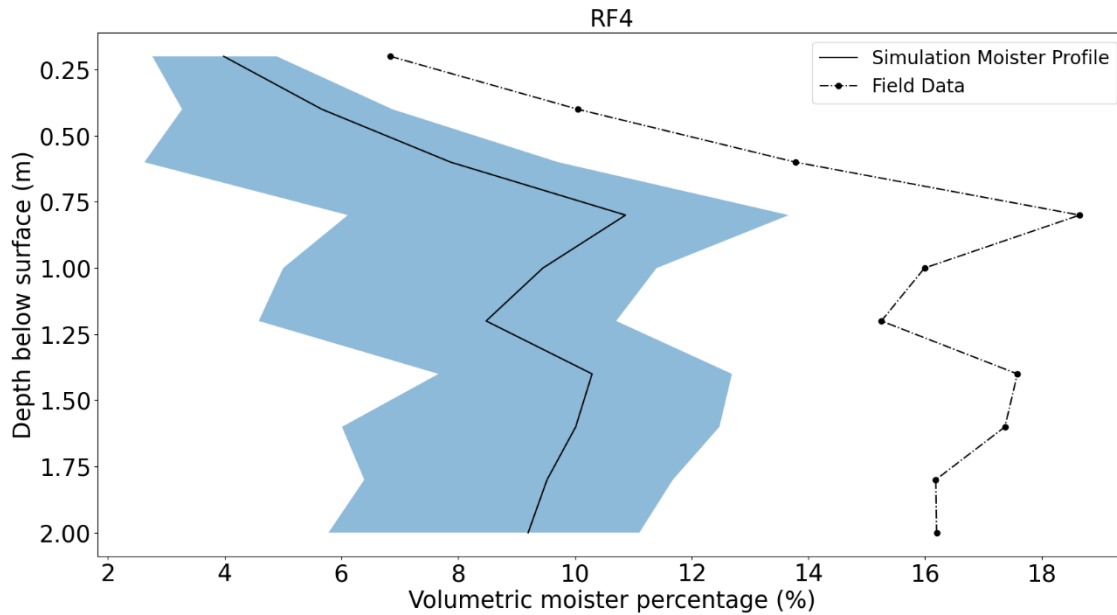


Figure 23: Modelled volumetric moisture percentage curve compared to the measured volumetric moisture curve for BH RF4

5.1.3.2 Oxygen profiles (PYROX)

The figures below show the modelled oxygen concentration compared to the measured concentration profiles for the study site. The predicted oxygen concentrations do not exactly match the measured concentrations; the model does, however, predict the profile well.

The rate of pyrite oxidation in in tailings material can be expressed as discussed in chapter 1 as:

$$(\partial U_A)/\partial t = D_1 x (\partial^2 U_A)/(\partial z^2) - q(z,t) \quad [7]$$

The term on the left, $(\partial U_A)/\partial t$, represent the change in pore oxygen concentration, $q(z,t)$ represents the change in volume due to the oxidation of pyrite. By determining the following main parameters from field – and laboratory measurements;

- 1) **a** – is the particle size defined at each node and this values where obtained by determining the particle size distribution of the material at each depth increment for each respective borehole;
- 2) **θ** – The volumetric moisture content was obtained from the unsaturated flow model;
- 3) **pyrite(wt%)** – The pyrite content was obtained from performing a sulphur speciation laboratory analysis (section 5.1.2.1);

The PYROX model calculate the rate of oxidation of pyrite based on the parameters discussed above. Based on this calculated rates, the software then calculate $q(z,t)$ for each time step and then solves equation 7. The pyrite oxidation rate could be predicted with moderate accuracy as the modelled oxygen concentration profiles match the general trend observed in the field observations. It can be clearly seen from the model results that the pyrite oxidation in the material is primarily a function of the degree of saturation of the material.

There where some uncertainties in the pyrite weight percentage and the porosity with depth. This difference in calculated versus measured oxygen concentrations are attributed to these uncertainties. In order to address this, a Monte Carlo modelling approach was followed where a log-normal distribution for both pyrite and porosity where assumed, the mode and standard deviation was approximated from the laboratory measured

data. The darker shaded areas in the graphs show the most likely scenario. It was also observed from the simulations that the model is more sensitive to porosity variance compared to variance in pyrite at each node.

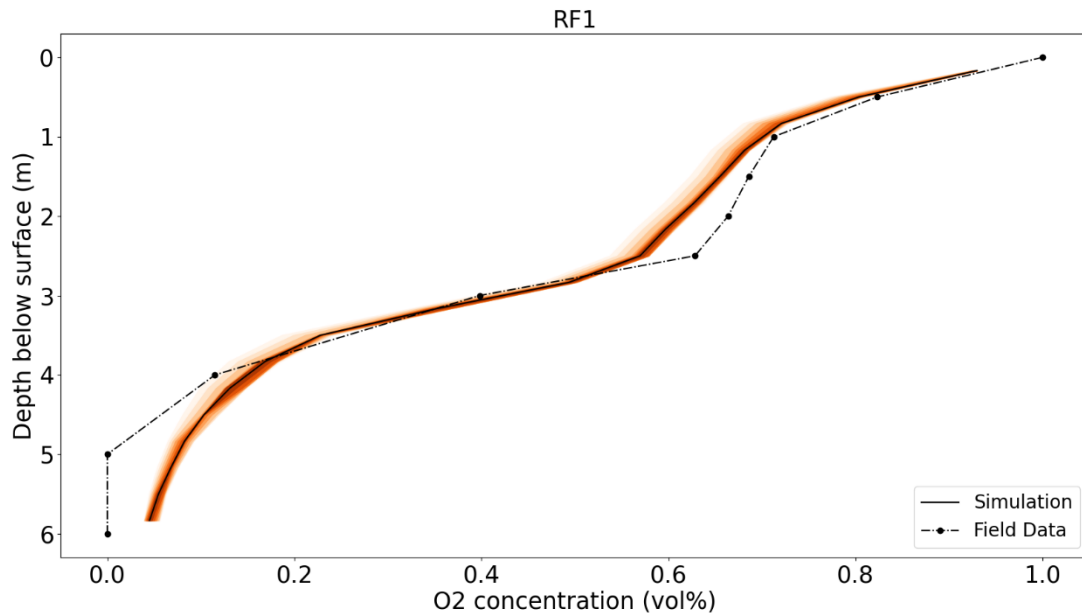


Figure 24: Modelled oxygen concentration curve (PYROX) compared to the measured oxygen concentration curve for BH RF1

In Figure 24 above, it can be seen that the predicted oxygen concentrations deviate from the measured values at depths between 1 and 2.5 metres and again at a depth of 3.5 metres and deeper. Borehole RF1 was located at the edge of the site and the assumption that oxygen only diffuses in from the surface is not completely valid for borehole. This may explain the differences between modelled and measured values. The model results do however show the significance of the influence of porosity and saturation on the rate of oxidation at this site and the change in gradient of the oxygen concentration profile could be predicted by the model.

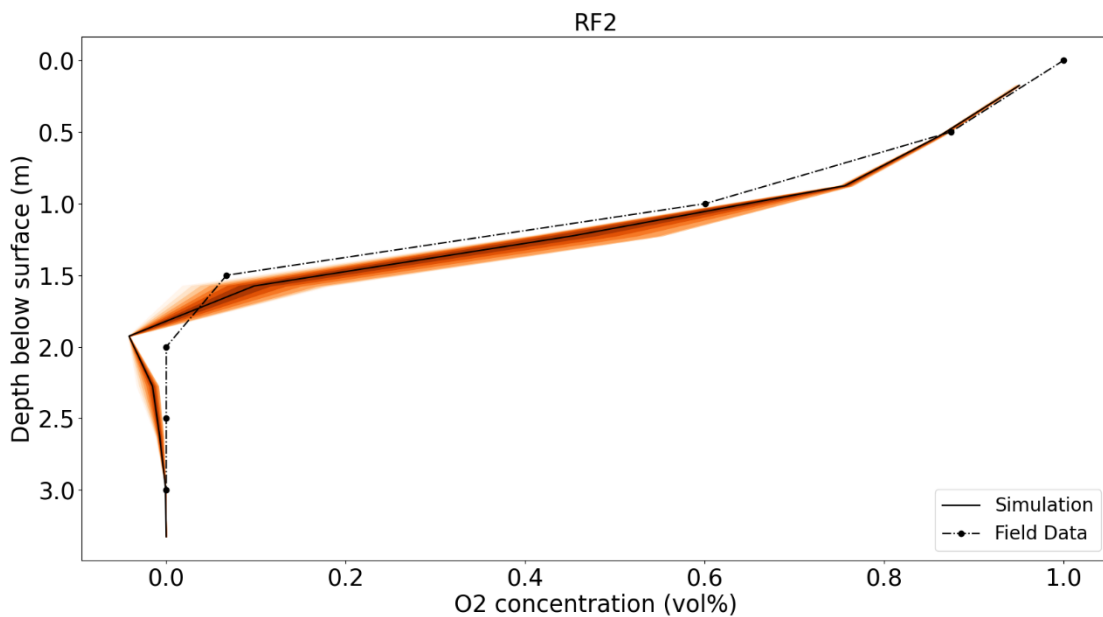


Figure 25: Modelled oxygen concentration curve (PYROX) compared to the measured oxygen concentration curve for BH RF2

CHAPTER 6: CONCLUSION

6.1 FIELD WORK

Due to difficulties in accessing the site, only drilling equipment that could be carried to the top of the tailings could be used. Only 8 boreholes could be drilled during the field campaign of the project. It would have been ideal if a much larger array of boreholes could be drilled to obtain a better understanding of the spatial variation of the measured parameters. It is also recommended for future work to plan for long term monitoring of these boreholes to also get a sense of the temporal variation.

6.2 LABORATORY ANALYSIS

In this study both static and kinetic geochemical laboratory analyses were performed. The results that were not directly utilized in the numerical modelling and were reported in appendices accompanying the report. It was observed that the data requirements to better understand the global behaviour of the geochemical evolution of the tailings are primarily hydrological in nature (parameters governing the volumetric moisture content of the material). This implies better understanding parameters such as particle size distribution, influence of preferential flow paths, downward migration the phreatic head and the spatial and temporal variation of soil moisture as a function of these parameters.

6.3 MODEL RESULTS

In this study it was shown that the unsaturated flow regime of a tailings storage facility may govern the rate of oxidation of pyrite though controlling the rate of oxygen ingress into the tailings. Several uncertainties such as the depth and downward migration rate of the phreatic head made calibrating the PYROX model problematic. Variance in soil moisture at the respective nodes of the PYROX model were calculated with SEEP/W by assuming that the phreatic head was static for the timespan of the model. This is a limitation of the model and it is accepted that it may very well not be the case. Furthermore, horizons of very fine particles (can be seen as nodes with a high moisture content in the moisture profiles) were observed. It was also observed that these horizons acted like barriers and shielded material underneath it from oxidation. The geochemical model assumed that the material in the unoxidized zone is homogeneous and did not compensate for this shielding effect or the possible existence of preferential flow paths like the fissures observed by Yibas et al. (2010).

In order to address the uncertainties mentioned above, a larger array of boreholes with greater depth (intercept the saturated zone in the tailings storage facility) will be required to get a sense of the spatial variability the parameters governing the unsaturated material moisture content. By fully understanding the unsaturated flow regime of tailings storage facilities more accurate field scale geochemical models can be constructed to model potential risks that may be associated with these sites.

The research conducted in this study was aimed to show that with the incorporation of physical parameters related to the hydrological functioning of a tailings storage facility, the global oxidation rate of pyrite can be determined. This rate is very important to understand the release of sulphates from the material as it was seen that factors such as stratification of the material may cause horizons that completely shield material below it from oxidation, effectively encapsulating it. Physical behaviour like this and the influence it has on the release of sulphates due to pyrite oxidation could never be determined from the data obtained from current strategies. The aim of this work was furthermore to show what parameters are important and should be considered when designing a fieldwork campaign for the purposes of determining a sulphate source term for a tailings storage facility.

Bibliography

Appelo, C.A.J., Postma, D., 2005. *Geochemistry, Groundwater and Pollution*, second ed. CRC Press, Amsterdam, The Netherlands.

Ardejani, F. D. Shokri, B.J. Moradzadeh, A. Soleimani, E. & Jafari, M.A. 2008. A combined mathematical geophysical model for prediction of pyrite oxidation and pollutant leaching associated with a coal washing waste dump. *Int. J. Environ. Sci. Tech.* 5, pp. 517-526.

ASTM. 2001. Standard test method for accelerated weathering of solid materials using a modified Humidity Cell, D 5744-96ASTM (2007) Standard test method for laboratory weathering of solid materials using a humidity cell, D5744-07, pp. 1-19

Bain, J.G. Mayer, K.U. Blowes, D.W. Frind, E.O. Molson, J.W.H. Kahnt, R. & Jenk, U. 2001. Modelling the closure-related geochemical evolution of groundwater at a former uranium mine. *Journal of Contaminant Hydrology*, 52, pp.109-135.

Brown, P. Luo, X.L., Mooney, & Pantelis, G. 1999. The modelling of flow and chemical reactions in waste piles. In: 2nd Internat. Conf. CFD in the Minerals and Process Industries. CSIRO, Melbourne, Australia, December 6-8, pp. 169-174.

Davis, G.B. & Ritchie, A.I.M. 1986(a). A model of oxidation in pyritic mine waste: part 1 equations and approximate solution. *Applied Mathematical. Modelling*, 10, pp. 314-322.

Davis, G.B. & Ritchie, A.I.M. 1986(b). A model of oxidation in pyritic mine waste: part 2 equations and approximate solution *Applied Mathematical. Modelling*, 10, pp. 314-322.

Davis, G.B. & Ritchie, A.I.M. 1986(c). A model of oxidation in pyritic mine waste: part 3 equations and approximate solution. *Applied Mathematical. Modelling*, 10, pp. 314-322.

Gardner, W. 1986. Early soil physics into the mid-20th century. *Advances in soil science*. Springer. p. 1-101).

Geo-Slope International, Ltd. (2019). SEEP/W for finite element seepage analysis. Available online at: <https://www.geoslope.com> (accessed 15 January 2019)

Hillel, D. 1980. Soil structure and aggregation. *Introduction to soil physics*: 40-52.

Lefebvre, R. Hockley, D. Smolensky, J. & Gélinas, P. 2001. Multiple transfer processes in waste rock piles producing acid mine drainage 1: Conceptual model and system characterization. *Journal of Contaminant Hydrology*, 52, pp. 137-164.

- Levenspiel, O. 1999. *Chemical Reaction Engineering*. 3d ed. New York: Wiley, City, New York, USA.
- Linklater, C.M. Sinclair, D.J. Brown, P.L. 2005. Coupled chemistry and transport modelling of sulphidic waste rock dumps at the Aitik mine site. Sweden. *Applied Geochemistry*, 20, pp. 275-293.
- Long, I. & French, B. 1967. Measurement of soil moisture in the field by neutron moderation. *European Journal of Soil Science*, 18(1):149-166.
- Mayer, K.U. Frind, & E. O. Blowes, D.W. 2002. Multicomponent reactive transport modelling in variably saturated porous media using a generalized formulation for kinetically controlled reactions. *Water Resources Research*, 38, 9, 1174, doi:10.1029/2001WR000862.
- MILLER, S., ROBERTSON, A. & DONAHUE, T. 1997. Advances in acid drainage prediction using the net acid generation (NAG) 4th international conference on acid rock drainage
- Molson, J.W., Fala, O. Aubertin, & M. Bussière, B. 2005. Numerical simulations of pyrite oxidation and acid mine drainage in unsaturated waste rock piles. *Journal of Contaminant Hydrology*, 78, pp 343-371.
- Pantelis, G. Ritchie, & A.I.M. Stepanyants, Y.A. A conceptual model for the description of oxidation and transport processes in sulphidic waste rock dumps. *Applied Mathematical Modelling*, 26(2002) 751-770.
- PRICE, W.A. 1997. Guidelines and recommended methods for the prediction of metal leaching and acid rock drainage at mine sites in British Columbia (DRAFT). British Columbia Ministry of Employment and Investment, Energy and Minerals Division, Smithers: BC, pp.143
- Reardon, E.J., & Moddle, P.M., 1985. Gas diffusion coefficient measurements on uranium mill tailings: Implications to cover layer design. *Uranium*, 2, 111-131.
- Skousen, J. Simmons, J. McDonald, L. M. Ziemkiewicz, P. Acid-Base Accounting to Predict Post-Mining Drainage Quality on Surface Mines. *J. Environ. Qual.*, 31, pp 2034-2044.
- SUNKAVALLI, S.P. 2014. Gap between Humidity Cell Testing Data and Geochemical Modeling of Acid Rock Drainage. ISSN: 2157-7587 HYCR, an open access journal
- Usher, B.H., Cruywagen, L-M., De Necker, E. & Hodgson, F.D.I., 2002. On-site and laboratory investigations of spoil in opencast collieries and the development of acid-base accounting procedures. *Water Research Commission*.
- Visvalingam, M. & Tandy, J. 1972. The neutron method for measuring soil moisture content – A review. *European Journal of Soil Science*, 23(4):499-511.

Wunderley, M.D. & Blowes, D.W. 1997. PYROX version 1.1 User Manual. Institute for Groundwater Research, Univ. of Waterloo, Waterloo, Ontario

Yibas, B. Pulles, W. Nengovhel, C. 2010. Kinetic development of oxidation zones in tailing dams with specific reference to the Witwatersrand gold mine tailings dams. Water Research Commission. Report Number 1554/1/10, 105 pp.

Younger, P. 2000. Predicting Temporal changes in total iron concentrations in groundwater flowing from abandoned deep mines: a first approximation. *Journal of Contaminant Hydrology*, 44, pp 47-69

APPENDIX A: ICP MS RESULTS

Table 11: 1:20 Leach test laboratory results

Sample:	1:20 LEACH												
	RF2.1	RF2.2	RF2.3	RF2.4	RF2.5	RF2.6	RF2.7	RF2.8	RF2.9	RF2.10	RF2.11	RF2.12	RF2.13
	mg/l	mg/l	mg/l	mg/l	mg/l	mg/l	mg/l	mg/l	mg/l	mg/l	mg/l	mg/l	mg/l
Be 9	4.09E-05	7.81E-05	ND	0.001825	0.001803	0.004086	0.003993	0.003811	0.0004276	0.0001488	ND	ND	ND
B 11	0.03126	0.02824	0.02193	0.02627	0.02233	0.0356	0.02075	0.02509	0.03993	0.03783	0.0733	0.1429	0.02745
Na 23	1.612	1.4	1.566	1.824	1.45	1.273	1.169	1.343	1.723	1.757	1.995	1.774	2.578
Mg 24	0.5252	0.9606	1.698	12.58	7.805	17.57	12.83	12.18	31	16.43	11.3	6.272	9.517
Al 27	0.07605	0.09076	0.1079	9.233	14.96	43.85	32.23	20.49	0.8756	0.3008	0.06474	0.0672	0.055
P 31	ND	ND	ND	ND	ND	ND	ND	ND	ND	ND	ND	ND	ND
K 39	0.6053	0.4568	0.2824	0.214	0.03366	ND	ND	0.09058	0.3024	0.3516	0.6945	0.7707	0.8664
Ca 43	3.261	238.6	340.8	458.4	307.5	184.6	112.8	107	180.4	125.6	164	233.2	195.3
Ti 47	0.001143	0.003841	0.001222	0.001867	0.009376	0.004319	0.00279	0.001107	0.0009477	0.001296	0.0008278	0.001325	0.0008165
V 51	0.0001385	ND	ND	ND	ND	0.0009608	ND						
Cr 53	0.001171	0.0007831	0.0006396	0.004621	0.02897	0.438	0.1012	0.005723	ND	ND	ND	ND	ND
Mn 55	0.1397	0.4982	0.02679	2.988	1.791	4.58	3.531	3.332	7.885	2.164	0.2388	0.09348	1.752
Fe 57	0.09529	0.2185	0.3768	1.458	3.055	82.12	20.71	7.567	2.285	0.6067	0.176	0.3085	0.1942
Co 59	0.0207	0.06573	0.01817	0.629	0.4962	1.614	1.126	1.031	1.091	0.3428	0.006478	0.01181	0.06785
Ni 60	0.05707	0.2184	0.008768	1.461	1.142	3.743	2.73	2.426	2.127	0.7852	0.008693	0.00543	0.2333
Cu 63	0.06666	0.1211	0.03848	0.3699	0.5286	1.958	1.214	0.9669	0.3305	0.1873	0.02343	0.02554	0.04769
Zn 66	0.1049	0.2047	0.01509	1.874	1.669	5.524	4.382	3.948	2.875	1.342	0.02296	0.01645	0.08446
As 75	0.00075	0.001564	0.003111	0.005059	0.008114	0.07991	0.0282	0.0392	0.0393	0.02572	0.006702	0.006175	0.01034
Se 82	0.0005257	0.001374	0.001859	0.003233	0.003596	0.007192	0.004728	0.005374	0.003031	0.002344	0.001738	0.002829	0.001576
Rb 85	0.001246	0.0008592	0.0006148	0.002364	0.001421	0.0007565	0.001037	0.001238	0.001365	0.001196	0.001309	0.001325	0.002117
Sr 88	0.004126	0.084	0.1052	0.1434	0.0891	0.05016	0.05168	0.0708	0.1589	0.124	0.1843	0.1835	0.06849
Mo 95	0.0003948	0.0001206	0.0005076	0.0001267	9.32E-05	0.000145	8.71E-05	0.0002014	0.0001374	0.0001404	0.002289	0.002715	0.0001358
Pd 105	ND	0.0001069	9.21E-05	0.001031	0.0008032	0.002188	0.001647	0.001626	0.00103	0.0002877	0.0001379	0.0001514	5.83E-05
Ag 107	ND	ND	ND	ND	ND	ND	ND	ND	ND	ND	ND	ND	ND
Cd 111	0.001449	0.002202	0.001244	0.00866	0.007334	0.02236	0.01759	0.01895	0.0164	0.00681	0.00131	0.001331	0.002497
Sb 121	7.58E-05	9.73E-05	0.0007104	0.0002056	0.0005152	0.0004676	0.0001211	0.000148	0.0002202	0.0002863	0.001197	0.001111	0.0003078
Ba 137	0.08897	0.1036	0.09855	0.1048	0.1029	0.09975	0.102	0.1158	0.1122	0.1057	0.09483	0.09151	0.09329
Pt 195	ND	ND	ND	ND	ND	ND	3.19E-05	ND	ND	ND	ND	ND	ND
Au 197	0.0001452	0.0001995	0.0007072	0.0001671	6.60E-05	3.64E-05	1.16E-05	3.83E-05	0.0001051	0.0002816	0.0004724	0.001654	0.0002902
Hg 202	9.71E-05	0.0001457	0.0001857	0.0001343	0.0001286	9.71E-05	0.0001428	5.71E-05	0.0001028	6.86E-05	0.0002685	0.0001028	8.00E-05

Updating current strategies for estimating a source term for a tailings storage facility

TI 205	ND	ND	ND	ND	8.51E-07	ND							
Pb 208	0.001205	0.001849	0.001272	0.00962	0.004868	0.002788	0.002134	0.002903	0.002359	0.001456	0.001397	0.001204	0.001164
Bi 209	5.98E-06	7.65E-05	5.39E-05	3.30E-06	2.75E-05	0.0000079	ND	ND	ND	3.30E-06	0.0001191	7.52E-06	2.92E-06
Th 232	ND	ND	ND	0.000239	2.91E-05	0.1671	0.005638	7.64E-05	5.64E-06	ND	ND	ND	ND
U 238	ND	0.002353	0.02506	0.2738	0.3486	1.41	1.268	1.167	0.1967	0.04302	0.01809	0.03007	0.0004291
SO4	2.58	601.05	873.76	1508.02	1123.78	1477.79	808.38	697.12	694.67	540.03	587.58	609.85	721.19
NO3	0.01	2.34	2.31	1.46	3.14	2.9	1.81	0.34	3.56	0.27	0.31	2.88	0.43
NH4	0.180386	0.1443088	0.0541158	0.6493896	0.3246948	0.3066562	0.2345018	0.3246948	0.2886176	0.3066562	0.2886176	0.6854668	0.7936984
Cl	0.46	1.78	1.04	1.07	1.13	5.21	1.61	0.69	2.02	0.41	0.98	4.62	1
pH	4.81	4.48	7.63	3.88	3.49	2.81	3.16	3.7	4.34	4.48	6.75	7.06	4.74
EC	0.04	1.03	1.38	1.99	1.61	2.28	1.27	0.9	1.12	0.78	0.85	1.05	0.99
TAL	1	0	37.5	0	0	0	0	0	0	0	17.5	40	2.5

Table 12: Humidity leach cell week 1 results

Sample:	RF1 OX	RF1 UNOX	RF1 TRANS	RF3 OX	RF3 UNOX	H ₂ O
	mg/l	mg/l	mg/l	mg/l	mg/l	mg/l
Be 9	0.000134	0.07627	0.02355	0.01737	ND	ND
B 11	0.1825	0.2776	0.03944	0.02272	0.016	ND
Na 23	18.36	53.19	5.527	5.228	7.079	1.838
Mg 24	273.1	451.4	129.9	41.26	48.08	0.2075
Al 27	0.05661	601.8	254.1	59.73	0.0155	ND
P 31	ND	ND	ND	ND	ND	ND
K 39	5.811	12.54	0.3055	1.777	4.101	ND
Ca 43	431.4	509.3	514.1	345.2	330.4	0.2454
Ti 47	0.001693	0.006877	0.002949	0.002929	0.0002986	ND
V 51	0.002338	0.001762	4.89E-08	ND	ND	ND
Cr 53	0.01247	2.416	2.653	0.2954	ND	ND
Mn 55	39	315.1	23.53	28.61	2.871	0.001344
Fe 57	0.6754	181.6	39.07	42.36	0.6047	ND
Co 59	4.169	41.55	7.112	7.055	0.3692	0.0001033
Ni 60	8.616	88.69	15.7	11.63	0.1281	ND
Cu 63	0.06648	17.89	3.691	3.667	0.01552	0.01279
Zn 66	1.803	116.3	37.4	23	0.06338	0.008066
As 75	0.006301	0.08588	0.01477	0.03473	0.01631	ND
Se 82	0.008894	0.1164	0.03229	0.02272	0.01144	ND
Rb 85	0.007979	0.02439	0.002902	0.0132	0.006382	0.0003555
Sr 88	0.1687	0.5137	0.3341	0.3324	0.4109	0.0003496
Mo 95	0.0007881	0.002909	0.0002251	0.0001312	0.0006727	ND
Pd 105	0.000616	0.04686	0.01077	0.008921	0.001041	ND
Ag 107	ND	ND	0.0002827	ND	ND	ND
Cd 111	0.008344	0.5488	0.0938	0.1003	0.001144	0.0009313
Sb 121	0.001858	0.001413	0.000888	0.001494	0.003116	ND
Ba 137	0.1566	0.134	0.1173	0.1195	0.1196	0.03552
Pt 195	0.0001988	8.69E-05	ND	ND	0.0003225	ND
Au 197	0.02252	0.001636	0.0000928	0.003823	0.01995	2.86E-05
Hg 202	0.005502	0.002102	0.001074	0.0009459	0.0006255	0.00036
Tl 205	ND	0.0002858	ND	ND	ND	ND
Pb 208	0.002254	0.264	0.1528	0.1772	0.001516	0.0009196
Bi 209	ND	ND	ND	ND	ND	ND
Th 232	ND	0.1474	0.1079	0.02224	ND	ND
U 238	0.356	20.56	6.153	5.598	0.3125	0.0003034
SO ₄	2132.30	10678.20	6377.37	3499.70	1929.11	0.29
NO ₃	3.10	14.37	5.26	7.85	2.42	0.38
NH ₄	2.04	9.15	0.43	3.36	6.67	0.05
Cl	13.20	49.55	13.56	7.49	8.00	2.76
pH	6.77	3.39	3.44	3.37	6.45	6.57
EC	3.01	7.37	4.78	3.44	2.74	0.03
TAL	150	0	0	0	67.5	22.5

Table 13: Humidity leach cell week 2 results

Sample:	RF1 OX	RF1 UNOX	RF1 TRANS	RF3 OX	RF3 UNOX	H ₂ O
	mg/l	mg/l	mg/l	mg/l	mg/l	mg/l
Be 9	ND	0.00403	0.004595	0.002259	ND	ND
B 11	0.009613	0.05735	0.0003289	0.01666	0.004477	ND
Na 23	5.33	4.625	2.924	2.923	3.279	1.4
Mg 24	29.76	23.9	19.29	4.649	11.44	0.5064
Al 27	ND	12.98	44.17	4.438	0.01245	ND
P 31	ND	ND	ND	ND	ND	ND
K 39	1.027	0.6437	ND	0.104	0.9071	ND
Ca 43	277.6	241.3	104.1	224.1	265.4	0.9532
Ti 47	0.0002058	0.001713	0.0003118	0.001597	ND	0.00174
V 51	ND	ND	ND	ND	ND	ND
Cr 53	ND	0.01285	0.1368	ND	ND	ND
Mn 55	1.855	20.64	5.719	6.101	0.751	0.001232
Fe 57	0.3124	0.7304	1.06	0.3233	0.3732	0.007962
Co 59	0.1443	3.134	1.412	1.627	0.2946	6.30E-05
Ni 60	0.07897	7.795	3.757	4.118	0.02914	ND
Cu 63	0.02313	1.266	0.5909	0.3525	0.0147	0.007336
Zn 66	0.05803	15.25	9.861	7.958	0.04467	0.2788
As 75	0.0035	0.0334	0.003909	0.01611	0.0178	ND
Se 82	0.003448	0.008249	0.004737	0.004254	0.003577	ND
Rb 85	0.002688	0.003301	0.001535	0.001999	0.001349	0.001546
Sr 88	0.1171	0.251	0.1022	0.1642	0.3	0.002087
Mo 95	0.001032	ND	ND	ND	0.002788	ND
Pd 105	7.19E-05	0.003721	0.002357	0.001531	0.0002447	ND
Ag 107	ND	ND	ND	ND	0.01003	ND
Cd 111	0.001463	0.06557	0.02825	0.02589	0.001309	0.002276
Sb 121	0.001626	2.73E-05	5.61E-05	0.0001638	0.004032	3.52E-05
Ba 137	0.1407	0.1264	0.1118	0.1161	0.1085	0.03611
Pt 195	4.42E-06	ND	ND	ND	4.42E-06	ND
Au 197	0.01147	0.0001024	2.28E-05	0.0005884	0.006227	8.45E-06
Hg 202	0.0003753	0.0005769	0.0003967	0.0002929	0.0002563	0.0002044
Tl 205	ND	ND	ND	ND	ND	ND
Pb 208	0.001451	0.1522	0.03881	0.158	0.001291	0.001738
Bi 209	ND	ND	ND	ND	ND	ND
Th 232	ND	ND	0.0004197	ND	ND	ND
U 238	0.3477	1.639	1.457	0.4929	0.188	0.0001798
SO ₄	1565.19	2074.82	905.02	745.18	1561.60	1.87
NO ₃	5.28	3.79	1.99	2.68	3.55	0.21
NH ₄	0.32	1.05	0.11	0.29	0.63	0.07
Cl	9.21	7.43	8.69	3.50	6.73	3.48
pH	6.58	3.76	3.45	3.84	6.37	6.59
EC	2.26	2.31	1.93	1.90	2.26	0.04
TAL	65	0	0	0	37.5	15

Table 14: Humidity leach cell week 3 results

Sample:	RF1 OX	RF1 UNOX	RF1 TRANS	RF3 OX	RF3 UNOX	H ₂ O
	mg/l	mg/l	mg/l	mg/l	mg/l	mg/l
Be 9	ND	0.003228	0.001769	0.001752	ND	ND
B 11	ND	0.005531	0.004016	0.002173	0.01284	ND
Na 23	3.282	2.416	2.412	2.088	2.292	1.415
Mg 24	9.05	6.864	8.247	1.914	4.13	0.5483
Al 27	ND	11.9	17.87	4.141	ND	ND
P 31	ND	ND	ND	ND	ND	ND
K 39	0.434	ND	ND	ND	0.2472	ND
Ca 43	165.1	118.6	48.09	120.2	169.3	3.316
Ti 47	0.0002228	0.0005404	ND	0.000865	ND	ND
V 51	ND	ND	ND	ND	ND	ND
Cr 53	ND	0.02397	0.04382	ND	ND	ND
Mn 55	0.3543	5.526	2.524	1.97	0.2833	0.001049
Fe 57	0.177	0.3229	0.1498	0.1675	0.1928	ND
Co 59	0.0382	1.142	0.5983	0.6638	0.09836	4.98E-05
Ni 60	0.02337	3.158	1.79	1.926	0.01078	ND
Cu 63	0.01357	1.102	0.3238	0.2762	0.02248	0.01181
Zn 66	0.02261	5.436	5.899	2.94	0.03087	0.07476
As 75	0.001266	0.03403	0.002386	0.01163	0.007642	ND
Se 82	0.001064	0.004093	0.001096	0.001901	0.001579	ND
Rb 85	0.002308	0.001111	0.001348	0.0008361	0.0007883	0.0016
Sr 88	0.07124	0.1118	0.05414	0.07478	0.1599	0.005259
Mo 95	0.0007348	ND	ND	ND	0.001402	ND
Pd 105	ND	0.001718	0.0009919	0.0009826	7.66E-05	ND
Ag 107	ND	ND	ND	ND	ND	ND
Cd 111	0.001121	0.02087	0.01378	0.01231	0.001127	0.001356
Sb 121	9.86E-04	0.0001559	8.55E-05	0.0001667	0.001407	8.98E-05
Ba 137	0.1008	0.08459	0.0918	0.08065	0.08212	0.03614
Pt 195	ND	ND	ND	ND	ND	ND
Au 197	0.0006267	3.62E-05	0.0000257	6.69E-05	0.002538	ND
Hg 202	0.0002838	0.0002594	0.0002105	0.0001953	0.0001129	0.0001892
Tl 205	ND	ND	ND	ND	ND	ND
Pb 208	0.001055	0.232	0.08321	0.08614	0.001123	0.001211
Bi 209	ND	ND	ND	ND	ND	ND
Th 232	ND	ND	ND	ND	ND	ND
U 238	0.07078	1.194	0.5566	0.3899	0.06345	0.0001315
SO ₄	972.73	1116.85	906.91	857.81	998.24	1.43
NO ₃	2.41	2.75	0.37	2.98	3.66	0.10
NH ₄	0.25	0.04	0.04	0.02	0.29	0.09
Cl	6.71	5.05	5.75	5.39	6.65	3.35
pH	7.54	3.83	3.90	4.26	7.35	7.37
EC	1.50	1.48	0.96	1.23	1.54	0.07
TAL	37.5	0	0	0	30	30

Table 15: Humidity leach cell week 4 results

Sample:	RF1 OX	RF1 UNOX	RF1 TRANS	RF3 OX	RF3 UNOX	H ₂ O
	mg/l	mg/l	mg/l	mg/l	mg/l	mg/l
Be 9	ND	0.002125	0.0004633	0.0002757	ND	ND
B 11	ND	ND	ND	ND	ND	ND
Na 23	2.818	2.817	2.658	2.505	3.043	1.512
Mg 24	1.975	4.177	3.278	1.069	3.932	0.6147
Al 27	0.004593	8.791	3.883	0.1023	ND	ND
P 31	ND	ND	ND	ND	ND	ND
K 39	0.01318	ND	ND	ND	0.1413	ND
Ca 43	22.9	49.55	16	39.73	164.6	5.443
Ti 47	0.0001694	0.0002091	ND	ND	ND	ND
V 51	ND	ND	ND	ND	ND	ND
Cr 53	ND	0.03872	0.003814	ND	ND	ND
Mn 55	0.03528	3.24	0.7606	0.453	0.3346	0.001076
Fe 57	0.03329	0.2851	0.04162	0.0215	0.1713	ND
Co 59	0.006905	0.6842	0.2003	0.1792	0.09268	6.46E-05
Ni 60	0.001637	1.882	0.5971	0.5132	0.0109	ND
Cu 63	0.01601	0.7426	0.07478	0.07046	0.03857	0.0234
Zn 66	0.01436	4.975	2.478	1.145	0.02289	0.1031
As 75	0.0002452	0.006196	0.0001285	0.001563	0.006738	ND
Se 82	ND	0.0009992	ND	9.69E-05	0.000967	ND
Rb 85	0.00145	0.001492	0.001512	0.001356	0.0006239	0.00164
Sr 88	0.0141	0.05364	0.02467	0.02694	0.151	0.007627
Mo 95	ND	ND	ND	ND	0.002132	ND
Pd 105	ND	0.0009546	0.0001677	8.01E-05	4.51E-05	ND
Ag 107	ND	ND	ND	ND	ND	ND
Cd 111	0.001055	0.01288	0.008094	0.004475	0.001102	0.001587
Sb 121	0.0002005	5.82E-05	3.81E-05	5.82E-05	0.001027	2.09E-05
Ba 137	0.09113	0.1003	0.1133	0.1041	0.1042	0.03814
Pt 195	ND	ND	ND	ND	ND	8.84E-05
Au 197	4.49E-05	2.67E-05	ND	ND	0.0009948	4.61E-06
Hg 202	0.0001892	0.0001922	0.0001526	0.0001251	9.46E-05	6.71E-05
Tl 205	ND	ND	ND	ND	ND	ND
Pb 208	0.001479	0.07751	0.02555	0.01514	0.001652	0.001728
Bi 209	ND	ND	ND	ND	ND	ND
Th 232	ND	ND	ND	ND	ND	ND
U 238	0.007512	0.7134	0.1195	0.03546	0.07736	0.0001267
SO ₄	125.36	666.62	260.75	288.15	932.18	1.77
NO ₃	0.40	0.32	0.25	0.34	2.49	0.24
NH ₄	0.05	0.07	0.07	0.04	0.20	0.04
Cl	4.56	4.57	4.75	4.15	6.41	3.30
pH	6.43	3.84	4.38	5.10	6.32	7.42
EC	0.31	0.82	0.39	0.49	1.45	0.08
TAL	37.5	0	0	2.5	35	40

Table 16: Humidity leach cell week 5 results

Sample:	RF1 OX	RF1 UNOX	RF1 TRANS	RF3 OX	RF3 UNOX	H ₂ O
	mg/l	mg/l	mg/l	mg/l	mg/l	mg/l
Be 9	ND	0.03763	0.01364	0.01617	ND	ND
B 11	ND	0.1549	0.06542	0.07685	0.05136	0.02877
Na 23	4.802	9.52	8.227	6.787	7.616	2.954
Mg 24	11.09	48.32	58.96	7.066	11.42	1.101
Al 27	ND	230.8	166.1	68.05	0.08512	0.03263
P 31	ND	ND	ND	ND	ND	ND
K 39	0.7027	0.4036	0.7192	1.072	1.49	0.4281
Ca 43	275.2	341.3	233.4	429.6	450.3	3.798
Ti 47	ND	0.006691	0.001678	0.004847	0.000862	0.000348
V 51	ND	0.000661	ND	ND	ND	ND
Cr 53	ND	1.602	0.3081	0.0522	ND	ND
Mn 55	0.5469	33.2	13.17	5.857	0.9516	0.001956
Fe 57	0.2907	60.95	0.9511	2.916	0.4625	0.0565
Co 59	0.07542	7.04	3.165	2.345	0.1414	ND
Ni 60	0.03722	20.64	9.117	7.462	0.03097	5.94E-06
Cu 63	0.02297	9.496	0.9969	2.064	0.02031	0.06987
Zn 66	0.08007	42.82	19.63	14.94	0.04817	0.3324
As 75	0.003489	0.08316	0.013	0.03963	0.01366	5.59E-05
Se 82	0.001289	0.02853	0.009414	0.01164	0.002748	ND
Rb 85	0.005132	0.001686	0.001378	0.001211	0.000754	0.001865
Sr 88	0.112	0.262	0.1588	0.1602	0.2713	0.003657
Mo 95	0.002054	0.000855	0.000238	7.19E-05	0.004619	1.24E-05
Pd 105	ND	0.009501	0.004119	0.004624	0.000263	2.19E-05
Ag 107	ND	ND	ND	ND	ND	ND
Cd 111	0.001262	0.07731	0.04518	0.03302	0.001566	0.002108
Sb 121	0.001526	0.000747	0.000299	0.000314	0.001993	5.81E-05
Ba 137	0.1207	0.1097	0.1062	0.09656	0.1156	0.03898
Pt 195	ND	0.000134	ND	ND	ND	ND
Au 197	0.000177	0.001005	0.000209	0.000151	0.001777	4.21E-05
Hg 202	0.000192	0.0073	0.003077	0.001734	0.001046	0.000894
Tl 205	ND	0.000144	7.02E-06	ND	ND	ND
Pb 208	0.001466	0.4316	0.1035	0.2521	0.001374	0.001192
Bi 209	ND	8.15E-05	8.04E-05	ND	0.000135	2.36E-05
Th 232	ND	0.1976	0.002832	0.002279	ND	ND
U 238	0.1177	6.339	1.857	1.833	0.08834	7.07E-05
SO ₄	1474.46	3762.26	2526.14	2172.60	1367.84	1.61
NO ₃	4.59	5.51	7.97	3.10	3.62	0.14
NH ₄	0.88	0.09	0.05	0.05	0.45	0.13
Cl	10.39	10.05	14.69	7.60	7.87	3.27
pH	7.40	2.80	3.49	3.25	6.55	6.92
EC	2.06	3.49	2.40	2.50	2.03	0.05
TAL	30	0	0	0	25	22.5

APPENDIX B: PARTICLE SIZE DISTRIBUTION

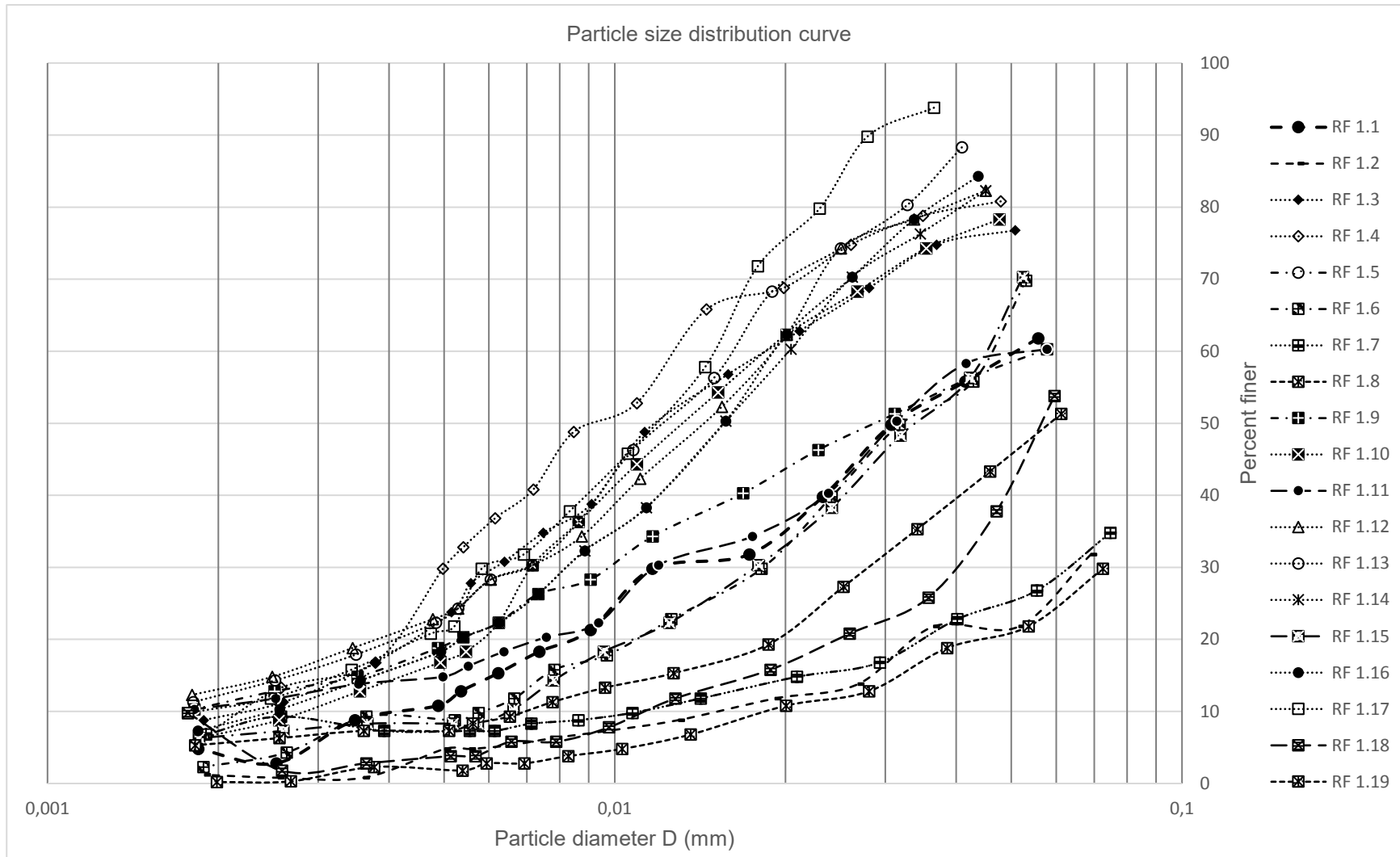


Figure 28: Particle size distribution curve for borehole RF 1

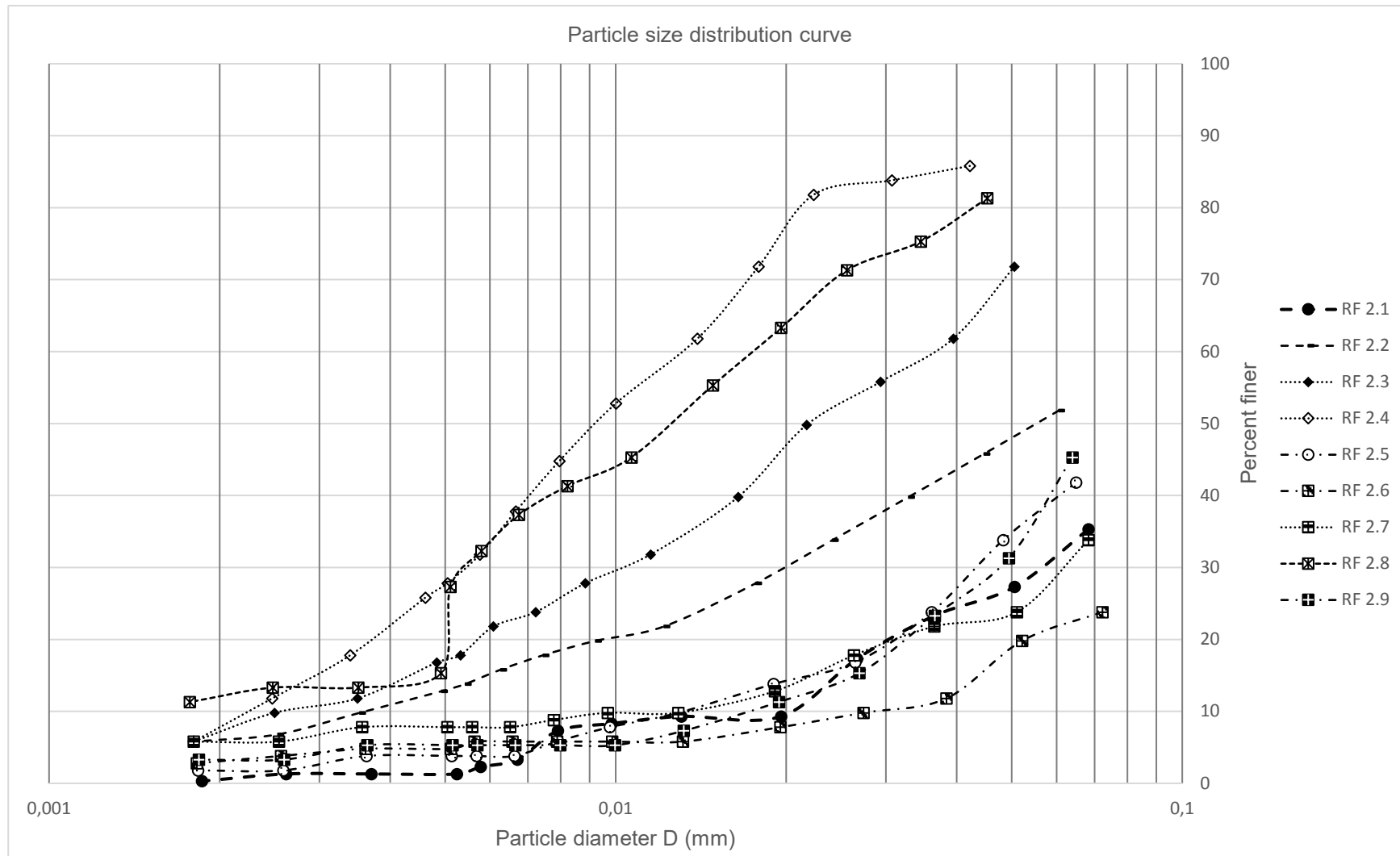


Figure 29: Particle size distribution curve for borehole RF 2

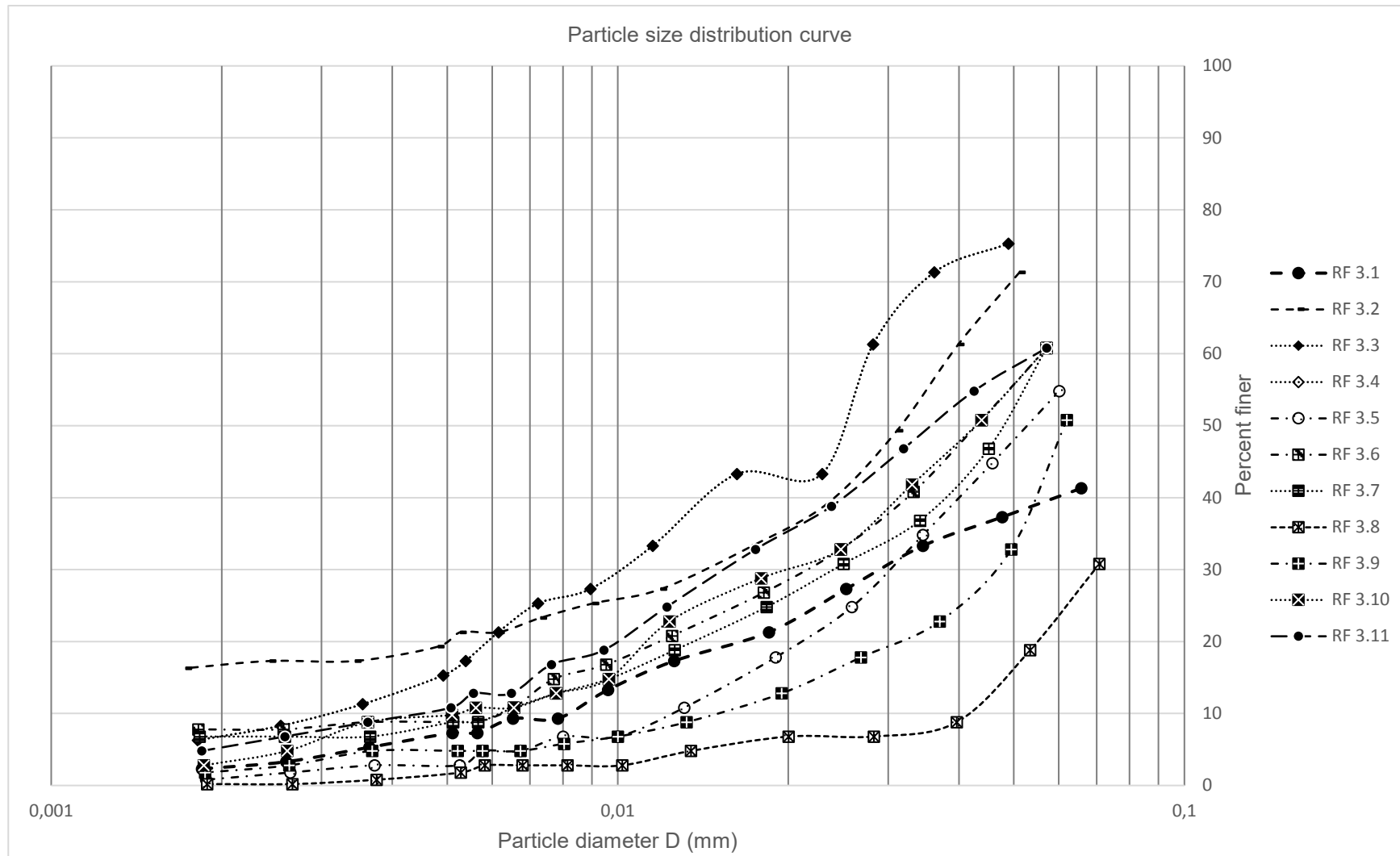


Figure 30: Particle size distribution curve for borehole RF 3

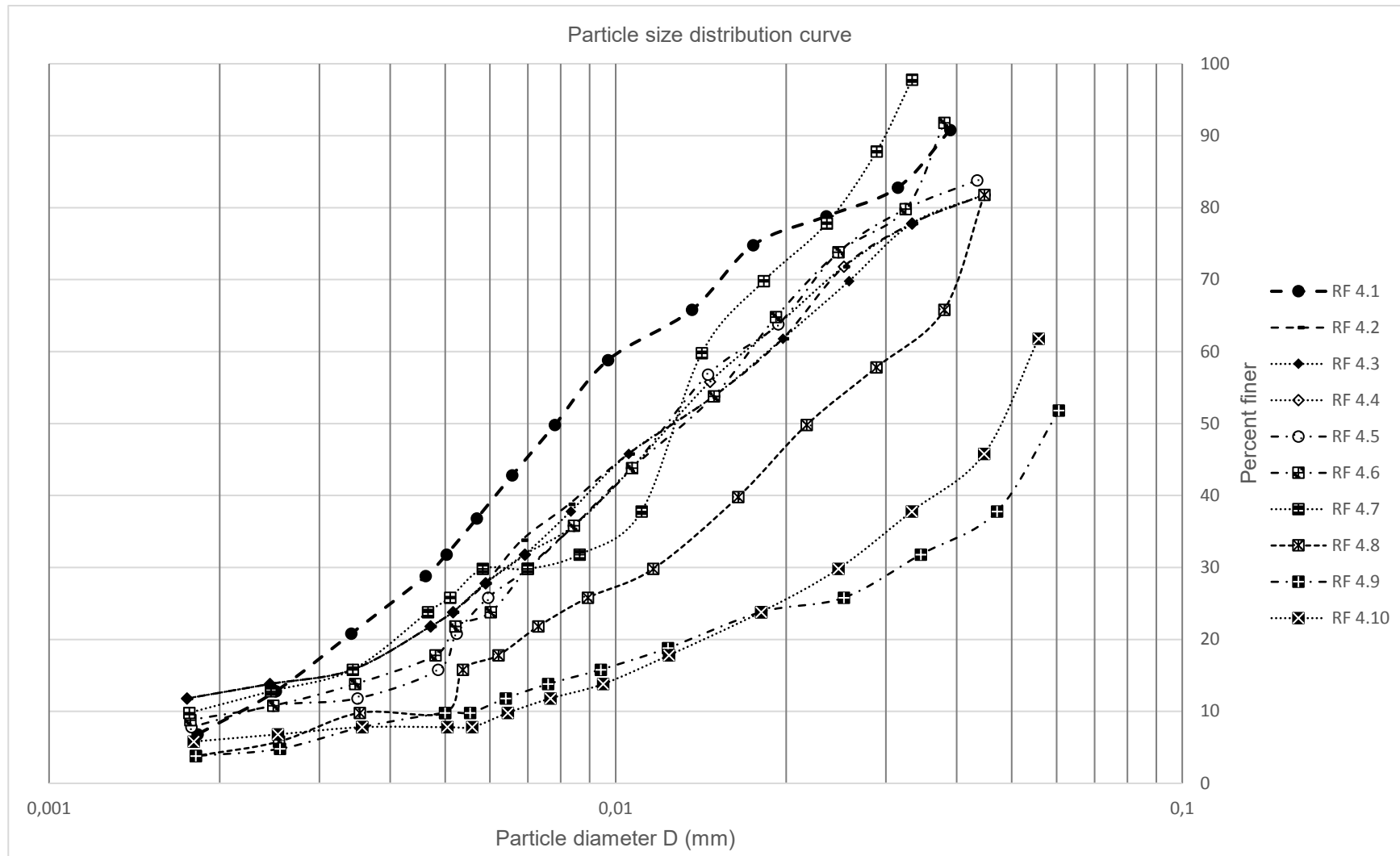


Figure 31: Particle size distribution curve for borehole RF 4

APPENDIX C: XRD RESULTS

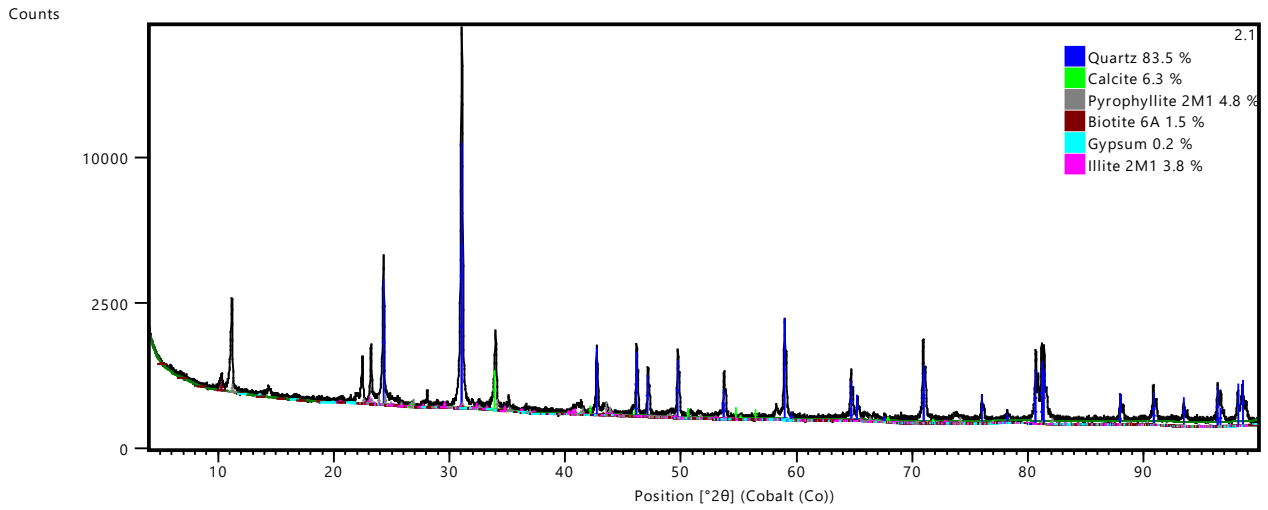


Figure 32: XRD analysis results for RF 2.1

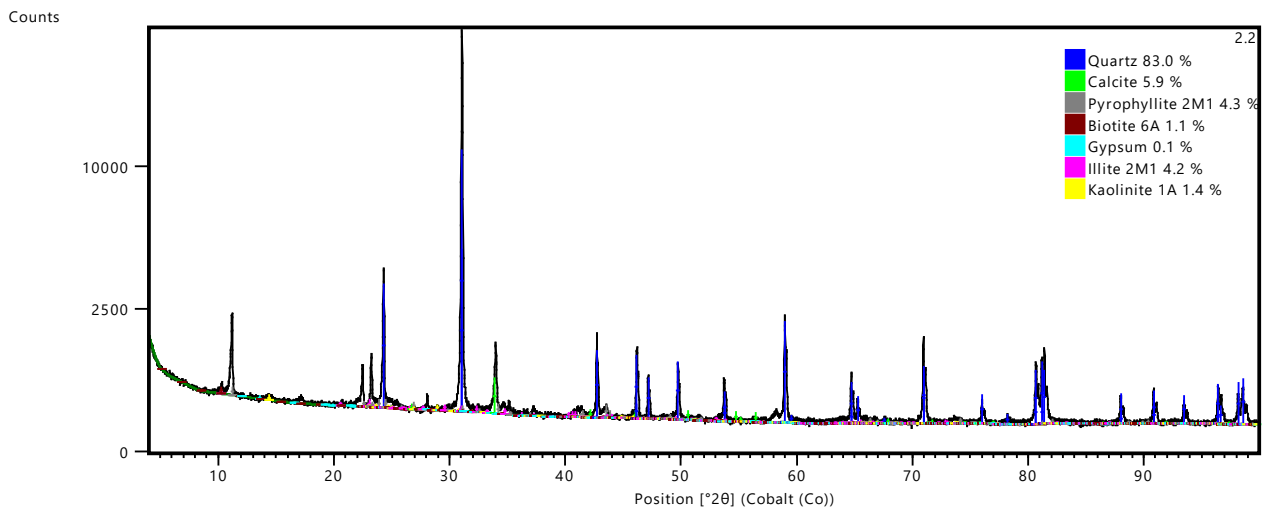


Figure 33: XRD analysis results for RF 2.2

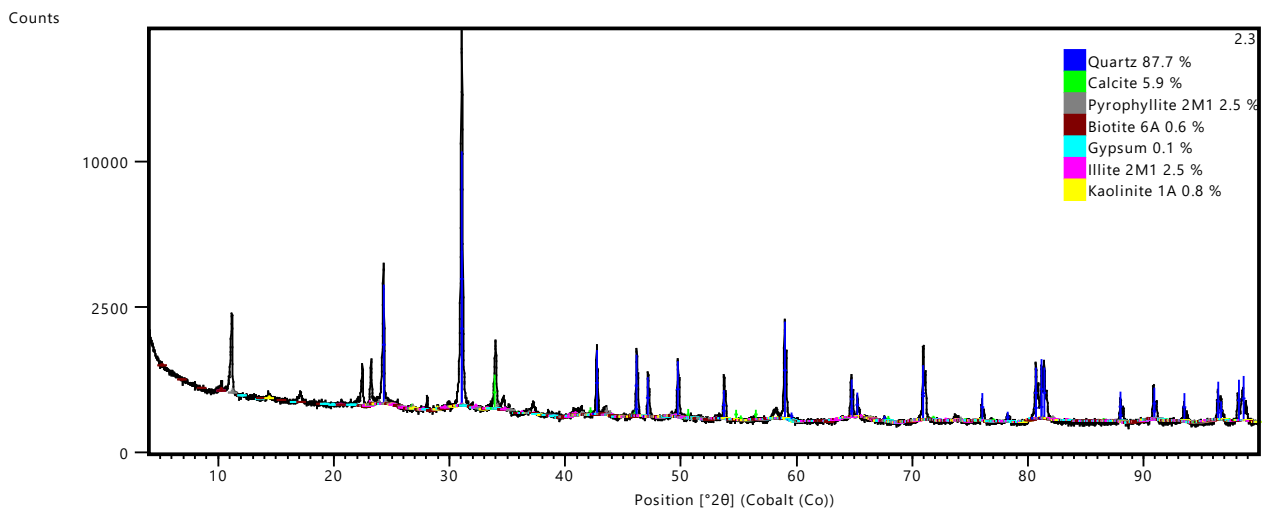


Figure 34: XRD analysis results for RF 2.3

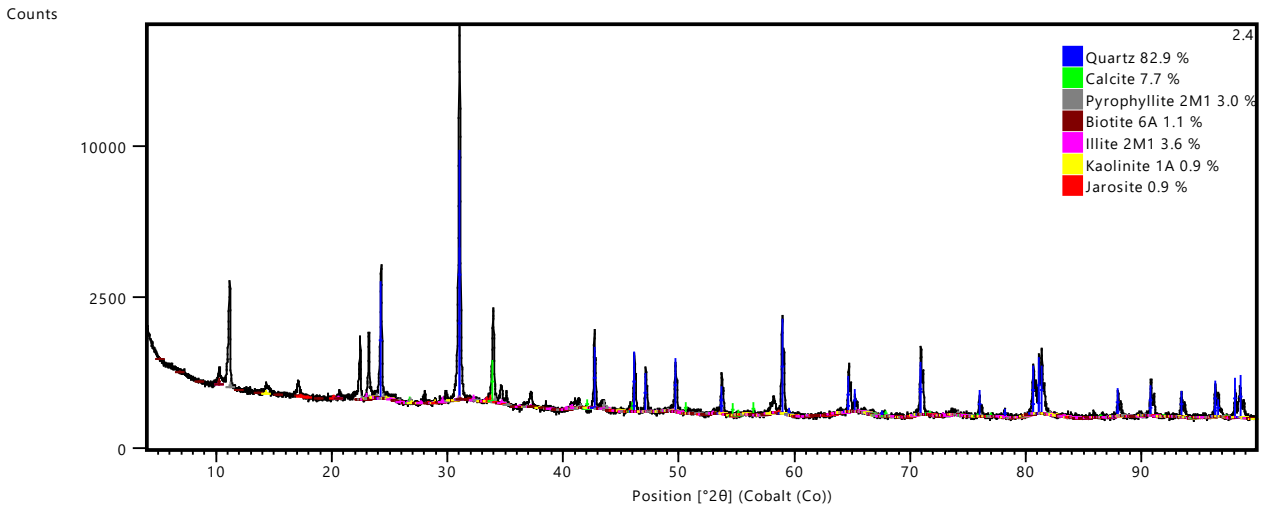


Figure 35: XRD analysis results for RF 2.4

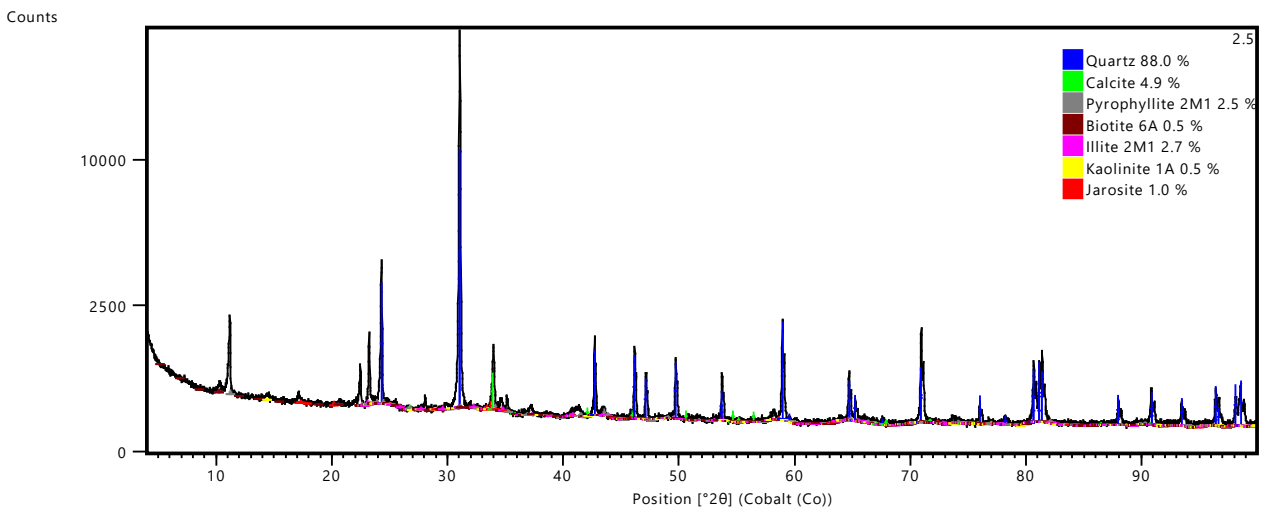


Figure 36: XRD analysis results for RF 2.5

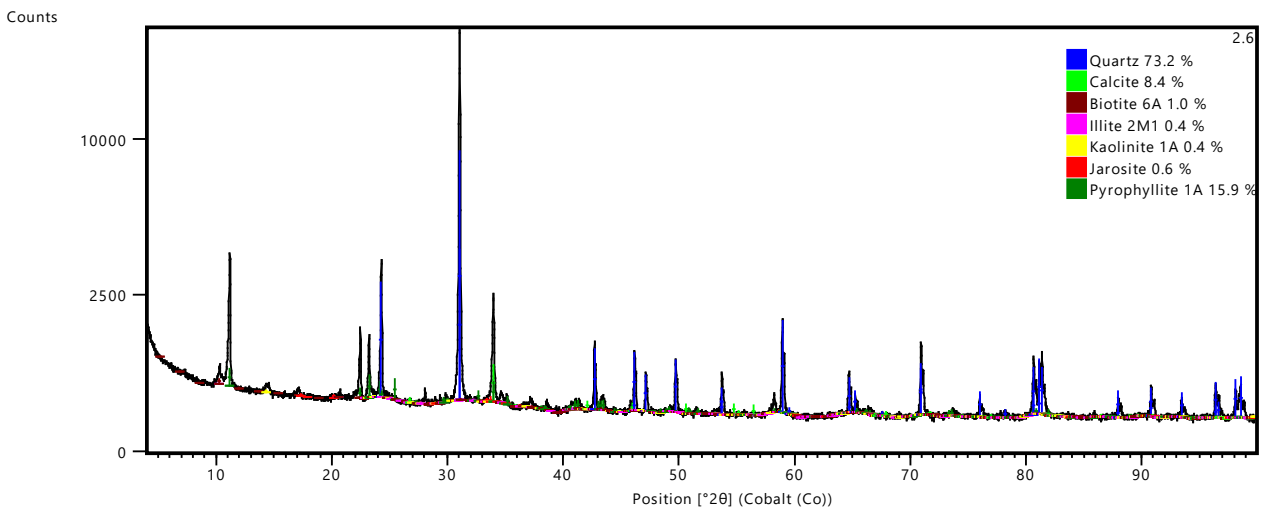


Figure 37: XRD analysis results for RF 2.6

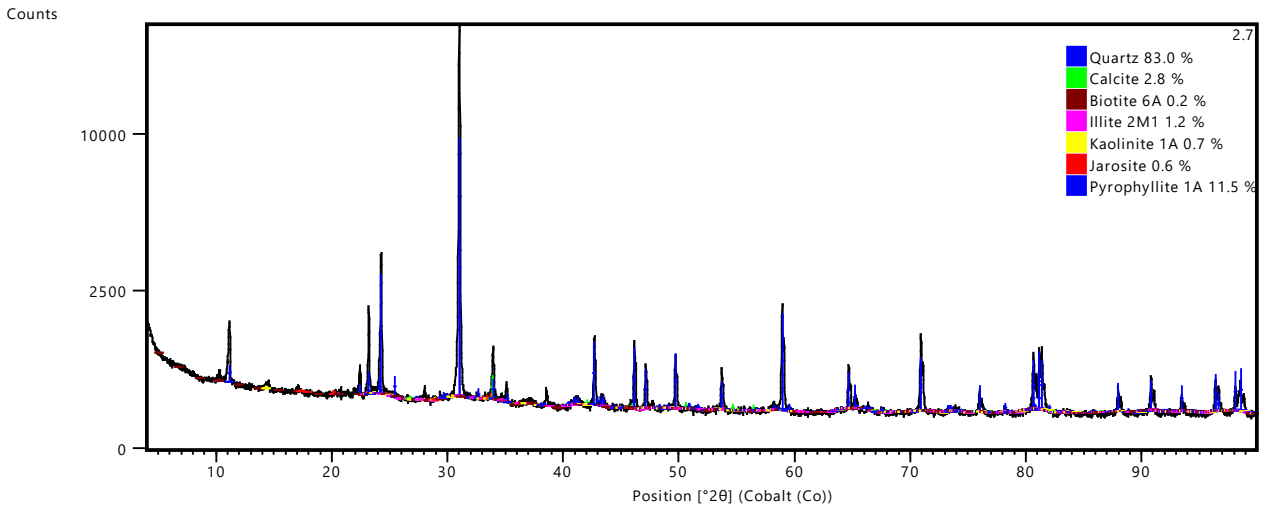


Figure 38: XRD analysis results for RF 2.7

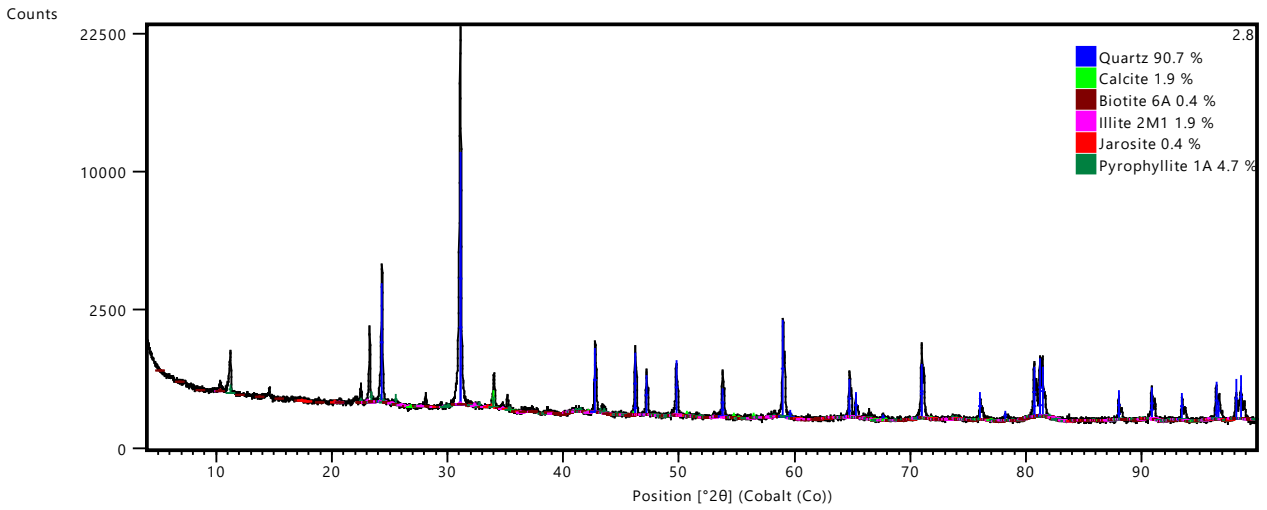


Figure 39: XRD analysis results for RF 2.8

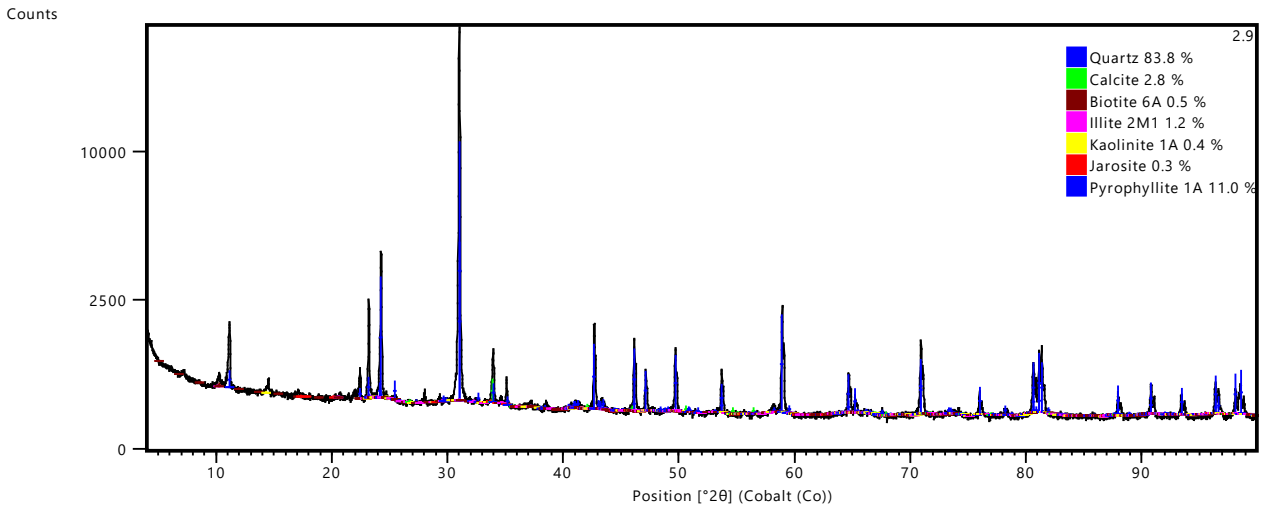


Figure 40: XRD analysis results for RF 2.9

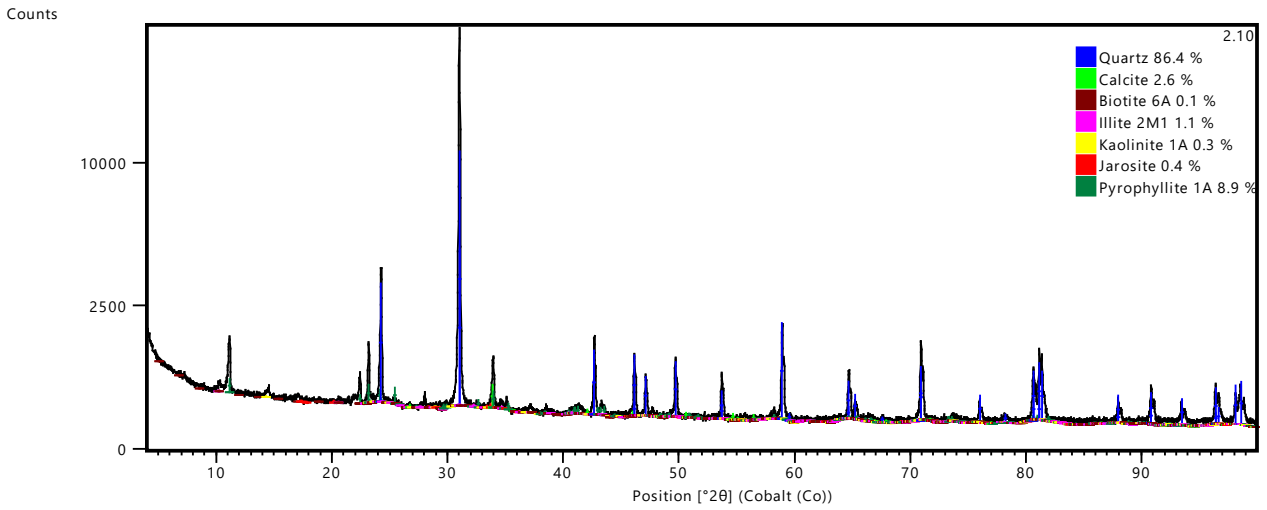


Figure 41: XRD analysis results for RF 2.10

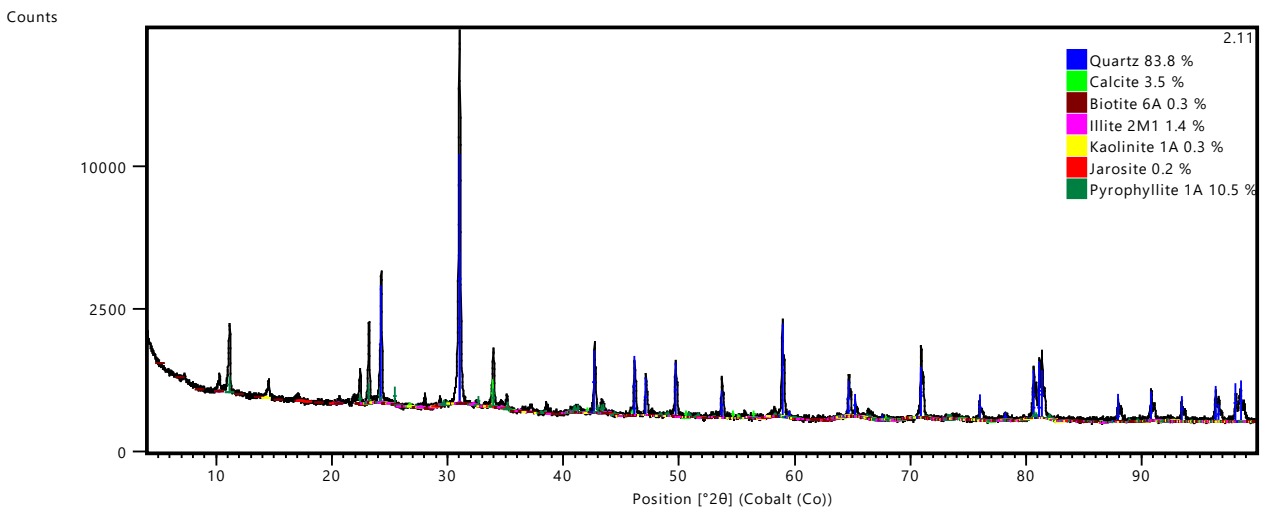


Figure 42: XRD analysis results for RF 2.11

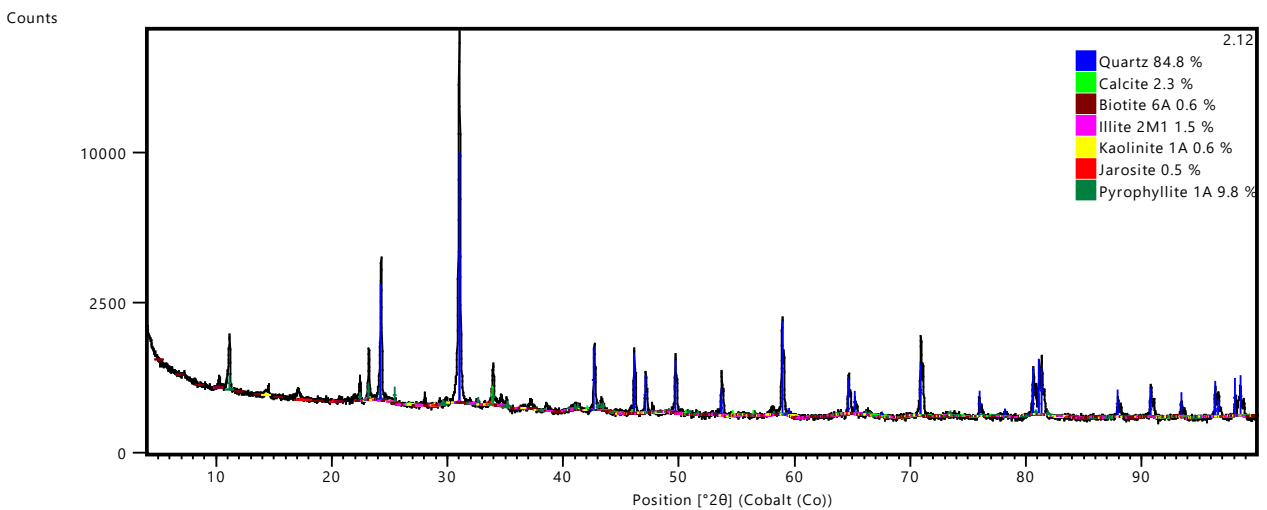


Figure 43: XRD analysis results for RF 2.12

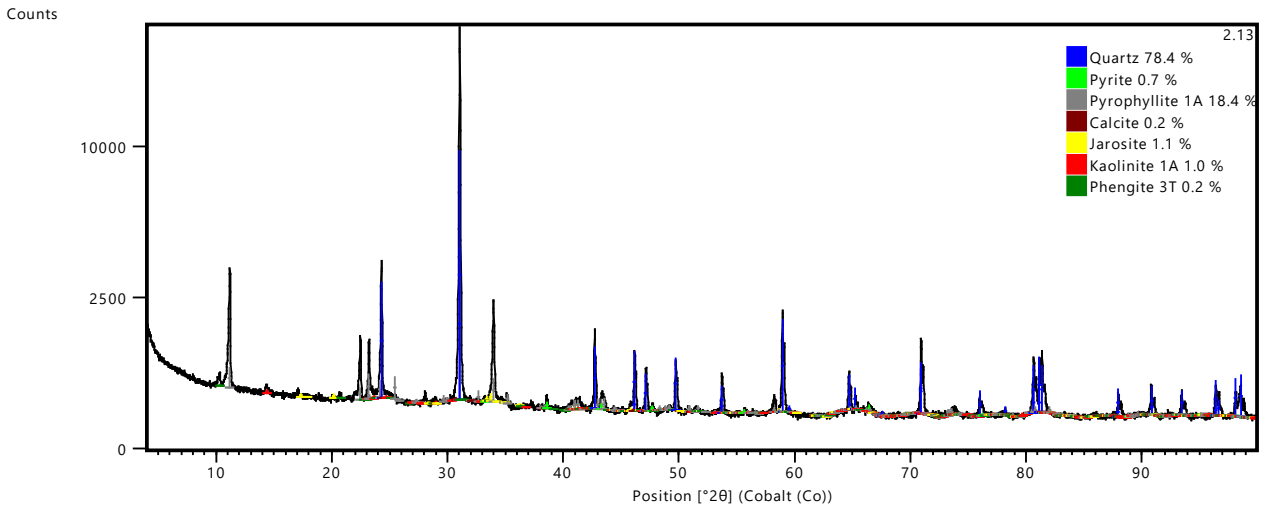


Figure 44: XRD analysis results for RF 2.13

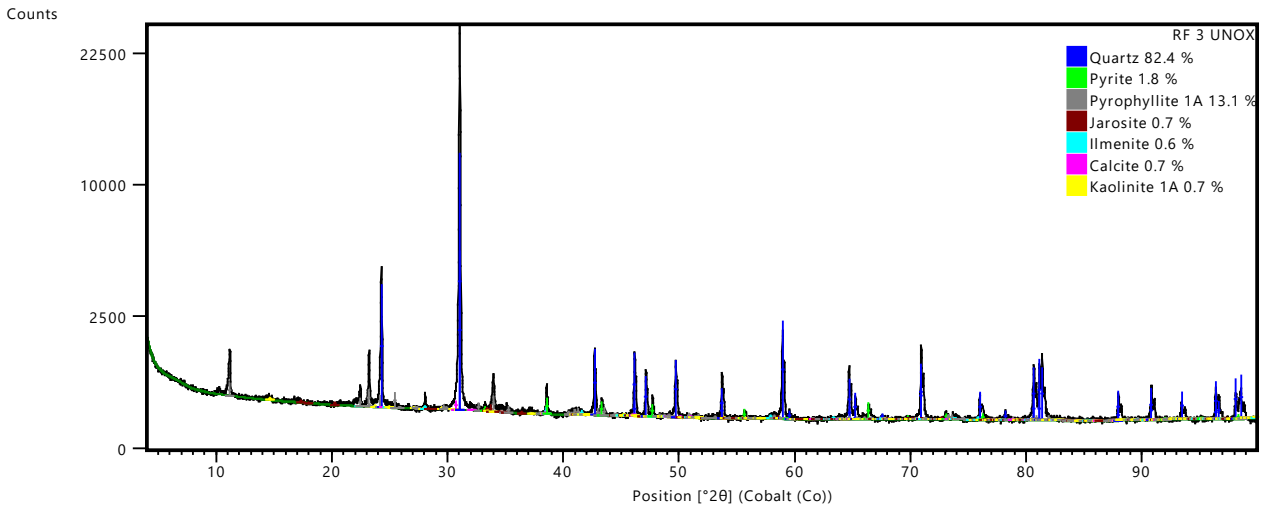


Figure 45: XRD analysis results for RF 3 unoxidized composite sample

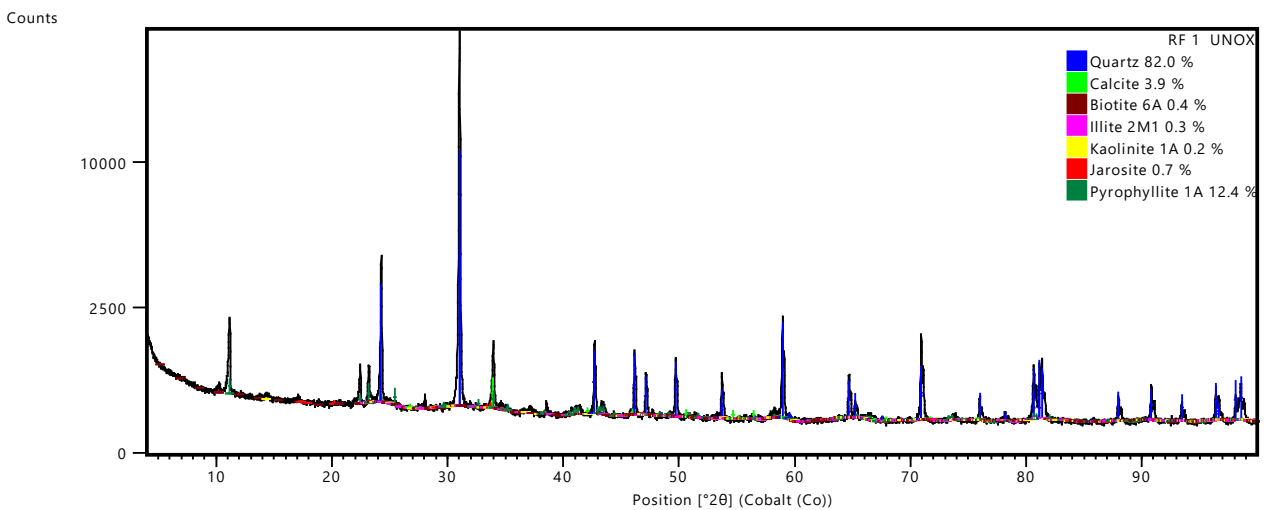


Figure 46: XRD analysis results for RF 1 unoxidized composite sample

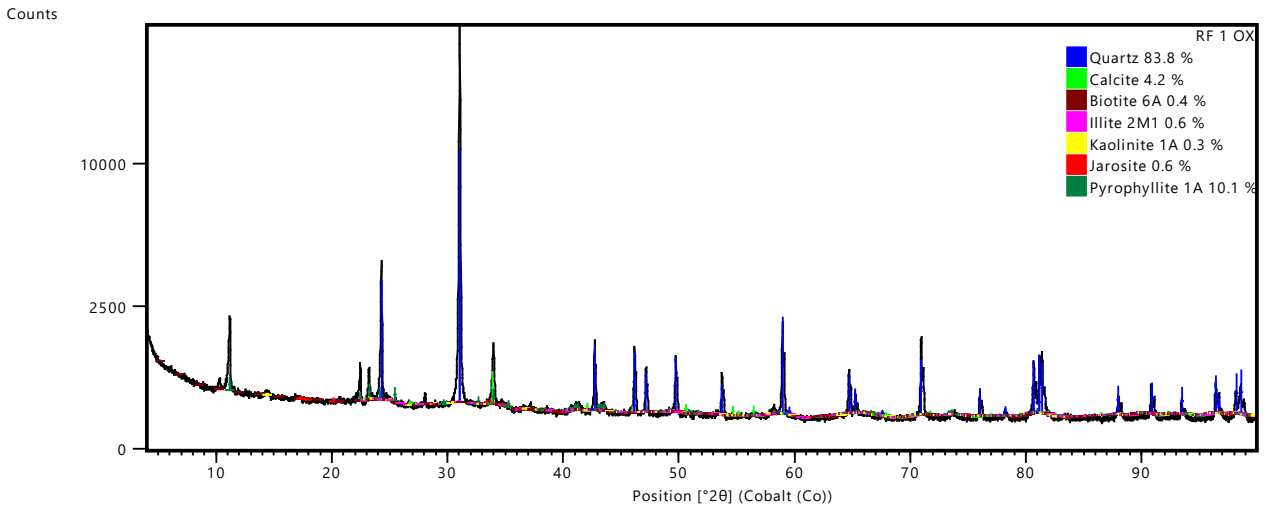


Figure 47: XRD analysis results for RF 1 oxidized composite sample

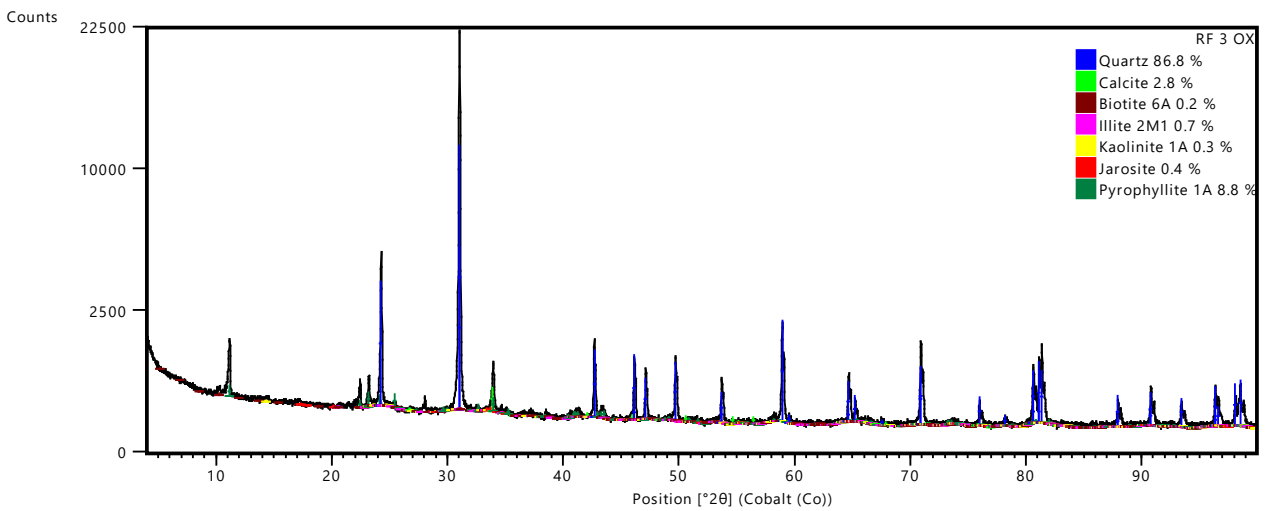


Figure 48: XRD analysis results for RF 3 oxidized composite sample

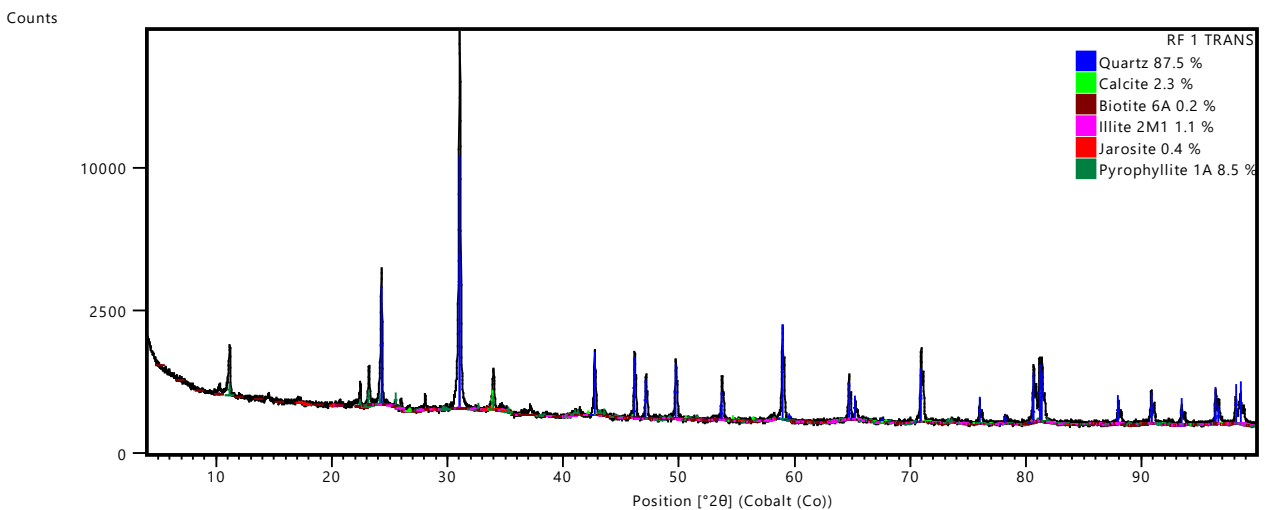


Figure 49: XRD analysis results for RF 1 transition zone sample

APPENDIX D: SULPHUR SPECIATION RESULTS

Table 17: RF 1 sulphur speciation data

Locality	Geo – Total Sulphur	Geo – Sulphide Sulphur	Geo – Sulphate Sulphur
	%	%	%
RF 1.1	0.07	0.023	0.047
RF 1.2	0.325	0.011	0.314
RF 1.3	0.5	0.02	0.48
RF 1.4	1.5	0.375	1.12
RF 1.5	0.905	0.321	0.583
RF 1.6	0.693	0.229	0.465
RF 1.7	1.07	0.423	0.648
RF 1.8	0.517	0.238	0.279
RF 1.9	1.14	0.719	0.418
RF 1.10	2.72	1.25	1.47
RF 1.11	1.43	0.916	0.517
RF 1.12	1.3	1.05	0.257
RF 1.13	1.14	0.677	0.46
RF 1.14	1.25	0.889	0.365
RF 1.15	1.08	0.897	0.185
RF 1.16	0.954	0.604	0.35
RF 1.17	1.15	0.747	0.398
RF 1.18	1.14	0.711	0.434
RF 1.19	1.03	0.843	0.192

Table 18: RF 2 sulphur speciation data

Locality	Geo – Total Sulphur	Geo – Sulphide Sulphur	Geo – Sulphate Sulphur
	%	%	%
RF 2.1	0.07	0	0.07
RF 2.2	0.664	0.037	0.627
RF 2.3	0.557	0.028	0.529
RF 2.4	1.18	0.501	0.675
RF 2.5	0.212	0.006	0.206
RF 2.6	0.844	0.574	0.27
RF 2.7	1.5	0.736	0.764
RF 2.8	1.6	1.03	0.571
RF 2.9	2.62	2.46	0.161

Table 19: RF 3 sulphur speciation data

Locality	Geo – Total Sulphur	Geo – Sulphide Sulphur	Geo – Sulphate Sulphur
	%	%	%
RF 3.1	0.381	0.042	0.339
RF 3.2	0.439	0.026	0.413
RF 3.3	1.2	0.613	0.589
RF 3.4	1.42	1	0.423
RF 3.5	1.12	0.663	0.454
RF 3.6	1.65	1.02	0.636
RF 3.7	1.52	0.974	0.547
RF 3.8	1.65	1.4	0.253
RF 3.9	1.88	1.27	0.618
RF 3.10	1.57	0.839	0.734
RF 3.11	1.19	0.901	0.29

Table 20: RF 4 sulphur speciation data

Locality	Geo – Total Sulphur	Geo – Sulphide Sulphur	Geo – Sulphate Sulphur
	%	%	%
RF 4.1	0.07	0	0.07
RF 4.2	0.664	0.037	0.627
RF 4.3	0.557	0.028	0.529
RF 4.4	1.18	0.501	0.675
RF 4.5	0.212	0.006	0.206
RF 4.6	0.844	0.574	0.27
RF 4.7	1.5	0.736	0.764
RF 4.8	1.6	1.03	0.571
RF 4.9	2.62	2.46	0.161